Weather Research Forecast Version 3.8
Meteorological Model Evaluation
Annual 2014 12-km CONUS

Prepared for:
US EPA

Prepared by:
UNC-Chapel Hill

September 7, 2016

UNC
INSTITUTE FOR
THE ENVIRONMENT

CONTENTS

TABLES

FIGURES

1.0 INTRODUCTION

The University of North Carolina (UNC) at Chapel Hill simulated annual meteorology for the 2014 calendar year to support emissions, photochemical, and dispersion modeling applications for this year. The simulated meteorological data will be used to support assessments of ozone, $PM_{2.5}$, visibility, and a variety of toxics.

The annual meteorology was simulated using the Weather Research and Forecasting model (WRF) at a 12-km horizontal resolution for the continental United States (CONUS). The WRF meteorological fields were processed using the Meteorology Chemistry Interface Process (MCIP) to generate Community Multiscale Air Quality (CMAQ)-ready input files. Additionally, the 2014 WRF meteorological fields were processed using the Mesoscale Model Interface Tool (MMIF) to generate input files for dispersion models. This report provides technical details about the WRF model configuration and the meteorological model performance evaluation for the 2014 calendar, which includes performance evaluation of 2-m temperature, 2-m mixing ratio, 10-m wind speed and direction, and accumulated monthly precipitation.

2.0 WRF MODEL CONFIGURATION

We used the Weather Research and Forecasting (WRF) model with the Advanced Research dynamic solver for this meteorological modeling study.[1] WRF is a next-generation mesoscale numerical weather prediction system designed to serve both operational forecasting and atmospheric research needs. WRF contains separate modules to compute different physical processes, such as surface energy budgets and soil interactions, turbulence, cloud microphysics, and atmospheric radiation. Within WRF, the user has many options for selecting the different schemes for each type of physical process. There is a WRF Preprocessing System (WPS) that generates the initial and boundary conditions used by WRF, based on topographic datasets, land use information, and larger-scale atmospheric and oceanic models. Below, we outline the model setup, model input, and options (e.g. parameterizations) that were used for the 2014 WRF simulations. The WRF options were selected based on numerical meteorological modeling research and the experience of scientists at the U.S. Environmental Protection Agency (USEPA), within the Office of Research and Development (ORD).[2,3,4]

A summary of the WRF input data preparation procedure used for this annual modeling exercise is provided below.

Model Selection: The publicly available version of WRF (version 3.8) was used for the 2014 meteorological simulation. This was the latest version of WRF available at the time the simulation was performed. WPS version 3.8 was also used to develop the model inputs.

Horizontal Domain Definition: The WRF 12-km configuration includes a 5-grid cell buffer in all directions to minimize any potential numeric noise along WRF domain boundaries, which can affect the air quality model meteorological inputs. Such numeric noise can occur near the boundaries of the WRF domain solution as the boundary conditions come into balance with the WRF numerical algorithms. The WRF horizontal domains are presented in Figure 2-1. The grid projection was Lambert Conformal with a pole of projection of 40 degrees north, -97 degrees east and standard parallels of 33 and 45 degrees.

Vertical Domain Definition: The WRF modeling was based on 36 vertical layers with a surface layer approximately 20 meters deep. The vertical domain is presented in both sigma and approximate height coordinates in Table 2-1.

Topographic Inputs: Topographic information for the WRF model was developed using the standard WRF terrain databases. The 12-km CONUS domain was based on the latest USGS GMTED2010 data.[5] This is 30-second (~900 m) data and replaces the old topography data (GTOPO30) available in prior WRF releases.

---

[1] Skamarock, W.C. and J.B. Klemp, 2008. A time-split nonhydrostatic atmospheric model for weather research and forecasting applications. *Journal of Computation Physics*, Volume 227, pp. 3465-3485.

[2] Pleim, J.E. and R.C. Gilliam, 2009. An indirect data assimilation scheme for deep soil temperature in the Pleim-Xiu land surface model. *Journal of Applied Meteorology and Climatology*, Volume 48, pp. 1362-1376.

[3] Gilliam, R.C. and J.E. Pleim, 2010. Performance assessment of the Pleim-Xiu LSM, Pleim surface-layer and ACM PBL physics in version 3.0 of WRF-ARW. *Journal of Applied Meteorology and Climatology,* Volume 49, pp. 760-774.

[4] Gilliam, R.C., J.M. Godowitch, and S.T. Rao, 2012. Improving the horizontal transport in the lower troposphere with four dimensional data assimilation. *Atmospheric Environment*, Volume 53, pp. 186-201.

[5] Global Multi-resolution Terrain Elevation Data 2010 (GMTED2010); https://lta.cr.usgs.gov/GMTED2010

Vegetation Type and Land Use Inputs: Vegetation type and land use information were based on the National Land Cover Database (NLCD) 2011.[6] This is a 9-second, ~250 m, dataset that includes fractional land use, which is advantageous for use with the land surface model applied (Pleim-Xiu). NLCD 2011 dataset (40-class) is only available for the CONUS and areas of Canada and Mexico are defined using the 20-class MODIS scheme.

Atmospheric Data Inputs: The initial and lateral boundary conditions were taken from the 12-km (Grid #218) North American Model (NAM) archives available from the National Climatic Data Center (NCDC) National Operational Model Archive and Distribution System (NOMADS) server.[7] Both the 6-hour analysis and 3-hour NAM forecast were used.

Time Integration: Third-order Runge-Kutta integration was used.

Diffusion Options: Horizontal Smagorinsky first-order closure with sixth-order numerical diffusion and suppressed up-gradient diffusion was used.

Water Temperature Inputs: The water temperature data were taken from the Group for High Resolution Sea Surface Temperature (GHRSST)[8]. The GHRSST product used has a horizontal resolution of 1 km.

Snow Inputs: Snow height and snow water equivalent within the CONUS were taken from the National Snow and Ice Data Center. Within the CONUS, the Snow Data Assimilation System (SNODAS)[9] data product was used to provide best available estimates of snow cover and snow water equivalent. The NAM fields were applied to provide snow estimates outside of the CONUS.

Data Assimilation: The objective analysis program (OBSGRID) was run to incorporate additional observational from the Meteorological Assimilation Data Ingest System (MADIS[10]) observation archive, including the MADIS metar, sao, and maritime observations. These data are then incorporated into the NAM boundary conditions and used within the WRF data assimilation. Specifically, the WRF model was run with analysis nudging (i.e., Four Dimensional Data assimilation [FDDA]). For winds and temperature, an analysis nudging coefficient of $1x10^{-4}$ was applied to the 12-km domain. For mixing ratio, an analysis nudging coefficient of $1.0x10^{-5}$ was applied to the 12-km domain. Analysis nudging for winds, temperature, and mixing ratio were applied above the planetary boundary layer.

An indirect data assimilation scheme was applied with the Pleim-Xiu land surface model, which uses the surface fields from the OBSGRID program. The first indirect data assimilation is a technique in which soil moisture is nudged according to the biases in 2-m air temperature and relative humidity between the

[6] National Land Cover Database 2011, http://www.mrlc.gov/nlcd2011.php.
[7] North American Model Analysis-Only, http://nomads.ncdc.noaa.gov/data.php; download from ftp://nomads.ncdc.noaa.gov/NAM/analysis_only/.
[8] Global High Resolution SST (GHRSST) analysis, https://www.ghrsst.org/ ; download from ftp://podaac-ftp.jpl.nasa.gov/allData/ghrsst/data/L4/GLOB/JPL/MUR/.
[9] National Operational Hydrologic Remote Sensing Center. 2004. *Snow Data Assimilation System (SNODAS) Data Products at NSIDC*, [January 2014 – December 2014]. Boulder, Colorado USA: National Snow and Ice Data Center. http://dx.doi.org/10.7265/N5TB14TC
[10] Meteorological Assimilation Data Ingest System. http://madis.noaa.gov/.

model- and observation-based analyses. The second is a technique that nudges the deep soil temperature according to the model bias in 2-m air temperature.

Physics Options: The physics options chosen for this application are presented in Table 2-2.

Application Methodology: The WRF model was executed as a continuous simulation with a 60-second integration time step. A 10-day spin-up period was applied. WRF was initialized on December 21, 2013 at 00Z and run through January 1, 2015. Model results were output every 60 minutes and output files were split at 24-hour intervals beginning at 00Z.

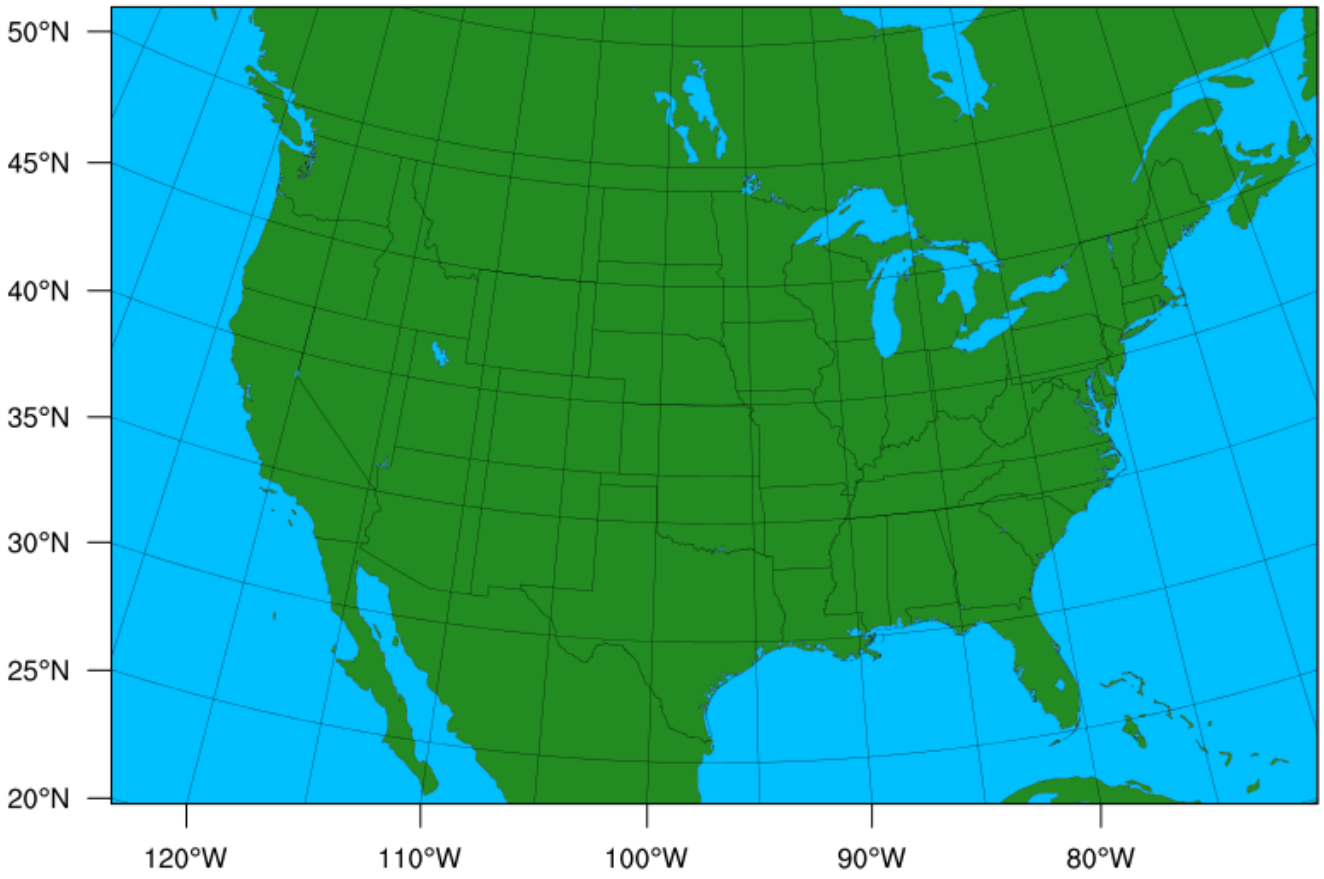

Figure 2-1. 12-km CONUS WRF modeling domain.

Table 2-1. Vertical layer definition for WRF simulations.

WRF Meteorological Model				
WRF Layer	Sigma	Pressure (mb)	Height (m)	Thickness (m)
36	0.0000	50.00	19313	3423
35	0.0500	98.15	15890	2243
34	0.1000	146.30	13648	1706
33	0.1500	194.45	11942	1392
32	0.2000	242.60	10551	1183
31	0.2500	290.75	9367	1034
30	0.3000	338.90	8333	921
29	0.3500	387.05	7412	832
28	0.4000	435.20	6580	761
27	0.4500	483.35	5820	702
26	0.5000	531.50	5117	652
25	0.5500	579.65	4465	610
24	0.6000	627.80	3856	573
23	0.6500	675.95	3283	541
22	0.7000	724.10	2742	412
21	0.7400	762.62	2330	298
20	0.7700	791.51	2032	289
19	0.8000	820.40	1742	188
18	0.8200	839.66	1554	185
17	0.8400	858.92	1369	182
16	0.8600	878.18	1188	178
15	0.8800	897.44	1010	175
14	0.9000	916.70	834	87
13	0.9100	926.33	748	86
12	0.9200	935.96	662	85
11	0.9300	945.59	577	84
10	0.9400	955.22	492	84
9	0.9500	964.85	409	83
8	0.9600	974.48	325	83
7	0.9700	984.11	243	82
6	0.9800	993.74	162	41
5	0.9850	998.56	121	40
4	0.9900	1003.37	80	40
3	0.9950	1008.19	40	20
2	0.9975	1010.59	20	20
1	1.0000	1013	0	

Table 2-2. Physics options used in the 12-km CONUS WRF Version 3.8 simulation of the 2014 calendar year.

WRF Treatment	Option Selected	Notes
Microphysics	Morrison 2-moment scheme[11]	6-class microphysics scheme that includes number concentrations for ice, snow, rain, and graupel.
Longwave Radiation	RRTMG[12]	Rapid Radiative Transfer Model (RRTM) for GCMs includes random cloud overlap and improved efficiency over RRTM.
Shortwave Radiation	RRTMG	Same as above, but for shortwave radiation.
Land Surface Model (LSM)	Pleim-Xiu[13]	Two-layer scheme with vegetation and sub-grid tiling.
Planetary Boundary Layer (PBL) scheme	ACM2[14]	Non-local upward mixing and local downward mixing.
Cumulus parameterization	Kain-Fritsch[15]	Deep and shallow convection sub-grid scheme using a mass flux approach with downdrafts and CAPE; moisture advection trigger applied.

[11] Morrison, H., G. Thompson, and V. Tatarskii, 2009. Impact of Cloud Microphysics on the Development of Trailing Statiform Precipitation in a Simulated Squall Line: Comparison of One- and Two-Moment Schemes. *Monthly Weather Review*, Volume 137, pp. 991-1007.

[12] Iacono, M.J., J.S. Delamere, E.J. Mlawer, M.W. Shepherd, S.A. Clough, and W.D. Collins, 2008. Radiative forcing by long-lived greenhouse gases: Calculations with AER radiative transfer models. *Journal of Geophysical Research*, Volume 113, D13103.

[13] Gilliam, R.C. and J.E. Pleim, 2010. Performance assessment of the Pleim-Xiu LSM, Pleim surface-layer and ACM PBL physics in version 3.0 of WRF-ARW. *Journal of Applied Meteorology and Climatology,* Volume 49, pp. 760-774.

[14] Pleim, Jonathan E., 2007. A Combined Local and Nonlocal Closure Model for the Atmospheric Boundary Layer. Part I: Model Description and Testing. *Journal of Applied Meteorology and Climatology*, Volume 46**,** pp. 1383–1395.

[15] Ma, Lei–Ming, and Zhe–Min Tan, 2009. Improving the behavior of the cumulus parameterization for tropical cyclone prediction: Convection trigger. *Atmospheric Research*, Volume 92**,** pp. 190–211.

3.0 MODEL PERFORMANCE EVALUATION APPROACH

The model evaluation approach was based on a combination of qualitative and quantitative analyses. The quantitative analysis was divided into monthly summaries of 2-m temperature, 2-m mixing ratio, and 10-m wind speed for each month to help generalize the model bias and error. The observed database for winds, temperature, and water mixing ratio used in this analysis was the National Oceanic and Atmospheric Administration (NOAA) Earth System Research Laboratory (ESRL) Meteorological Assimilation Data Ingest System (MADIS). The locations of the MADIS monitoring sites within the 12-km CONUS are shown in Figure 3-1.

The quantitative model performance evaluation of WRF using surface meteorological measurements was performed using the publicly available AMET evaluation tool.[16] AMET calculates statistical performance metrics for bias, error and correlation for surface winds, temperature and mixing ratio and can produce time series of predicted and observed meteorological variables and performance statistics. This evaluation only summarizes the meteorological model performance using bias and error model performance statistics metrics with select plots to enhance potential users' understanding of model performance. However, we provide an online source so data users can independently judge the adequacy of the model simulation. Overall comparisons are offered herein to judge the model efficacy for 2014, but this review does not necessarily cover all potential user needs and applications.

We evaluate the model near surface temperature, mixing ratio (humidity), wind speed, and wind direction bias and error. The equations for the model bias and error are given below.

$$\text{Bias} = \frac{1}{N}\sum_{i=1}^{N}\left(P_i - O_i\right)$$

$$\text{Error} = \frac{1}{N}\sum_{i=1}^{N}\left|P_i - O_i\right|$$

For the wind direction difference statistics, a difference called wind displacement was applied. Wind displacement is the difference in the U and V vectors of the modeled and observed winds. The displacement is calculated as:

$$\textbf{Wind Displacement} = \textbf{abs}\left((U_m - U_o + V_m - V_o\right) \textbf{ X (1km/1000m) X (3600s/hr) X 1hr)}$$

Where U_m and V_m are the U and V components respectively of the modeled wind vector, and U_o and V_o are the U and V components of the observed wind vector.

We also evaluated the WRF spatial field of accumulated monthly precipitation against the observed monthly precipitation estimates from the Parameter-elevation Relationships on Independent Slopes Model (PRISM) interpolation procedure. The PRISM interpolation uses approximately 13,000 precipitation measurement sites across the CONUS and interpolates them to a < 1 km grid using

[16] AMET evaluation tool; https://www.cmascenter.org/help/documentation.cfm?MODEL=amet&VERSION=1.1&temp_id=99999.

regression weights based primarily on the physiographic similarity of stations to the grid cell.[17] Factors considered are location, elevation, coastal proximity, topographic facet orientation, vertical atmospheric layer, topographic position, and orographic effectiveness of the terrain. The PRISM interpolation approach represents a significant improvement over other techniques used to spatially interpolate observed precipitation that failed to account for factors that influence precipitation away from the observations, such as orographic effects. However, it is still an interpolation technique that may not always capture all effects on precipitation and is just limited to precipitation within the CONUS. The PRISM interpolation procedure will be particularly challenged during summer convective precipitation events (thunderstorms) that can be very spotty and isolated. Such events can occur between the rainfall monitoring sites, and so would not be present in the observations, and hence, the PRISM analysis fields. In our comparison, we regrid PRISM precipitation estimates to take a difference between WRF and PRISM for each month to help illuminate the WRF precipitation errors.

Lastly, model evaluation includes comparison with shortwave downward radiation measurements. Shortwave downward radiation measurements are taken at Surface Radiation Budget Network (SURFRAD)[18] and Integrated Surface Irradiance Study (ISIS)[19] monitor locations. The SURFRAD network consists of seven sites and the ISIS network consists of nine sites across the United States, shown in Figure 3-2. Both networks are operated by NOAA, with SURFRAD sites existing as a subset of ISIS monitors that provide higher-level radiation information not used in this evaluation.

[17] Daley, C., M. Halbleib, J. Smith, W. Gipson, M. Doggett, G. Taylor, J. Curtis and P. Pasteris, 2008. Physiographically sensitive mapping of the climatological temperature and precipitation across the conterminous United States. *International. Journal of Climatology*, Volume 28, pp 2031-2064.

[18] http://www.srrb.noaa.gov/surfrad

[19] http://www.esrl.noaa.gov/gmd/grad/isis/index.html

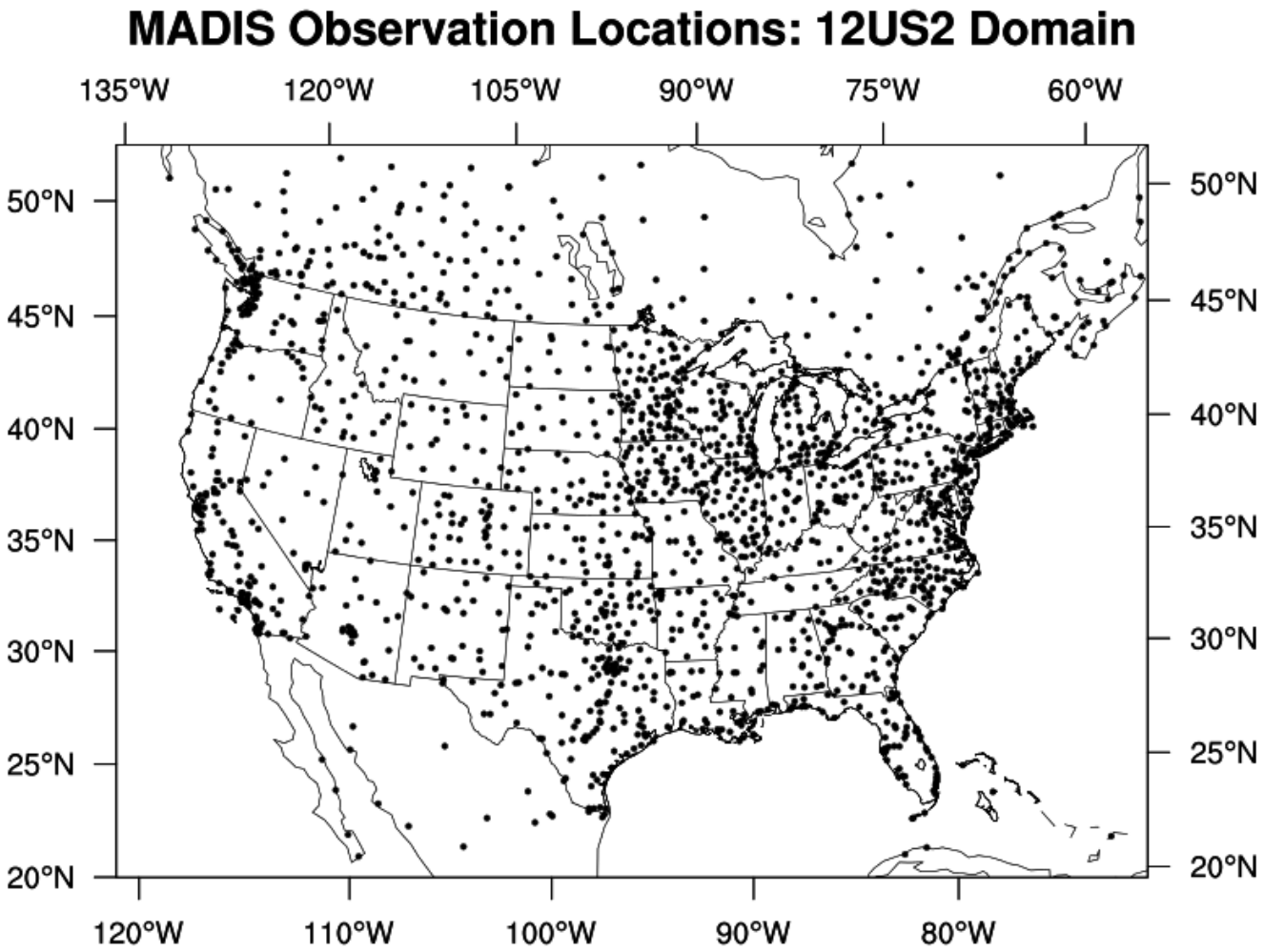

Figure 3-1. Locations of MADIS surface meteorological modeling sites with the WRF 12-km CONUS modeling domain.

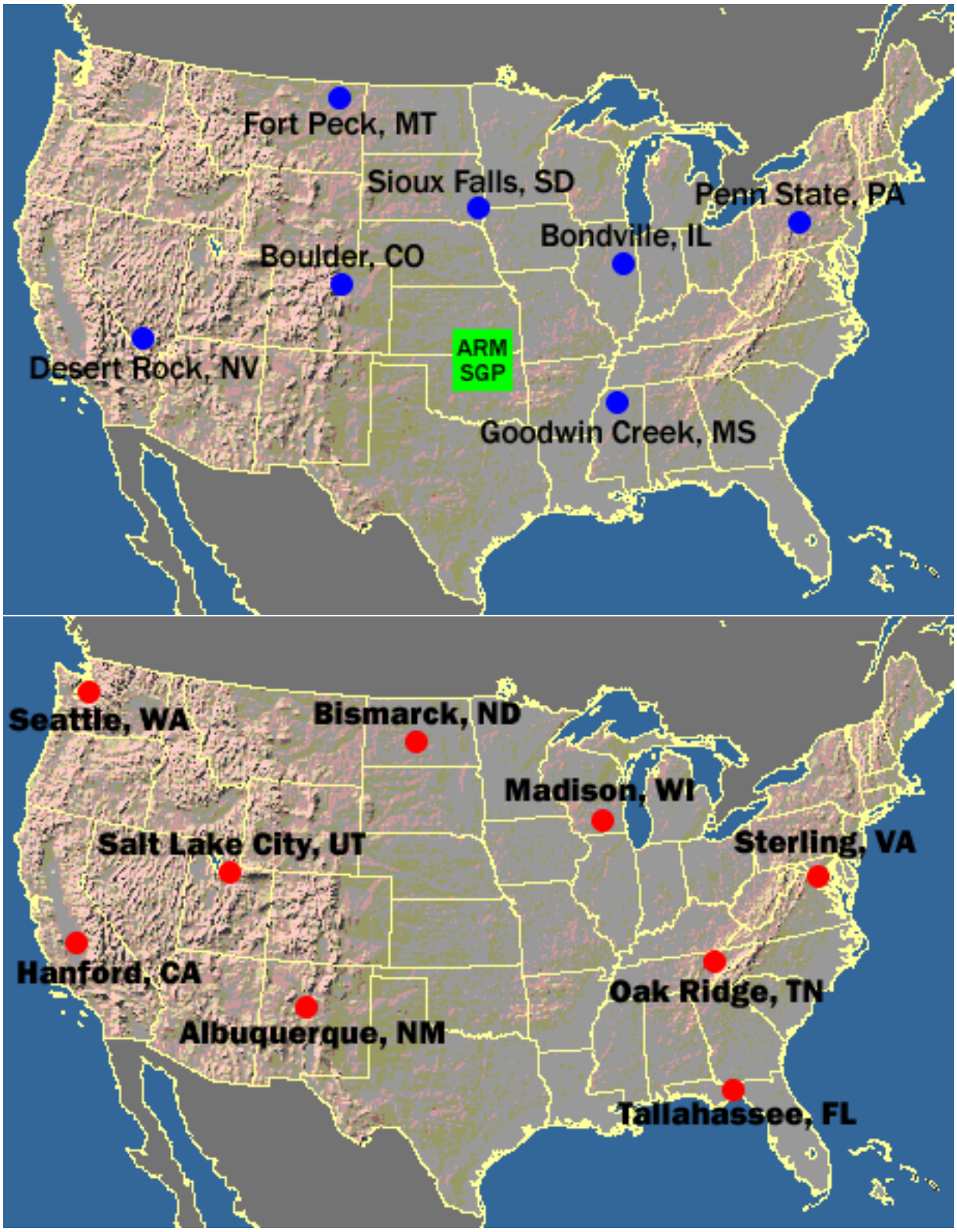

Figure 3-2. Location of SURFRAD (top) and ISIS (bottom) radiation monitors.

4.0 WRF MODEL PERFORMANCE EVALATUION RESULTS

Model Evaluation Results for 2-m Temperature

The temperature bias on average for the CONUS for all months is smaller than ±1K with a temperature error less than 2K, Figure 4-1. On average, there is a warm bias during the summer and fall months and a cool bias during the winter and spring months. The largest error occurs during the winter months of January and February.

Figure 4-2 shows the diurnal temperature statistics for January and July. The diurnal plot illustrates a cool bias in January (winter) that exists throughout the day; however, the bias is largest during the night and early morning and improves during the afternoon hours. The error during January (winter) is also largest during the night and early morning. The opposite is true for July (summer), with a general warm bias throughout the day. The bias and error for July (summer) is largest during the afternoon/evening hours and smallest during the early morning hours.

Figure 4-3 illustrates that the cool bias during the winter months (January and February) is more dominant for the eastern half of the CONUS (Great Plains and eastward). However, some portions of the western CONUS (Rocky Mountains and westward) have a warm bias during the winter. Similar spatial patterns in the bias continue into the spring, but are generally smaller than in the winter, as shown in Figure 4-4. However, there is a transition to a warm bias in portions of the eastern half of the CONUS that reaches a maximum by July; seen in Figure 4-5 and Figure 4-6. Large portions of the Midwest into the Northeast have the largest warm bias during the summer months. Interestingly, we see there is some difference between the western CONUS and eastern CONUS, with a cool bias for many locations throughout the western half of the CONUS – Rocky Mountains and west. By October, November and into December – Figure 4-7 and Figure 4-8 – the warm bias for the eastern half of the CONUS reverse back to a cool bias for many locations.

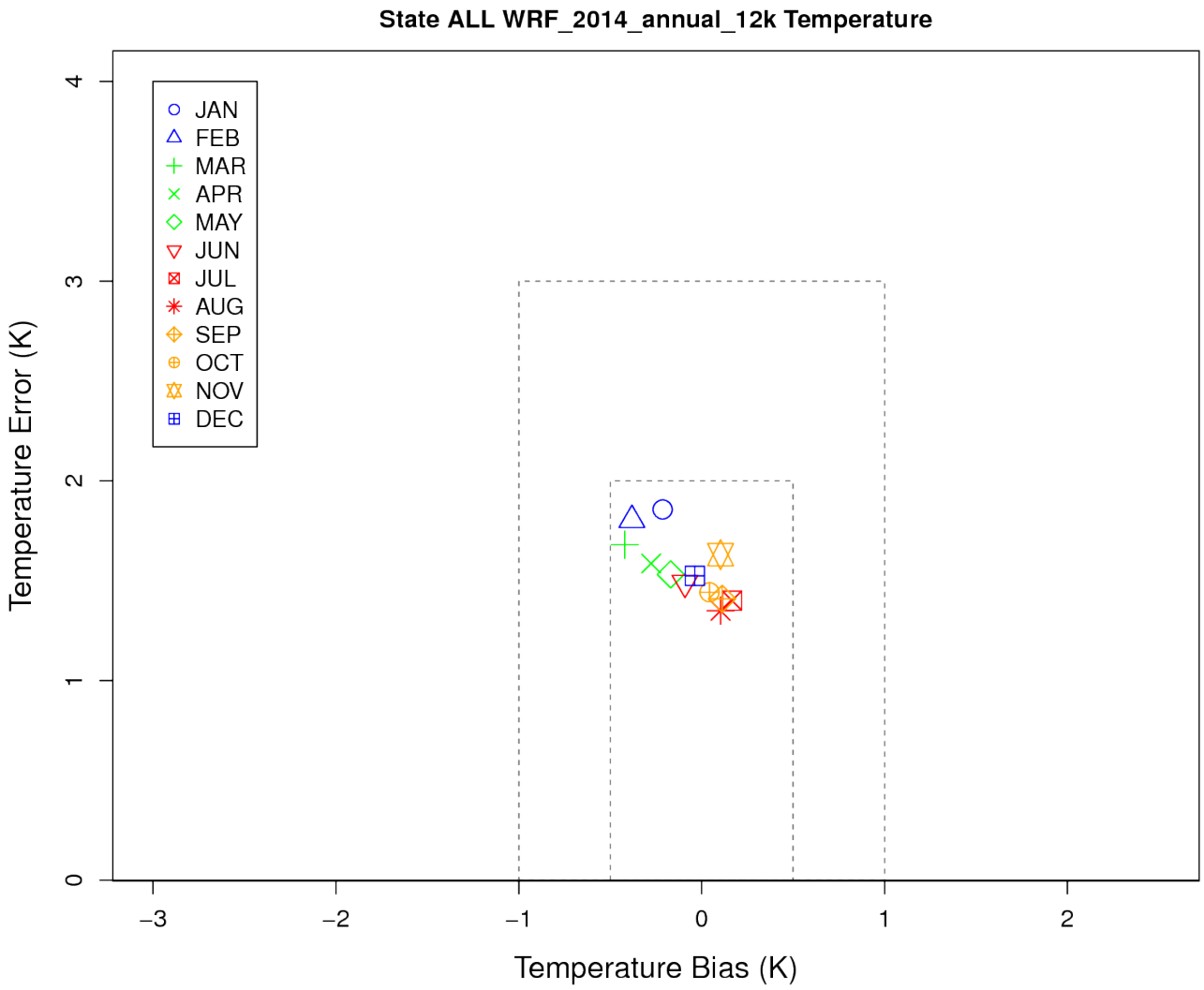

Figure 4-1. Soccer plot of monthly 2-m temperature error and bias averaged over the 12-km CONUS domain for the 2014 calendar year.

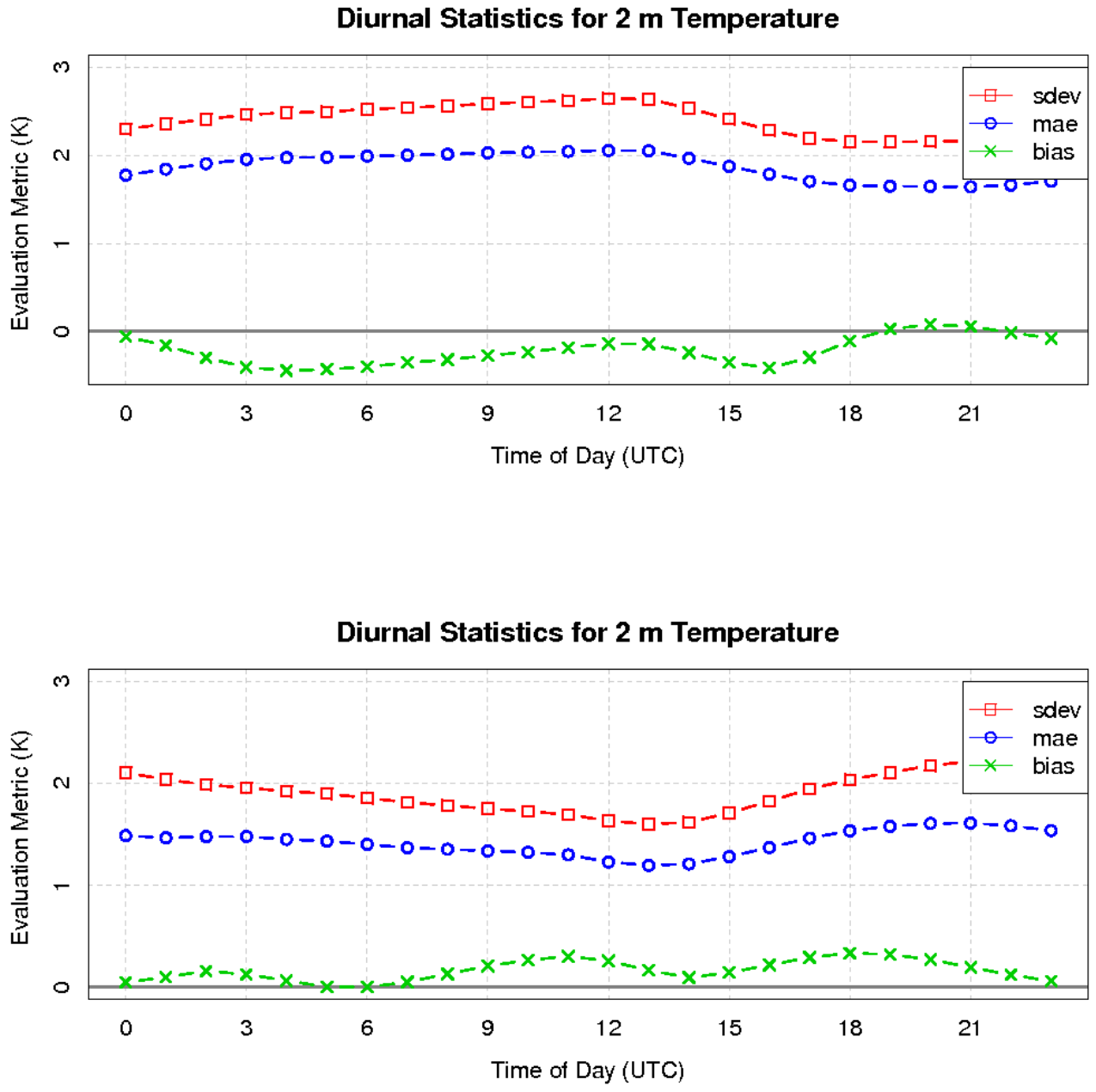

Figure 4-2. Diurnal 2-m temperature error and bias (°C) averaged over the 12-km CONUS domain for January (top) and July (bottom) 2014.

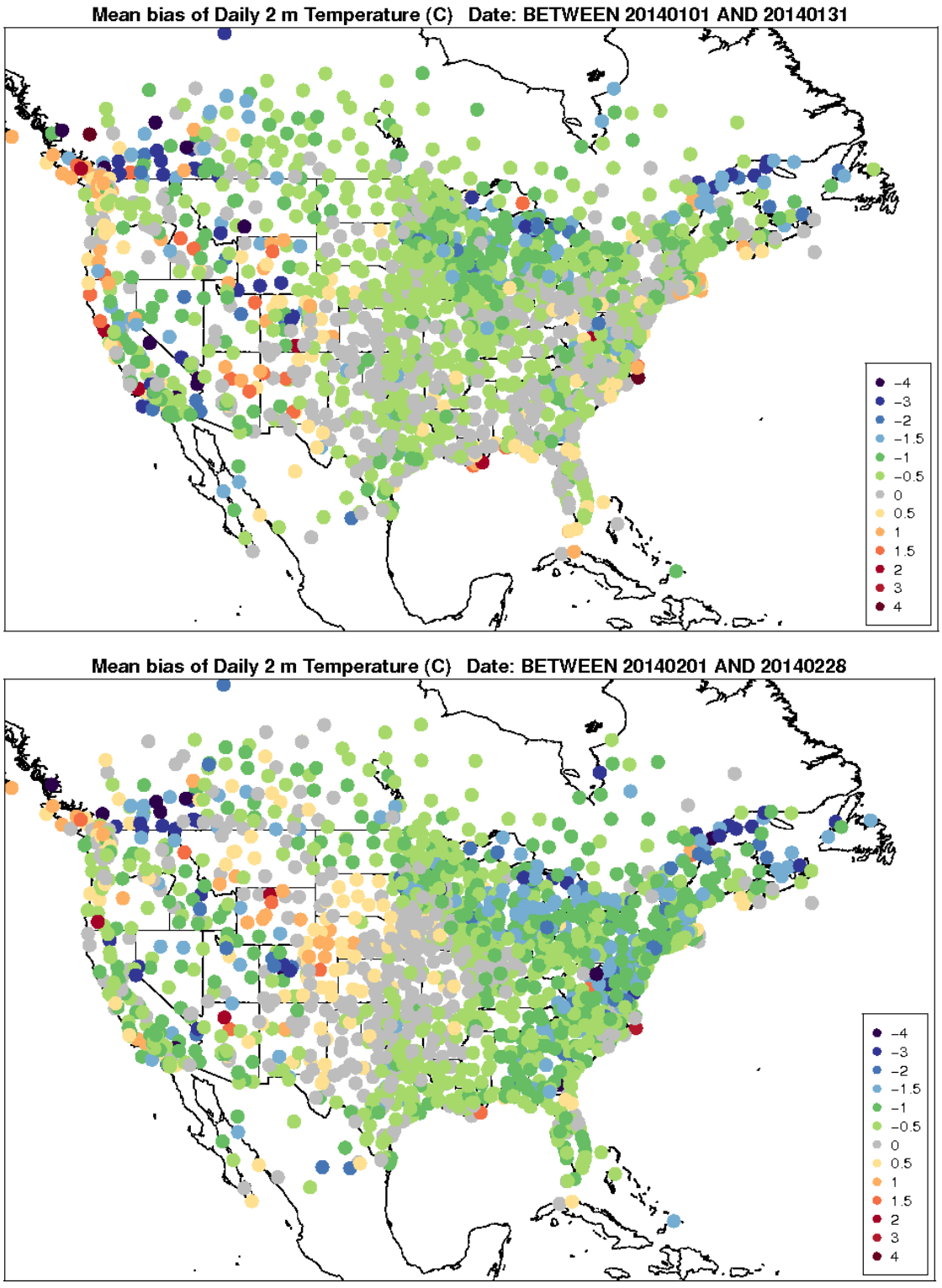

Figure 4-3. Spatial distribution of 2-m temperature bias (°C) within the 12-km CONUS domain for January (top) and February (bottom).

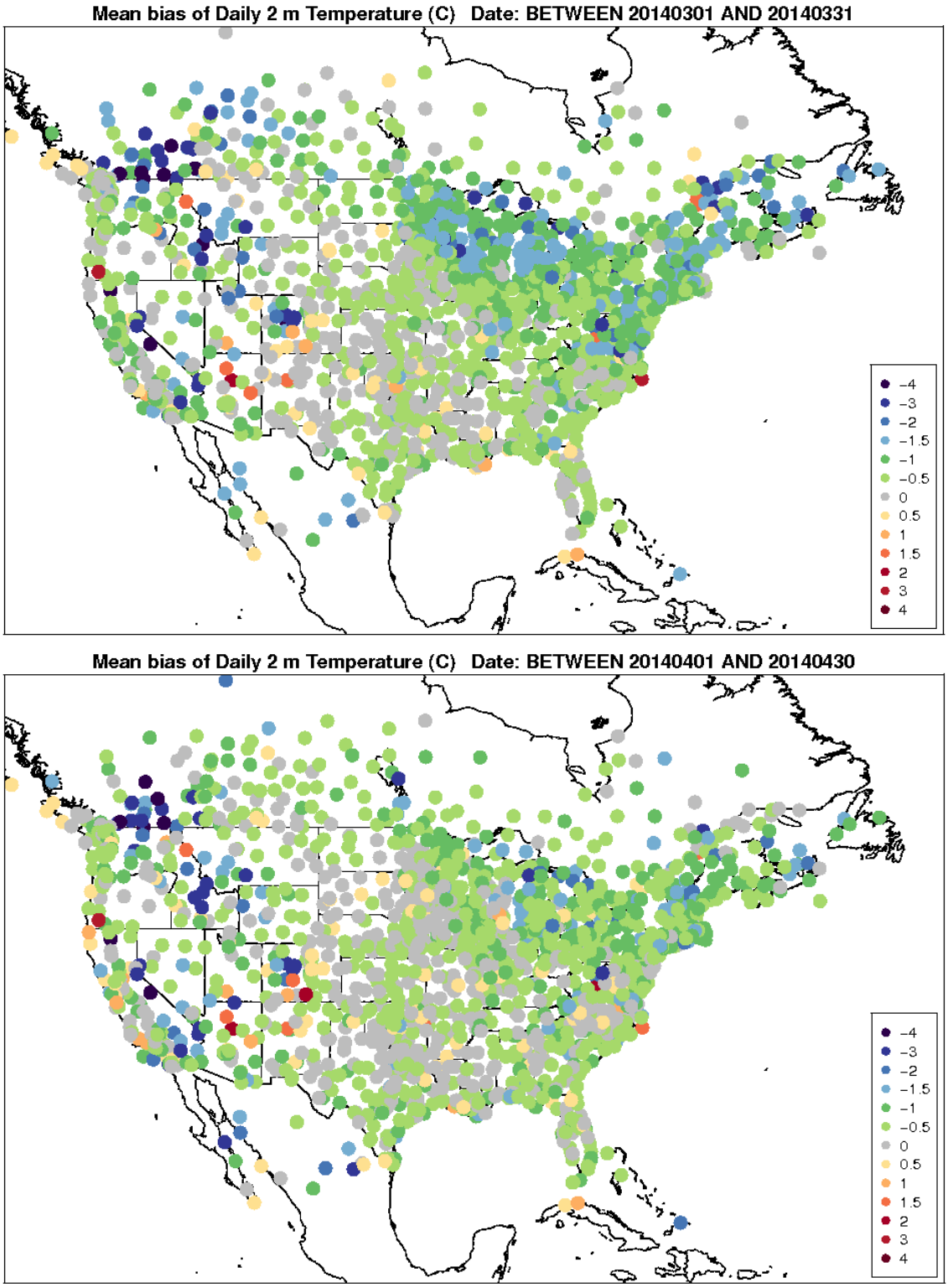

Figure 4-4. Spatial distribution of 2-m temperature bias (°C) within the 12-km CONUS domain for March (top) and April (bottom).

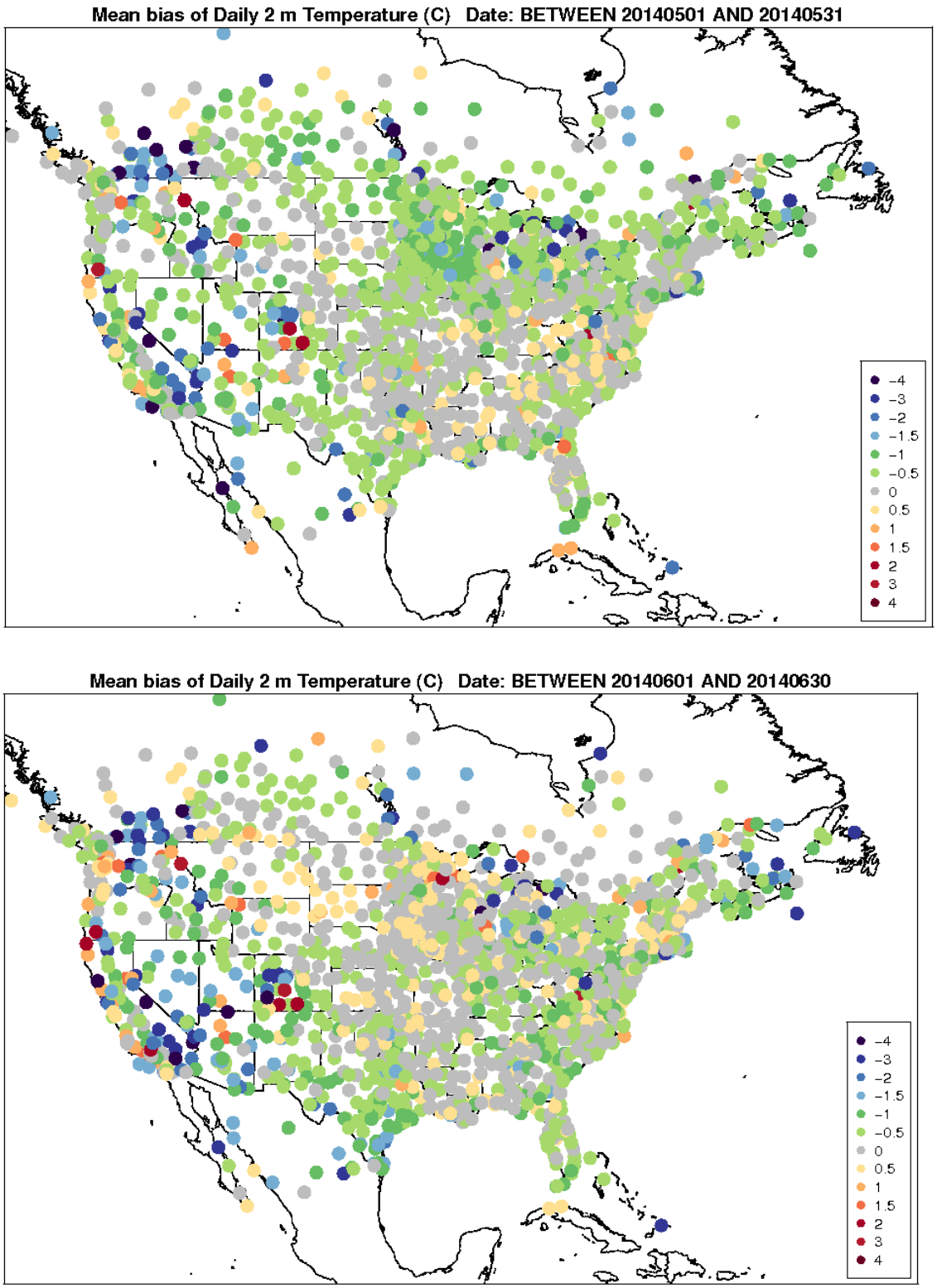

Figure 4-5. Spatial distribution of 2-m temperature bias (°C) within the 12-km CONUS domain for May (top) and June (bottom).

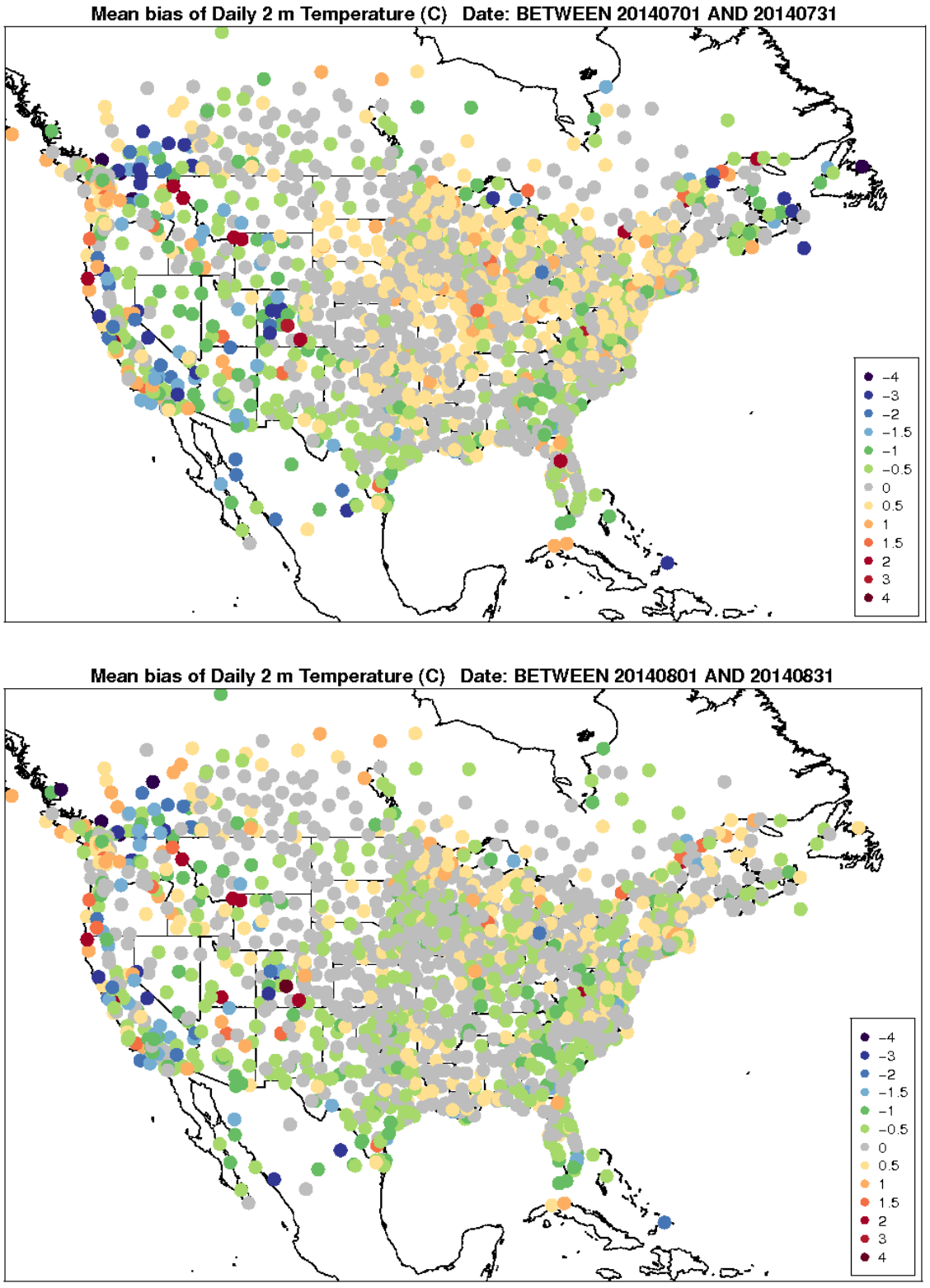

Figure 4-6. Spatial distribution of 2-m temperature bias (°C) within the 12-km CONUS domain for July (top) and August (bottom).

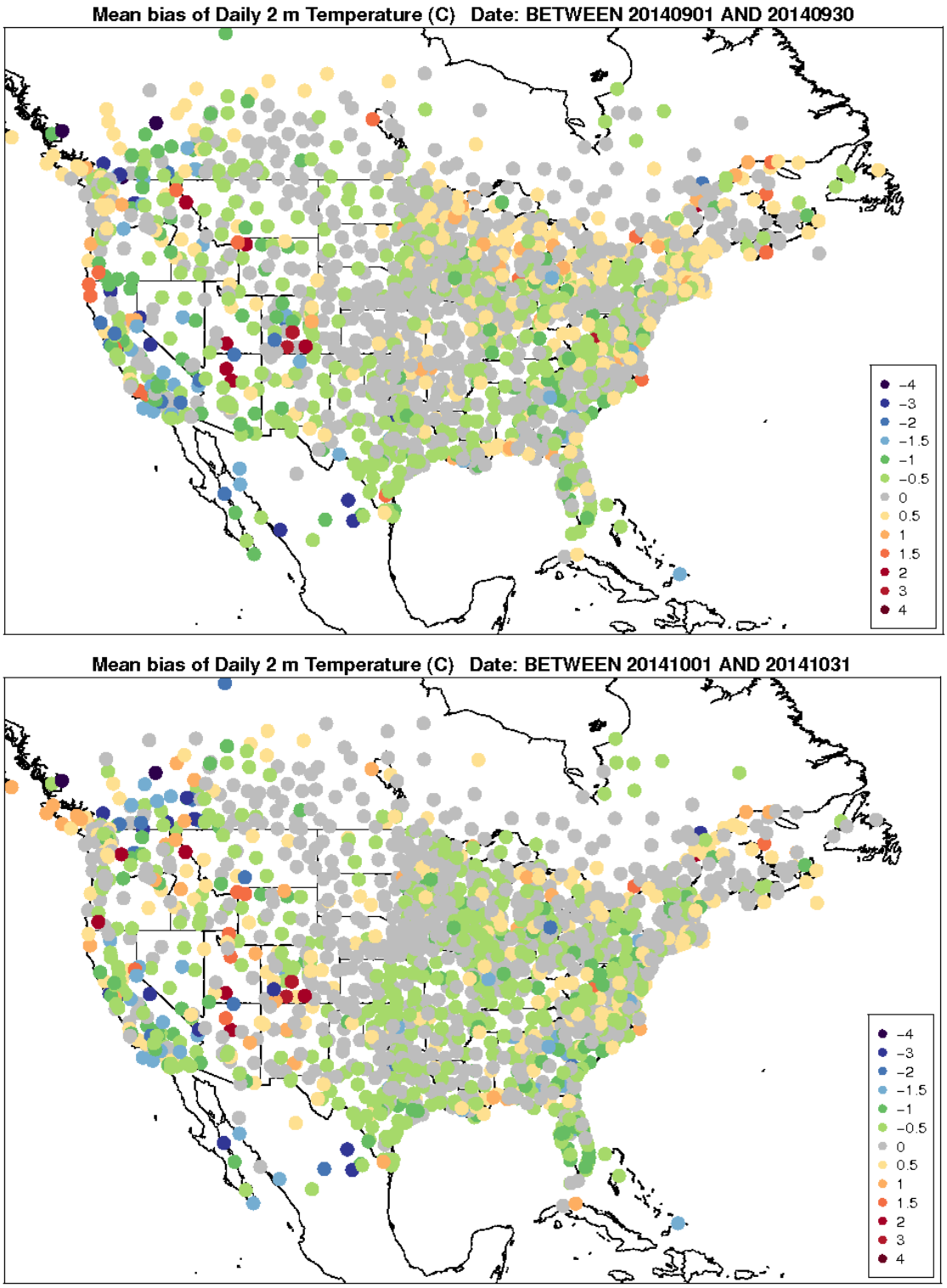

Figure 4-7. Spatial distribution of 2-m temperature bias (°C) within the 12-km CONUS domain for September (top) and October (bottom).

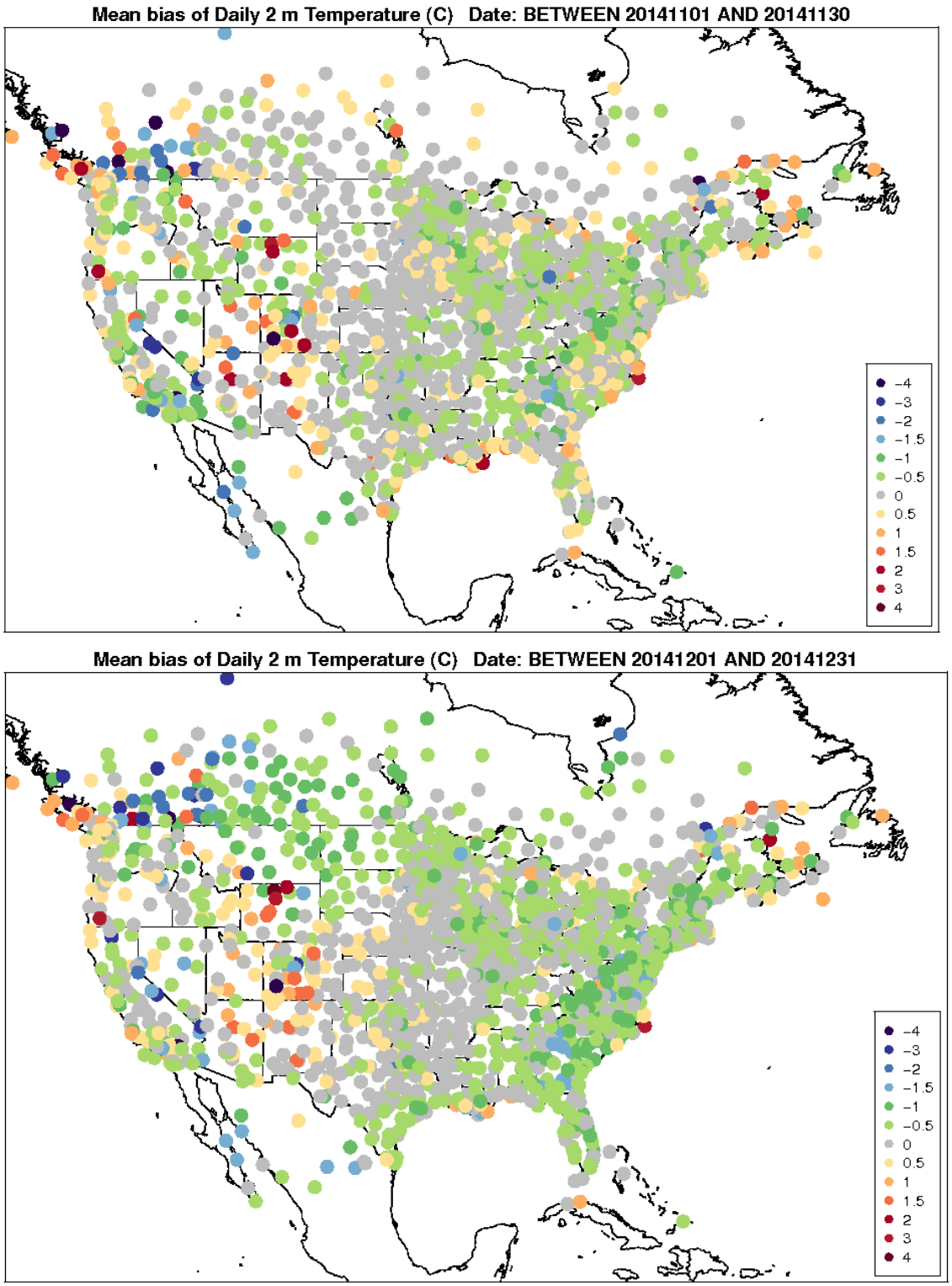

Figure 4-8. Spatial distribution of 2-m temperature bias (°C) within the 12-km CONUS domain for November (top) and December (bottom).

Model Evaluation Results for 2-m Mixing Ratio

In general, there is a positive bias for the mixing ratio for the CONUS in 2014, shown in Figure 4-9. The mixing ratio error is largest during the summer months (June, July, August) and smallest during the winter, when the moisture capacity of the atmosphere is reduced. Overall, outside of the summer months, the remainder of the year has a bias smaller than ±0.5 g/kg and an error less than 1.0 g/kg.

The diurnal statistics of the mixing ratio illustrate differences in the behavior of the mixing ratio bias between January (winter) and July (summer), seen in Figure 4-10. During the winter months, a positive bias and larger error is seen in the mixing ratio between late afternoon and evening hours. The positive bias becomes smaller and becomes slightly negative overnight into the early morning hours. However, during the summer, the bias/error is typically small and slightly negative during the afternoon into early evening. The bias then quickly becomes positive and large overnight into the early morning hours.

During winter (January and February), many locations throughout the CONUS have a mixing ratio bias smaller than ±0.5 g/kg, seen in Figure 4-11. A noticeable negative bias extends from Texas into the central U.S. during the winter months. During the spring months (March and April), Figure 4-12, large areas with a positive bias begin to be seen within the CONUS, especially along the eastern coast of the U.S. and the upper Midwest. However, negative bias can be found from the central Plains and locations west. From late spring (May) throughout the summer (June, July, August), positive bias becomes larger over the western half of the CONUS, especially in the Southwest regions of the U.S., with bias upwards of 2-3 g/kg, Figure 4-13 and Figure 4-14. The large positive bias found for large regions within the U.S. are quickly reduced by October, Figure 4-15. In November and December, the mixing ratio bias becomes slightly negative for the eastern half of the CONUS, Figure 4-16.

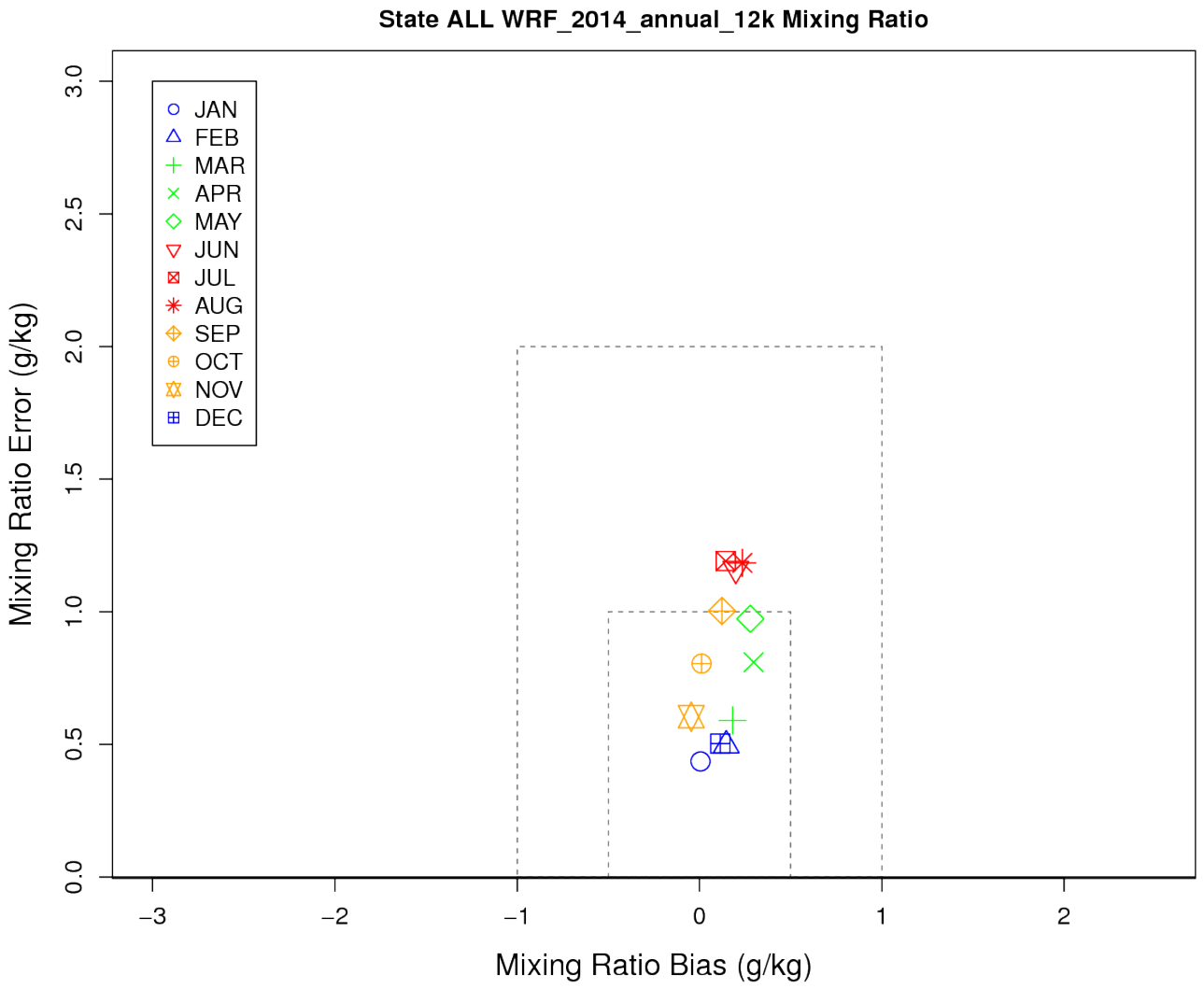

Figure 4-9. Soccer plot of monthly 2-m mixing ratio error and bias (g/kg) averaged over the 12-km CONUS domain for the 2014 calendar year.

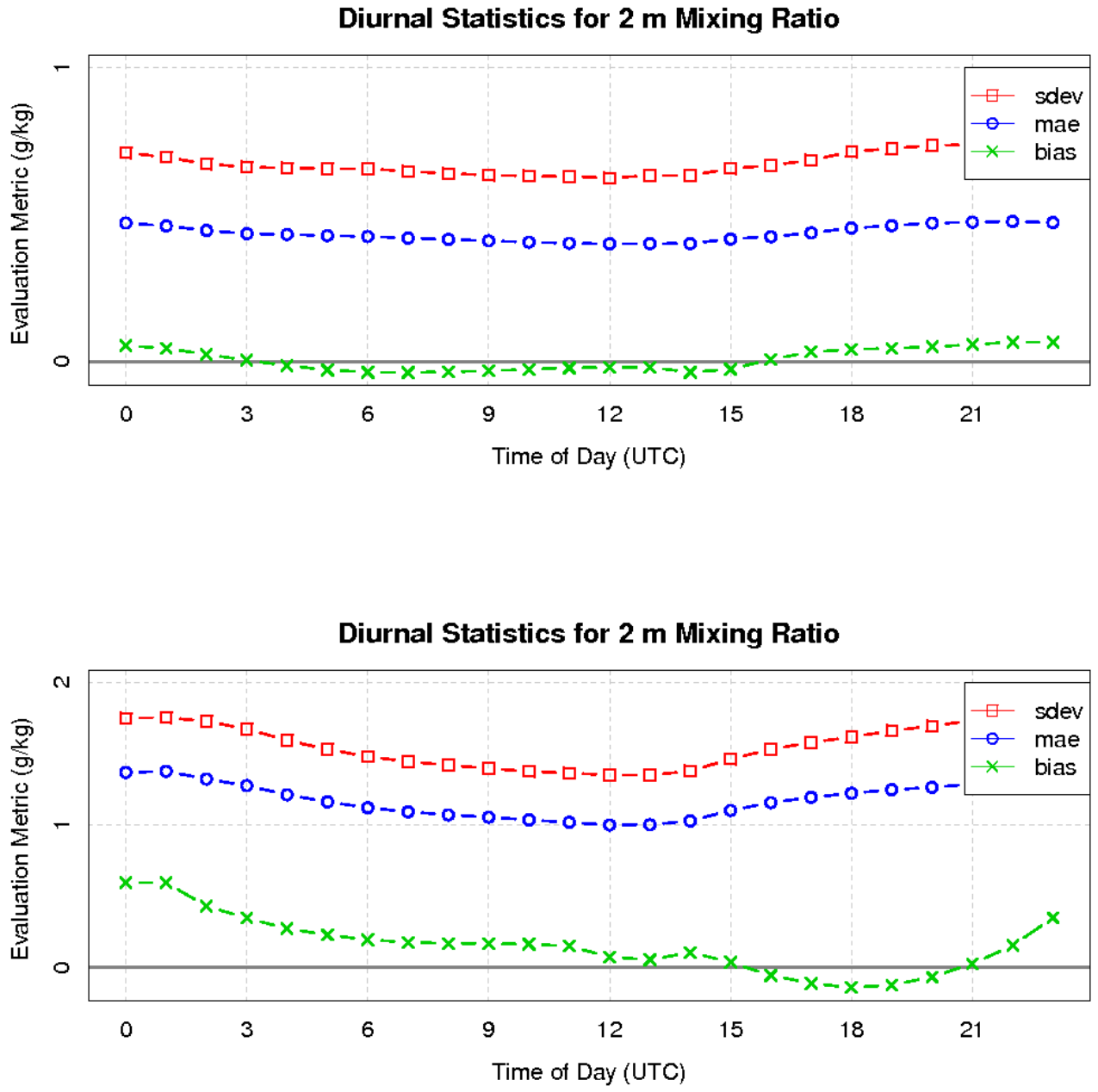

Figure 4-10. Diurnal 2-m mixing ratio error and bias (g/kg) averaged over the 12-km CONUS domain for January (top) and July (bottom) 2014.

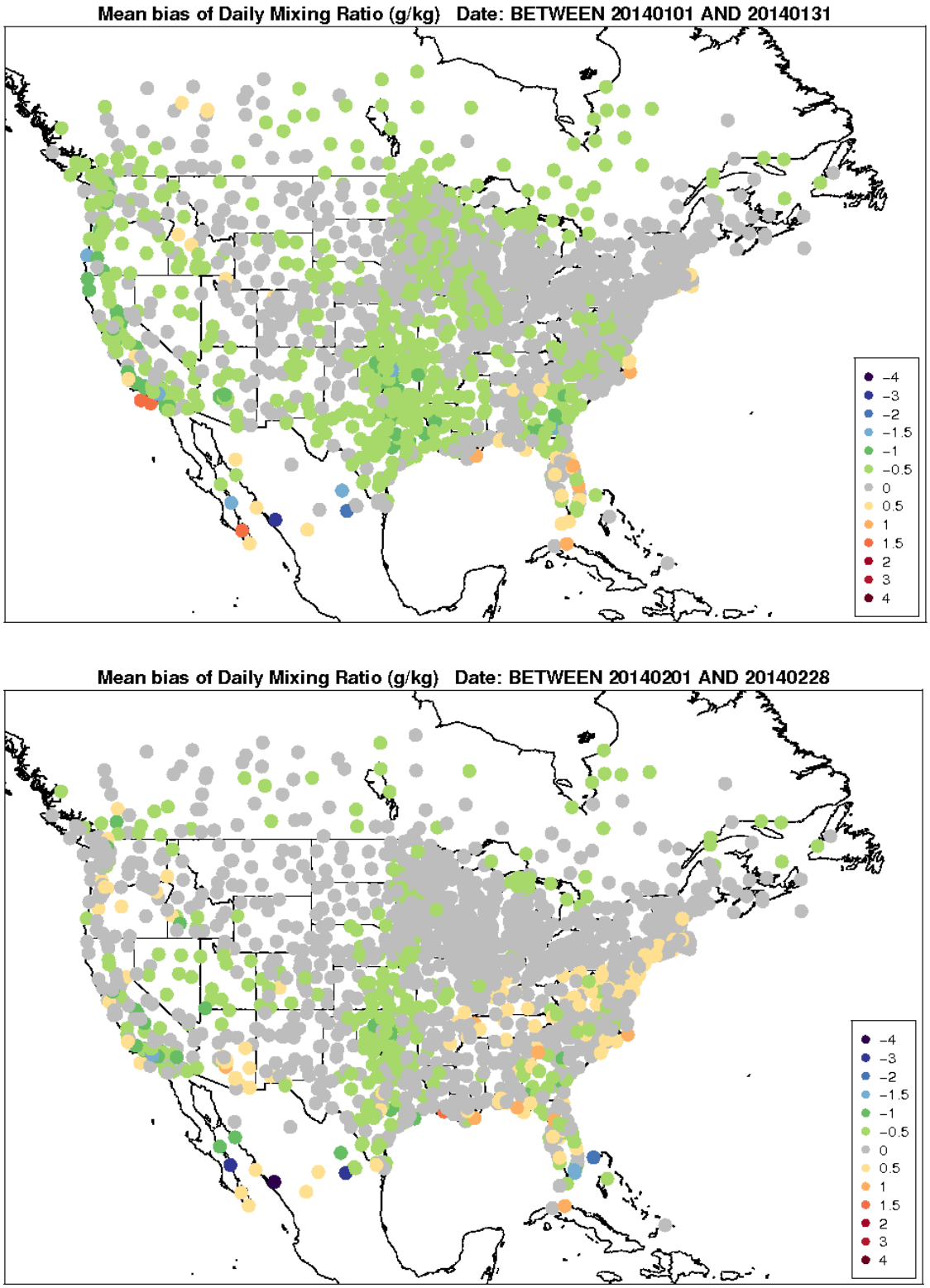

Figure 4-11. Spatial distribution of 2-m mixing ratio bias (g/kg) within the 12-km CONUS domain for January (top) and February (bottom).

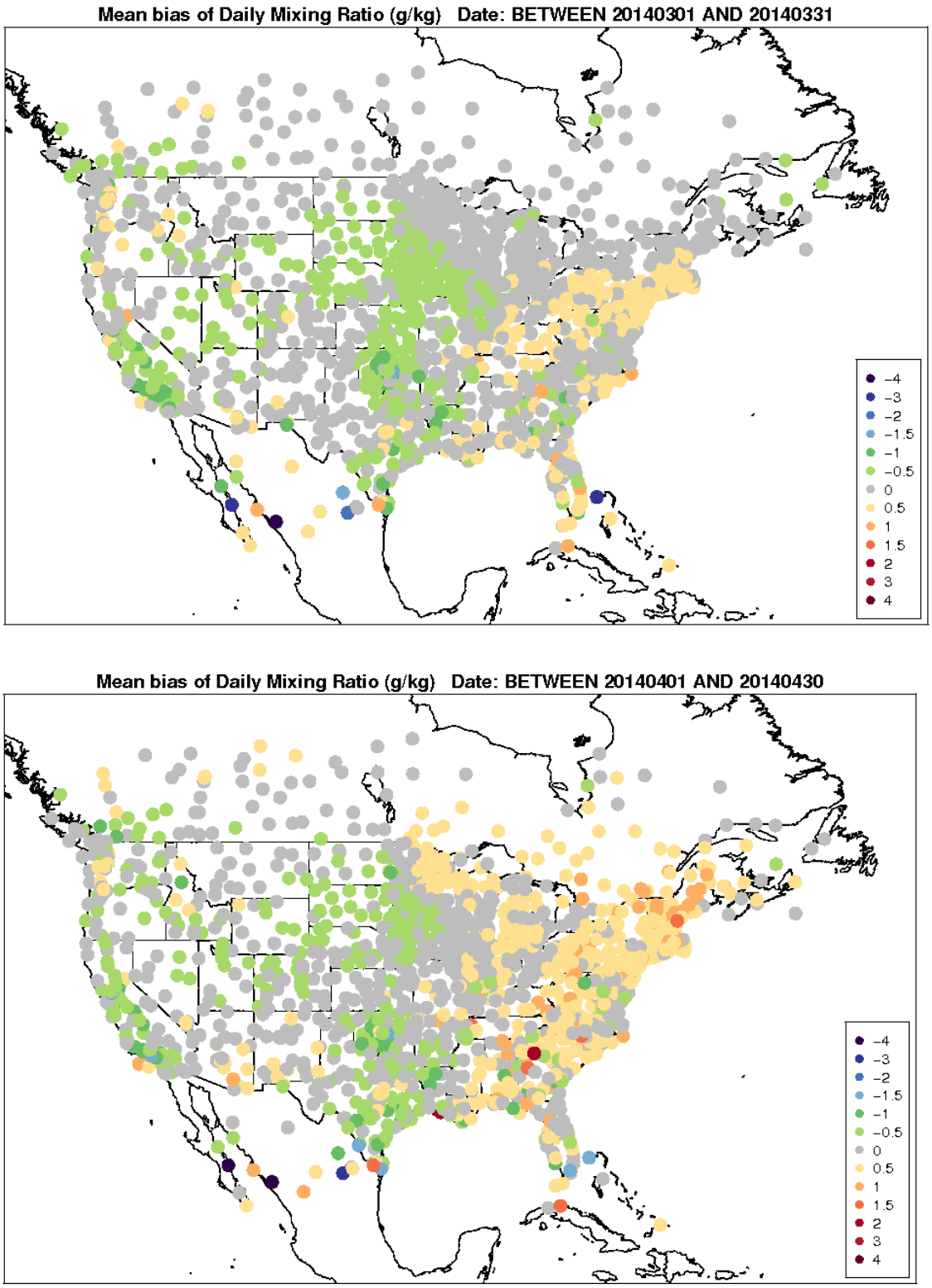

Figure 4-12. Spatial distribution of 2-m mixing ratio bias (g/kg) within the 12-km CONUS domain for March (top) and April (bottom).

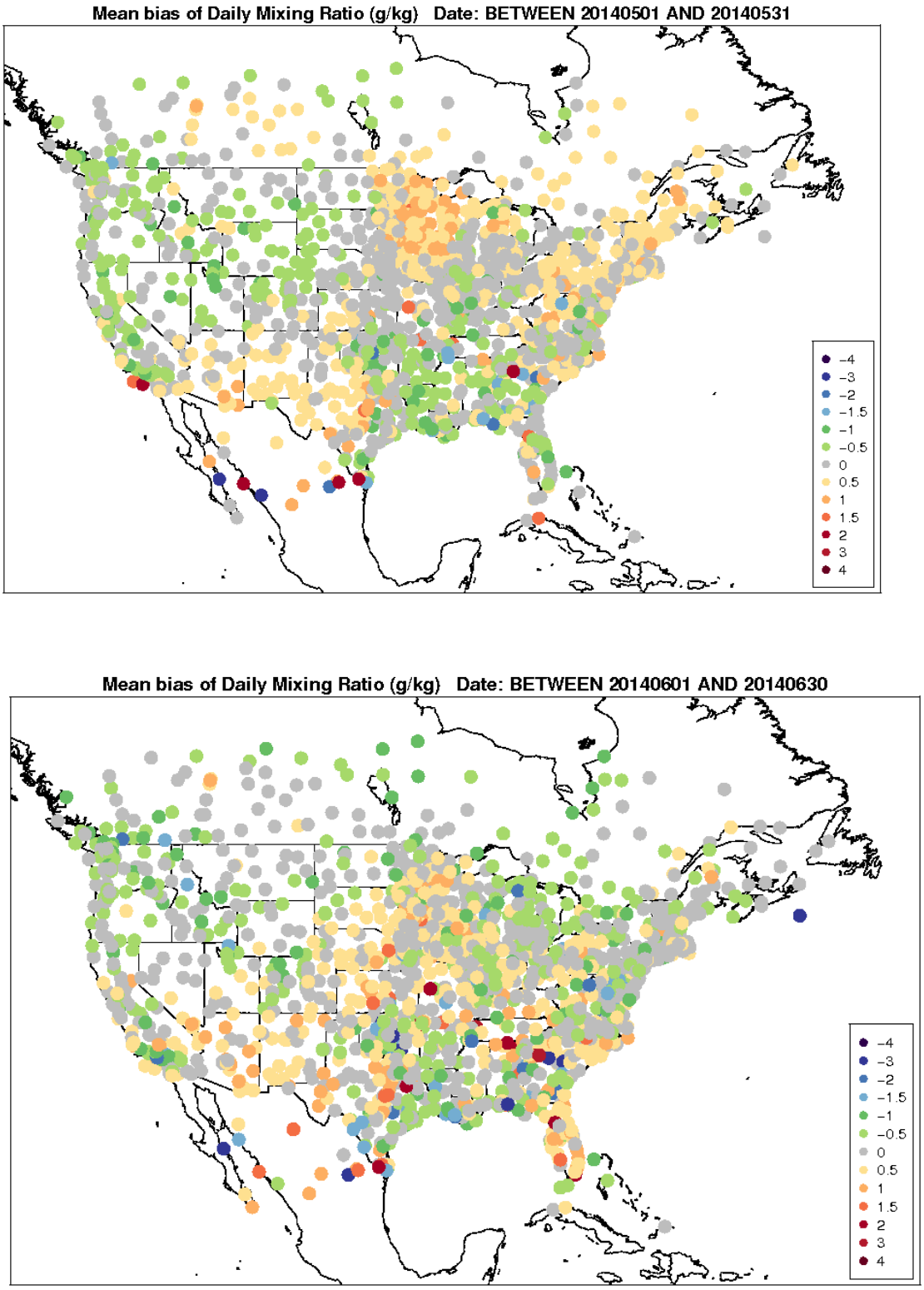

Figure 4-13. Spatial distribution of 2-m mixing ratio bias (g/kg) within the 12-km CONUS domain for May (top) and June (bottom).

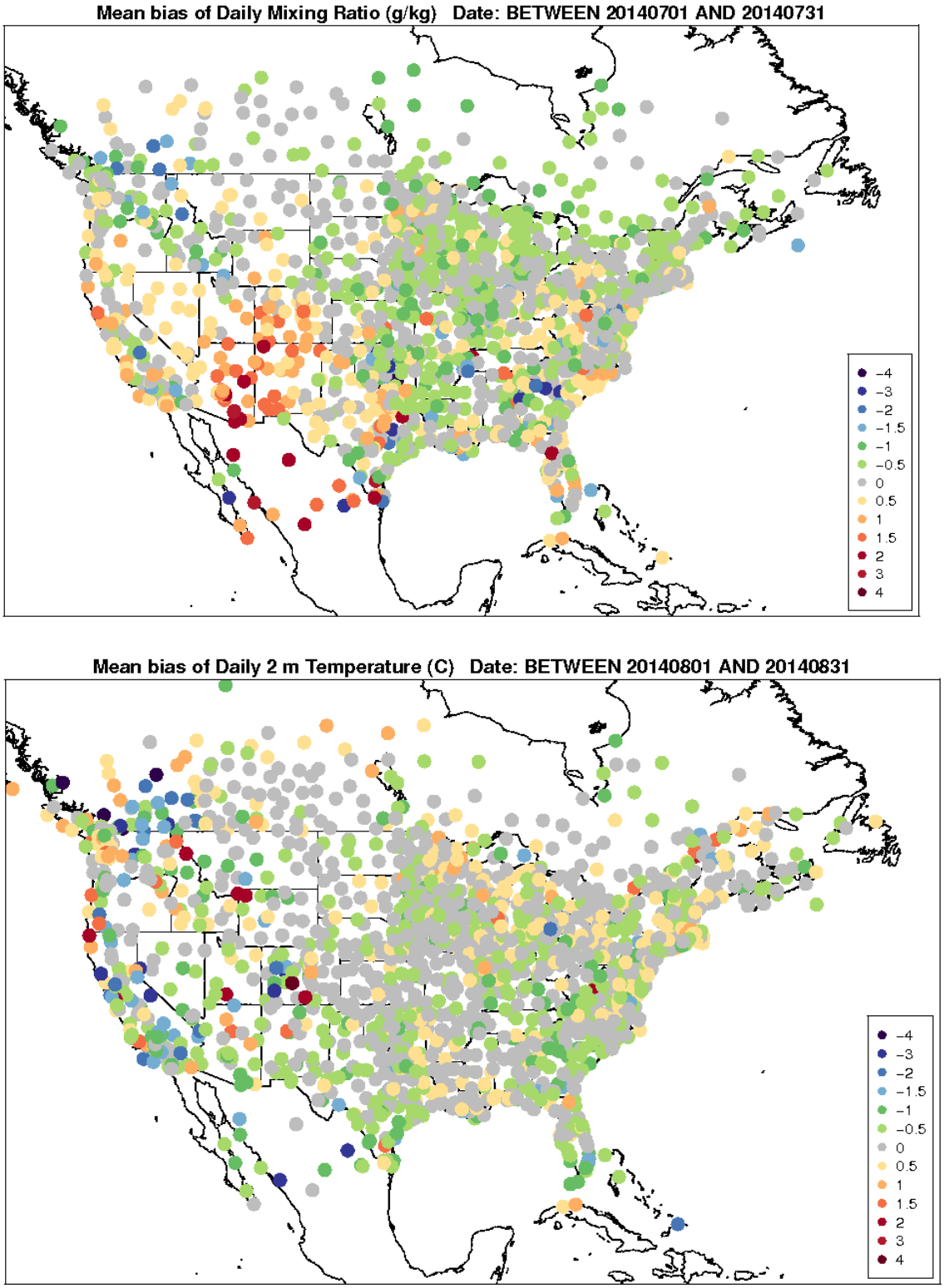

Figure 4-14. Spatial distribution of 2-m mixing ratio bias (g/kg) within the 12-km CONUS domain for July (top) and August (bottom).

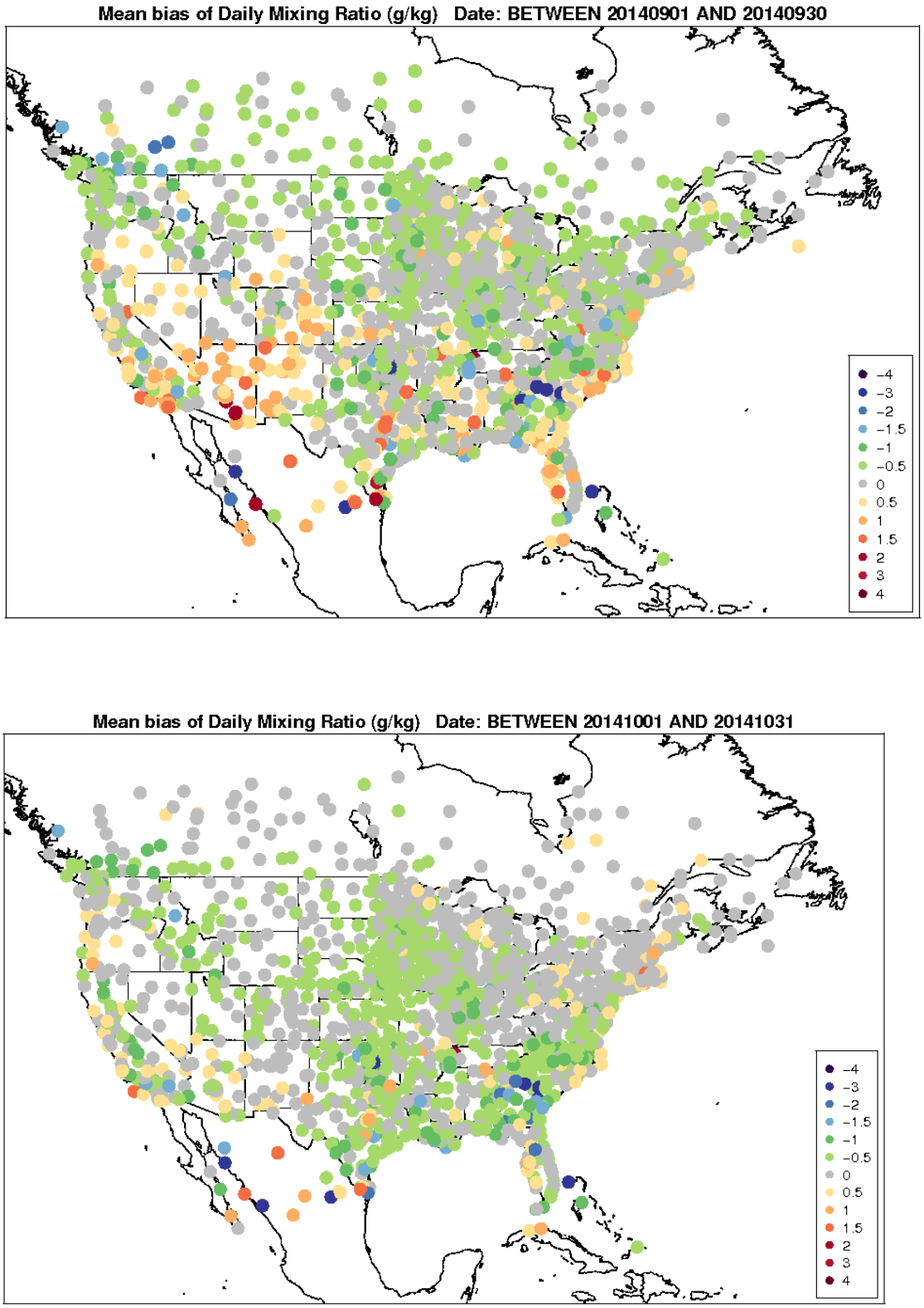

Figure 4-15. Spatial distribution of 2-m mixing ratio bias (g/kg) within the 12-km CONUS domain for September (top) and October (bottom).

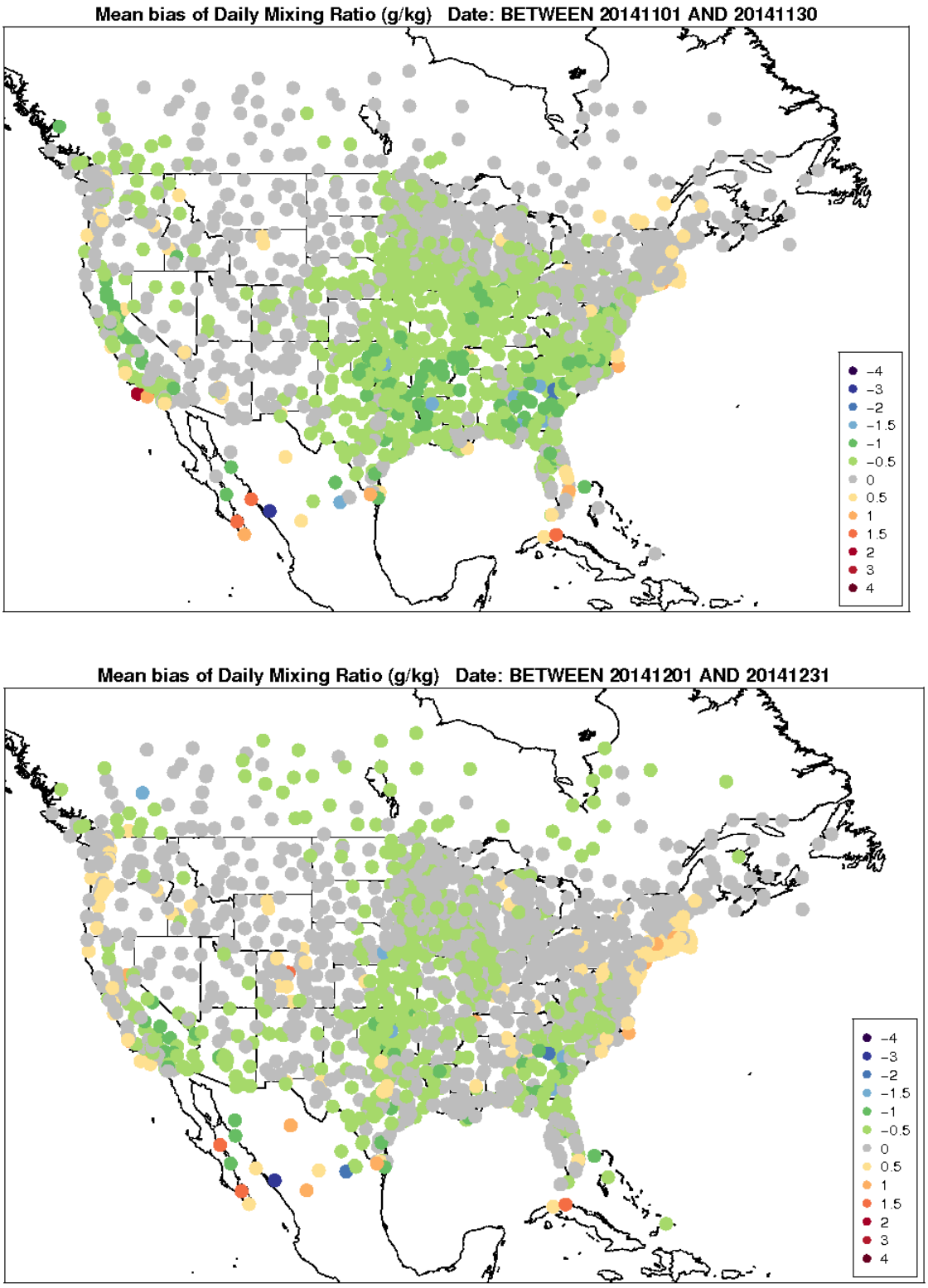

Figure 4-16. Spatial distribution of 2-m mixing ratio bias (g/kg) within the 12-km CONUS domain for November (top) and December (bottom).

Model Evaluation Results for 10-m Wind Speed

All months on average for the CONUS have a wind speed bias smaller than ±0.5 m/s and wind speed error less than 2 m/s, shown in Figure 4-17. Unlike 2-m temperature and mixing ratio, the differences in the bias between winter and summer months are similar with slightly better performance for wind speed during the summer.

The diurnal statistics illustrate the 10-m wind bias is typically larger and negative during the afternoon and evening hours for both January (winter) and July (summer); see Figure 4-18. However, the bias is smaller than 0.5 m/s. The bias is closer to zero during the night and early morning. There is also a persistent diurnal error, around 1.3 m/s, for winter and summer months.

The spatial pattern illustrates the complexity in the wind speed bias throughout the CONUS. During the winter months (January and February), Figure 4-19, the wind speed bias is generally positive for many locations from the Carolinas into the Northeast U.S. However, from the Great Plains and westward, many locations experience a negative bias. This pattern continues into the spring months (March, April), Figure 4-20. By summer (June, July, August), Figure 4-21 and Figure 4-22, some of the largest positive wind speed bias locations are around the Great Lakes region. In addition, positive wind speed bias exists for many stations within the Northeast U.S. Some of the largest negative wind speed biases during the summer months occur for locations in the western half of the CONUS, from the Rocky Mountains, west.

We find the largest bias occurs during the fall season (October, November), Figure 4-23 and Figure 4-24. Some of the locations with the largest positive bias are found around the Great Lakes and Northeast, especially in coastal locations. The largest negative bias locations tend to occur over the western half of the CONUS, especially in the Rocky Mountains. The poor wind speed performances in these locations are likely related to complex processes not resolved by the 12-km horizontal resolution.

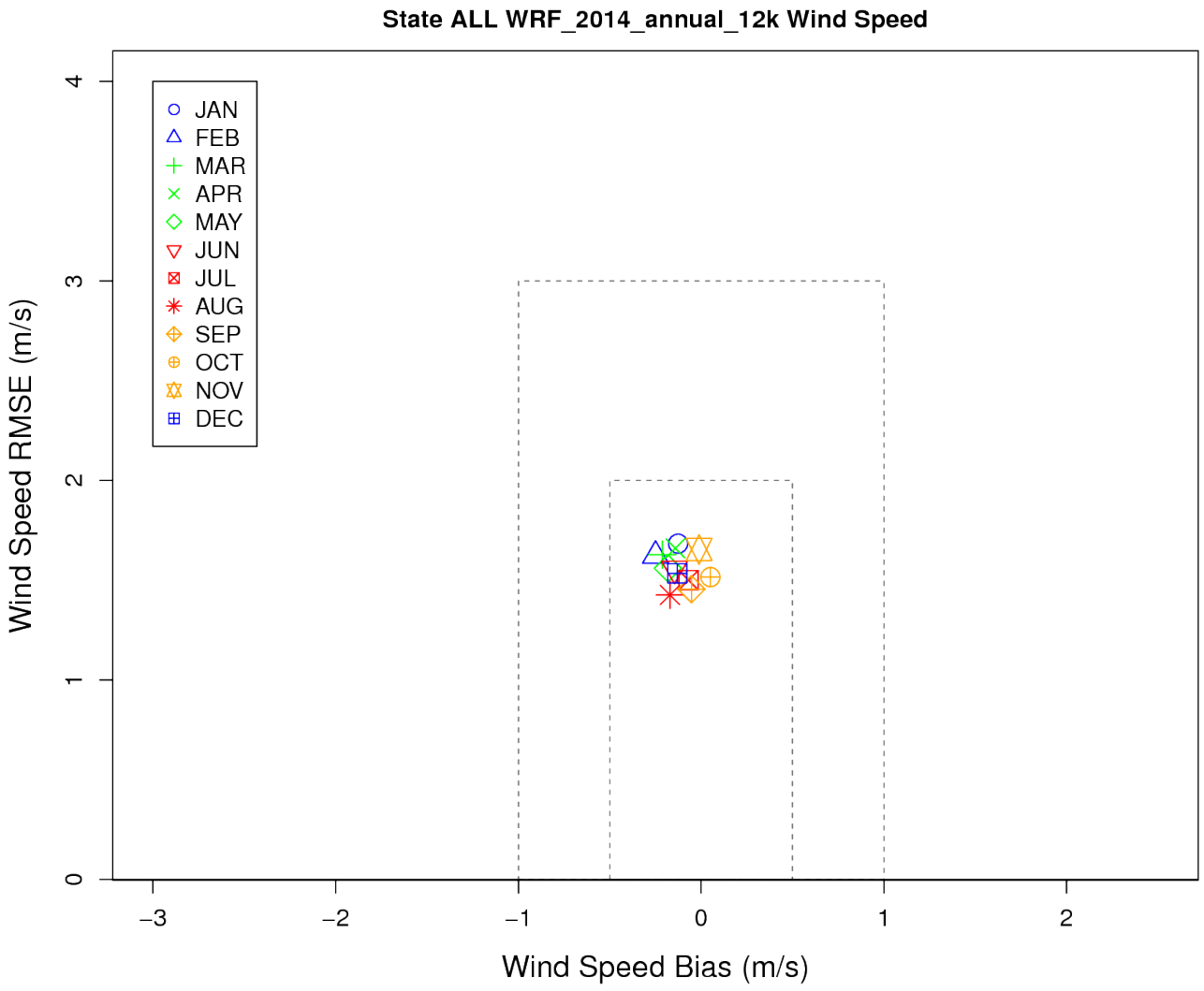

Figure 4-17. Soccer plot of monthly 10-m wind speed error and bias (m/s) averaged over the 12-km CONUS domain for the 2014 calendar year.

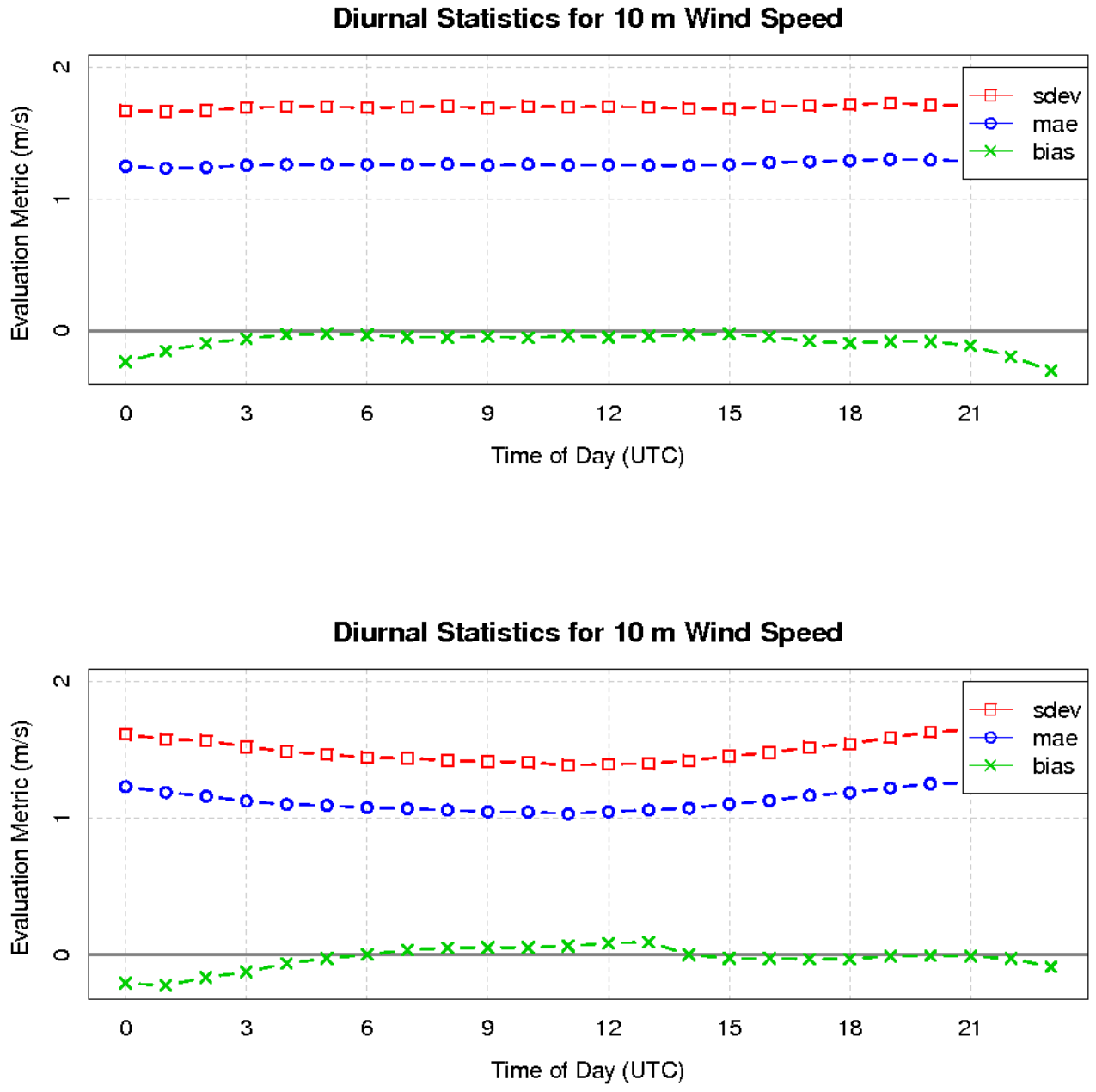

Figure 4-18. Diurnal 10-m wind speed error and bias (m/s) averaged over the 12-km CONUS domain for January (top) and July (bottom) 2014.

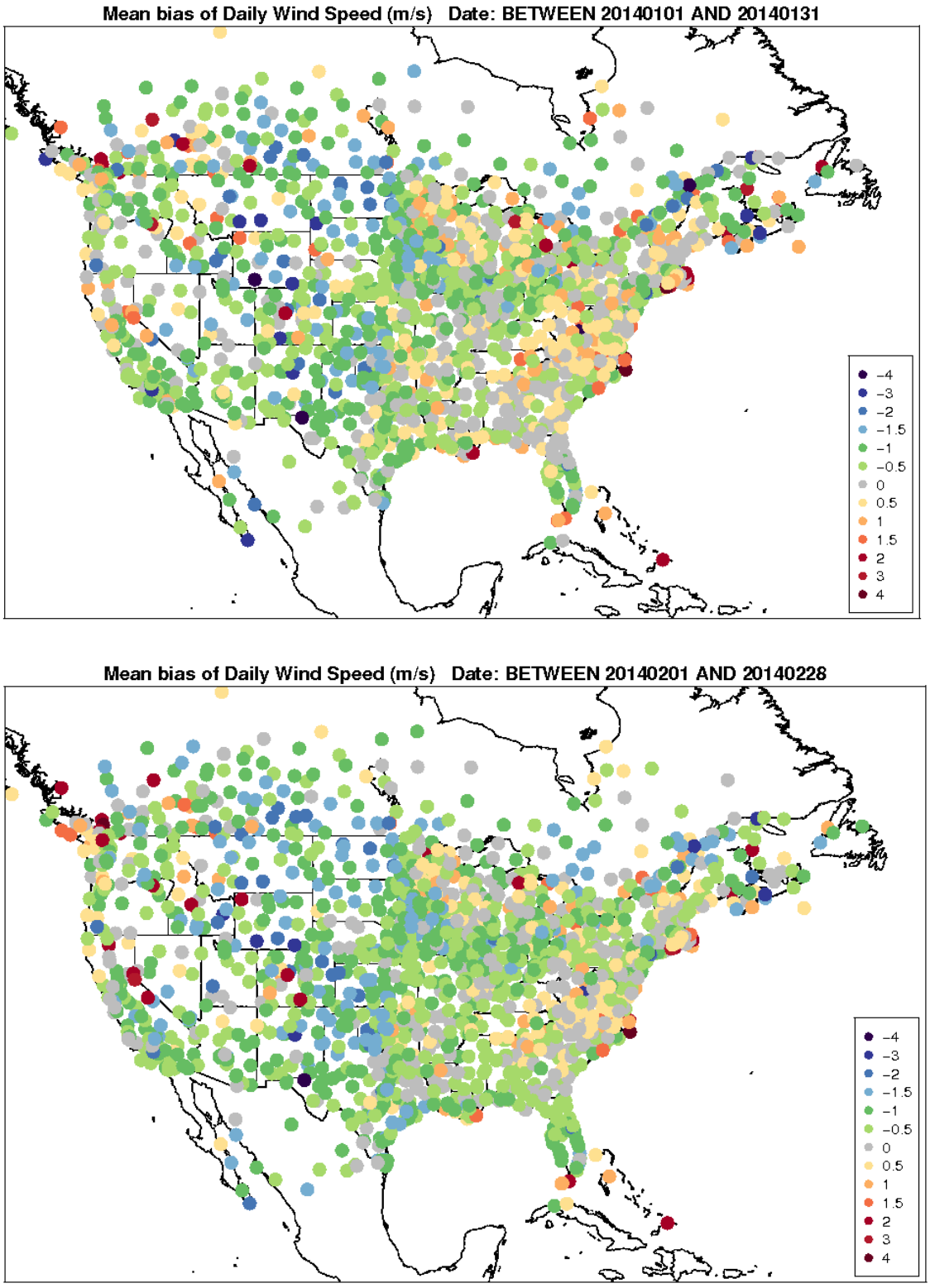

Figure 4-19. Spatial distribution of 10-m wind speed bias (m/s) within the 12-km CONUS domain for January (top) and February (bottom).

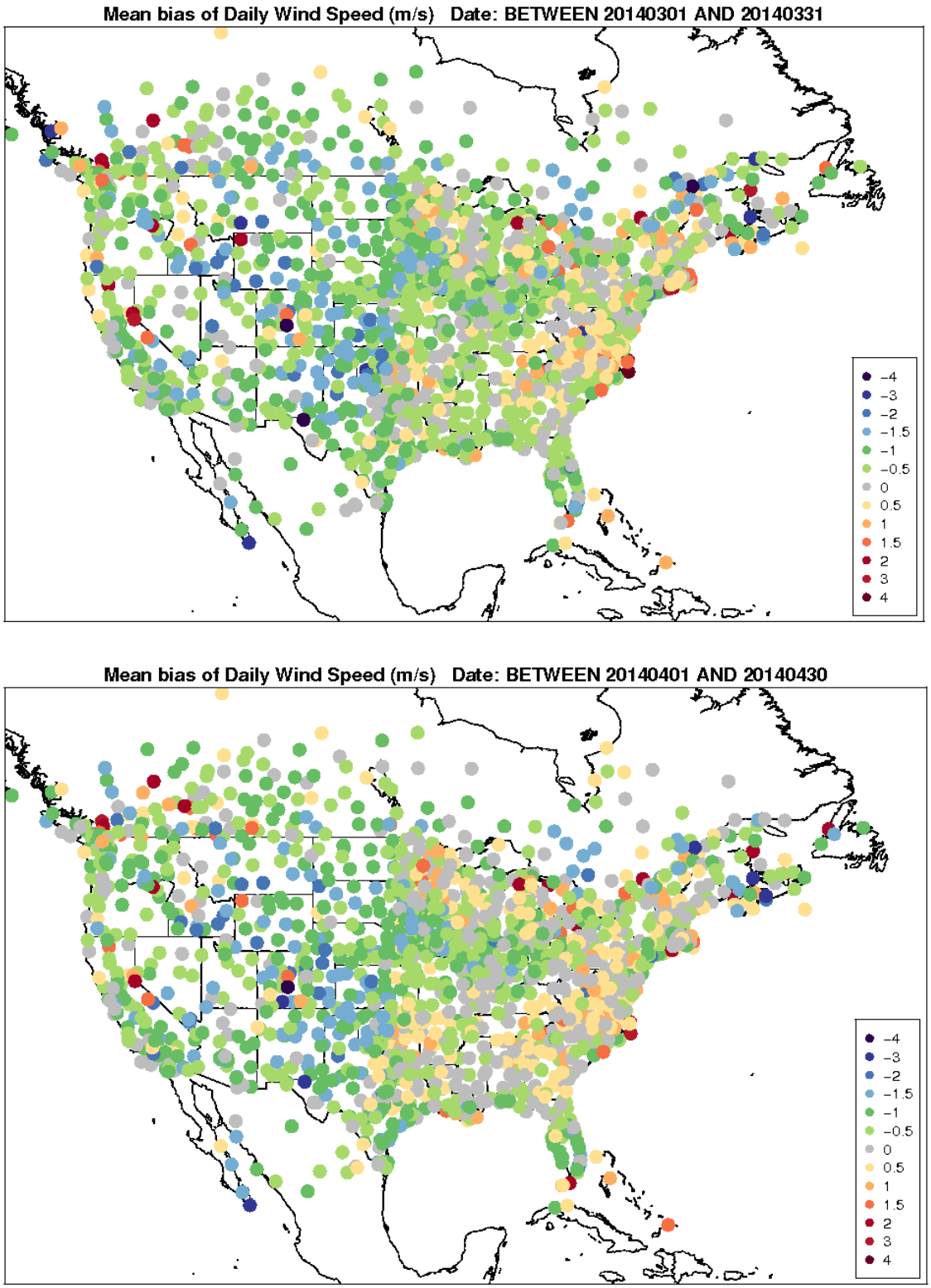

Figure 4-20. Spatial distribution of 10-m wind speed bias (m/s) within the 12-km CONUS domain for March (top) and April (bottom).

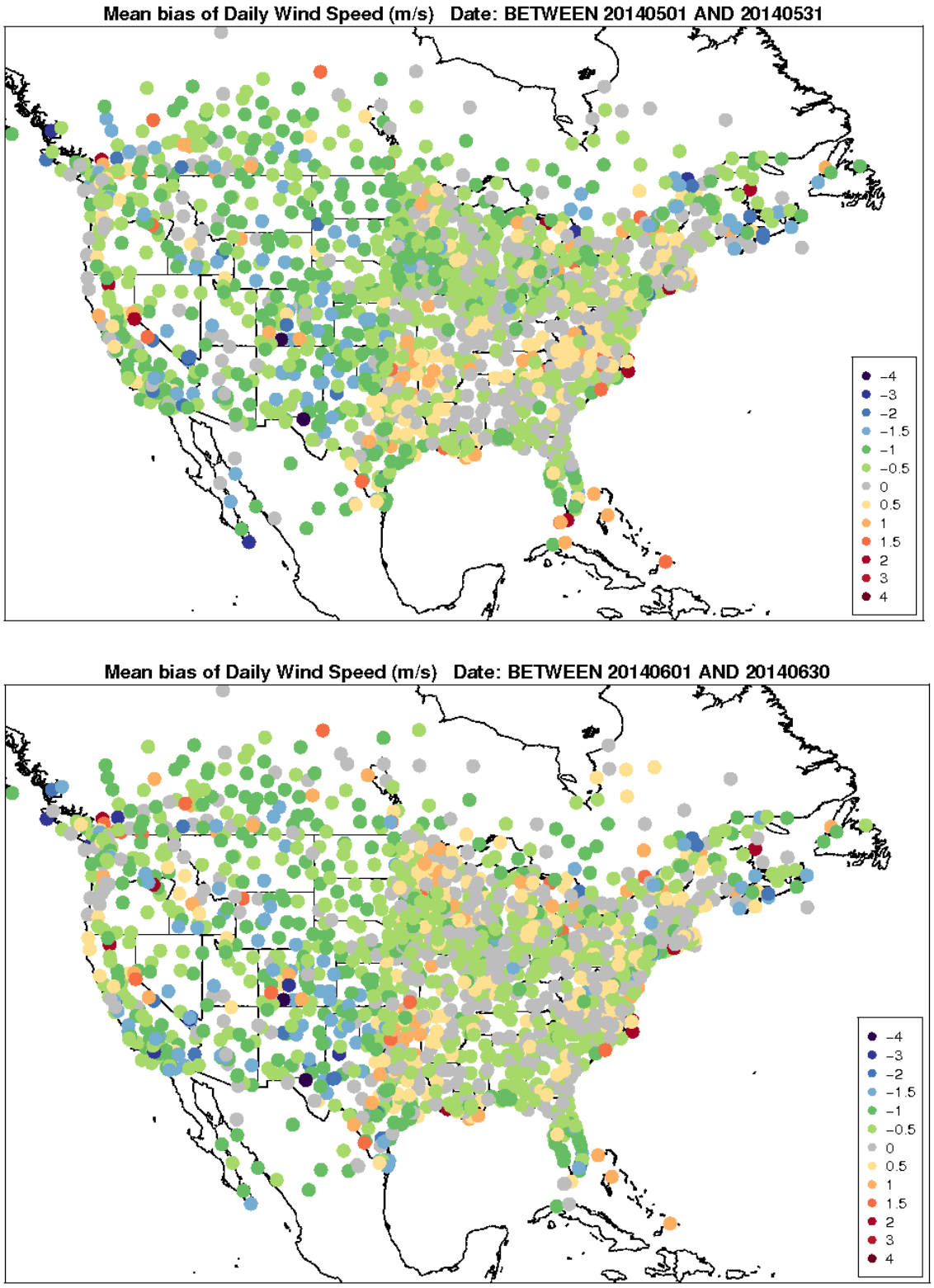

Figure 4-21. Spatial distribution of 10-m wind speed bias (m/s) within the 12-km CONUS domain for May (top) and June (bottom).

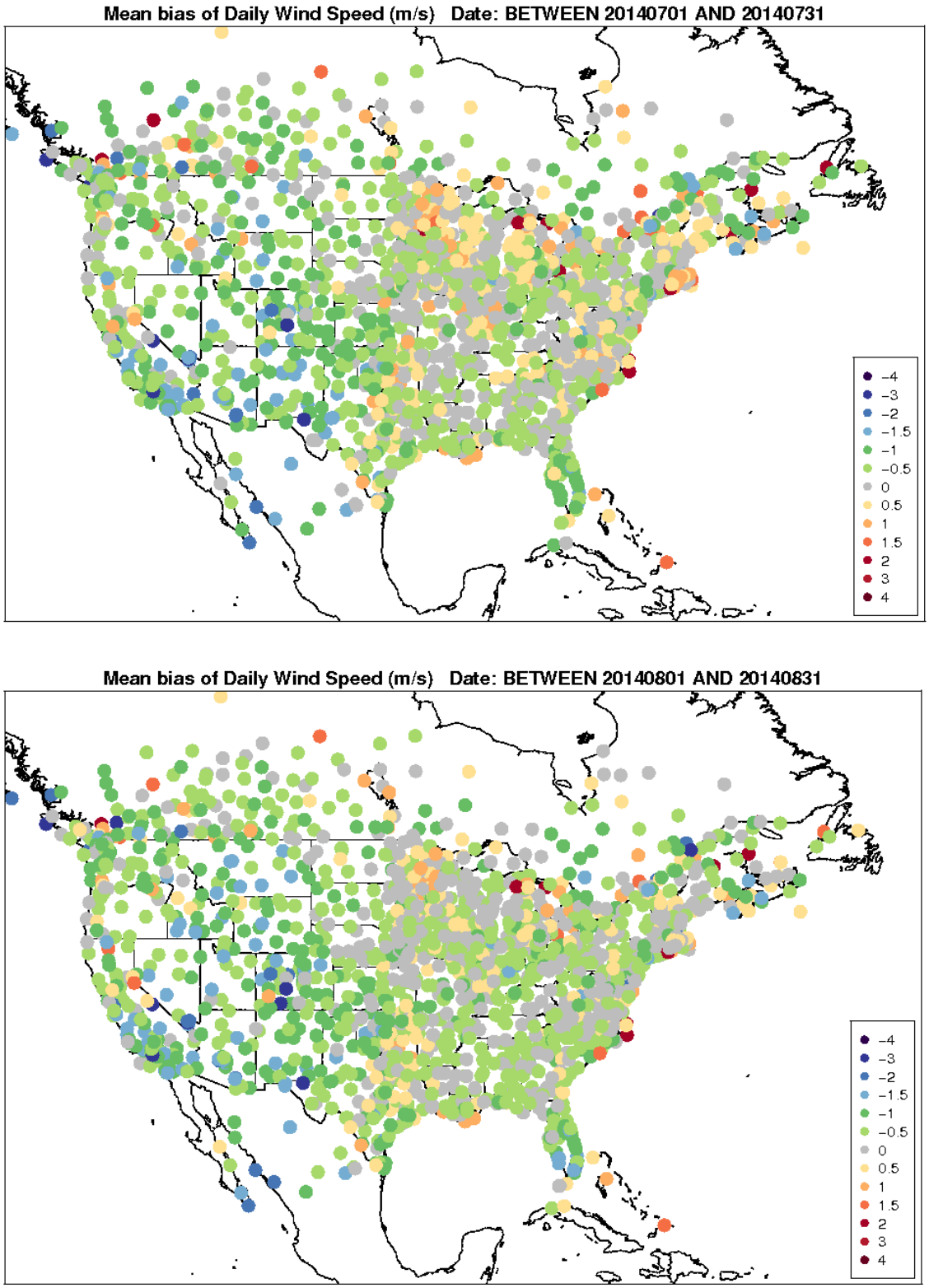

Figure 4-22. Spatial distribution of 10-m wind speed bias (m/s) within the 12-km CONUS domain for July (top) and August (bottom).

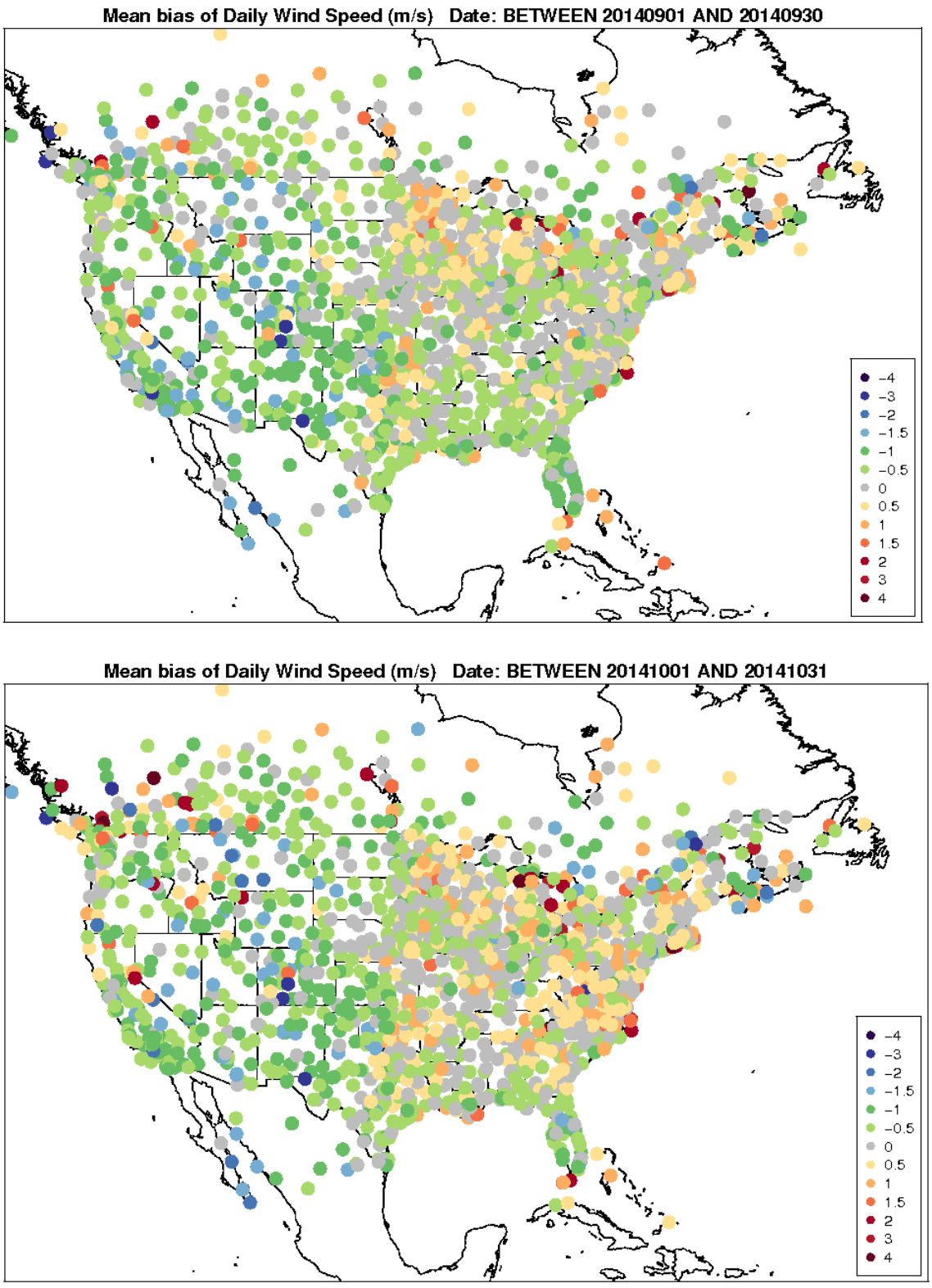

Figure 4-23. Spatial distribution of 10-m wind speed bias (m/s) within the 12-km CONUS domain for September (top) and October (bottom).

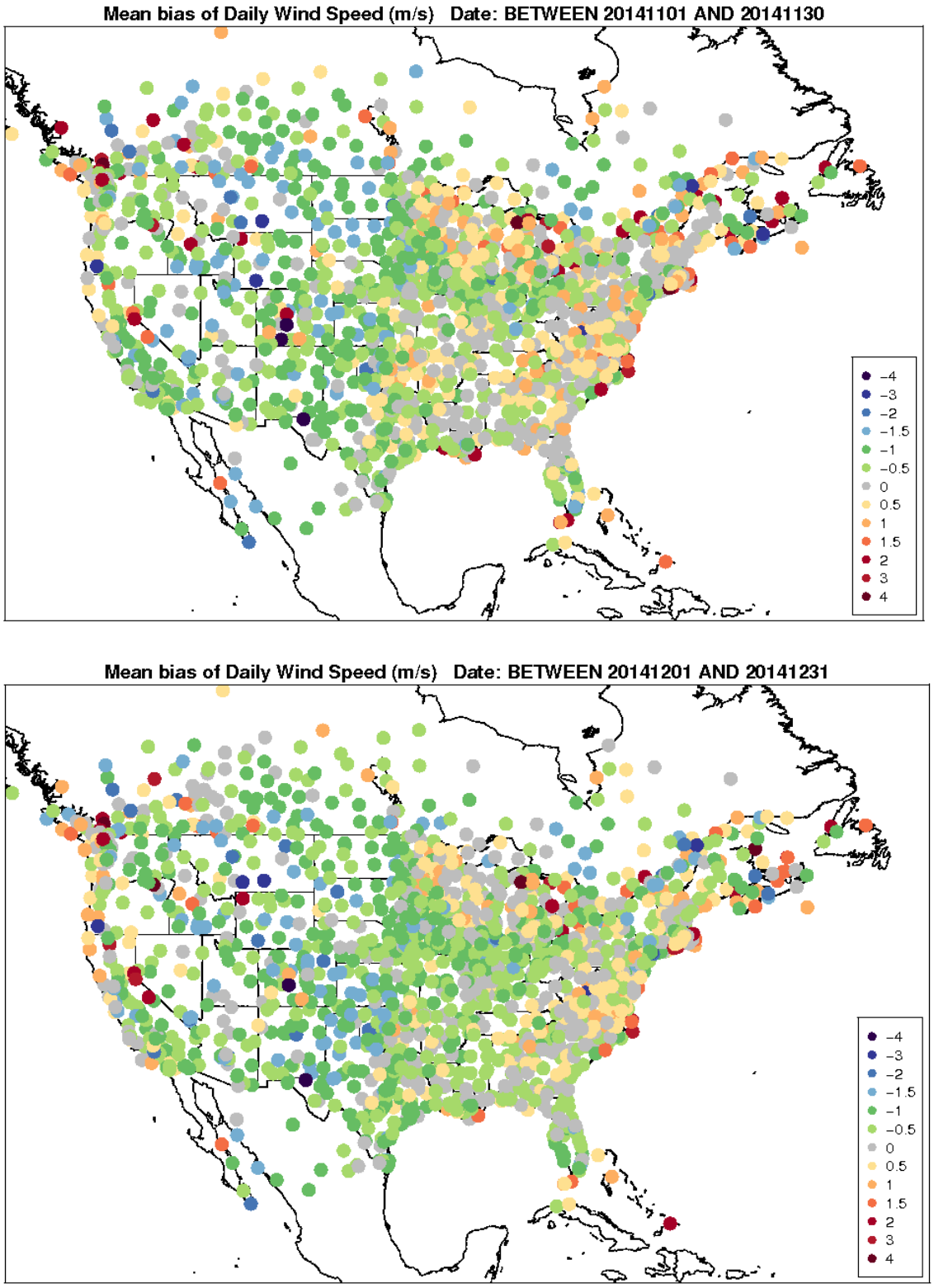

Figure 4-24. Spatial distribution of 10-m wind speed bias (m/s) within the 12-km CONUS domain for November (top) and December (bottom).

Model Evaluation Results for 10-m Wind Direction

The 10-m wind direction error for the CONUS is less than 60 degrees for all months, shown in Figure 4-25. The largest wind direction bias and errors occur during the summer (June, July, August). The best performing months are during the late fall and early winter (October, November, December).

Figure 4-26 illustrates the diurnal statistics for January (winter) and July (summer) and confirms that the average error increases during the summer, by approximately 5 to 10 degrees. Diurnally, the bias is fairly consistent throughout the day during January; however, in July the bias and errors increase overnight and during the early morning hours.

In prior analyses, we illustrated the spatial bias for station locations within the CONUS. For wind direction, we focus on the mean absolute error rather than bias. We focus on the mean absolute error of wind direction because wind direction is a vector field. (Please refer to Section 5 for additional plots including the spatial bias plots of wind direction.) During the winter months (January, February), the mean absolute error is largest for the western states within the CONUS, Figure 4-27. The large errors over the western states within the CONUS are likely a result of the model's inability to resolve the complex topography and can be found in all months. During the winter months, the mean absolute errors are also larger within the Southeast U.S., with best performance for locations within the Midwest U.S. In the spring months (March, April), the errors typically increase across the eastern half of the CONUS, especially for locations along the Appalachian Mountains, Figure 4-28. Additionally, the errors increase by 10 to 20 degrees for locations within the Midwest U.S. During the summer (June, July, August), the wind direction errors increase within the Southeast U.S. by more than 30 degrees, compared to winter and spring, Figure 4-29 and Figure 4-30. The best performing locations are centered along the climatologically favored region for a strong low-level jet during the summer (from Texas into the Midwest). During the fall (October, November), the wind direction errors are typically smaller than the summer months, by as much as 30 degrees, for locations within the Midwest U.S., Figure 4-31 and Figure 4-32.

Wind vector displacement (km) on average for the CONUS domain is shown in Figure 4-33. The top panel illustrates the hourly wind displacement and the bottom panel the monthly wind displacement. The mean wind displacement for both hourly and monthly is approximately 5-km. The hourly data illustrates that the mean wind vector displacement increases during the afternoon and early evening hours. However, the monthly wind vector displacement is distributed across the year. Overall, the mean wind vector displacement is around 5-km and smaller than the model horizontal resolution of 12-km; thus, negligible impacts due to wind displacement are expected.

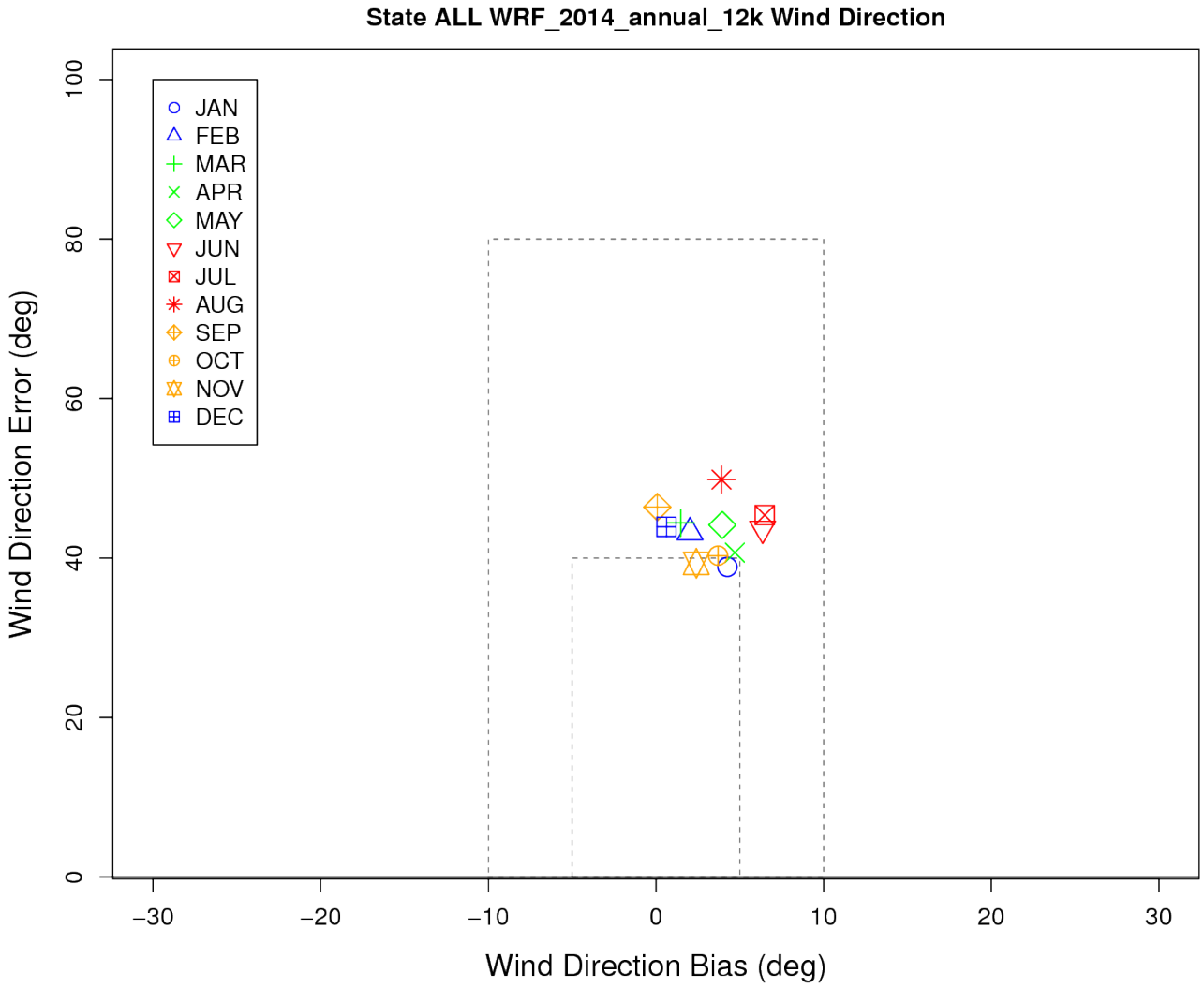

Figure 4-25. Soccer plot of monthly 10-m wind direction error and bias averaged over the 12-km CONUS domain for the 2014 calendar year.

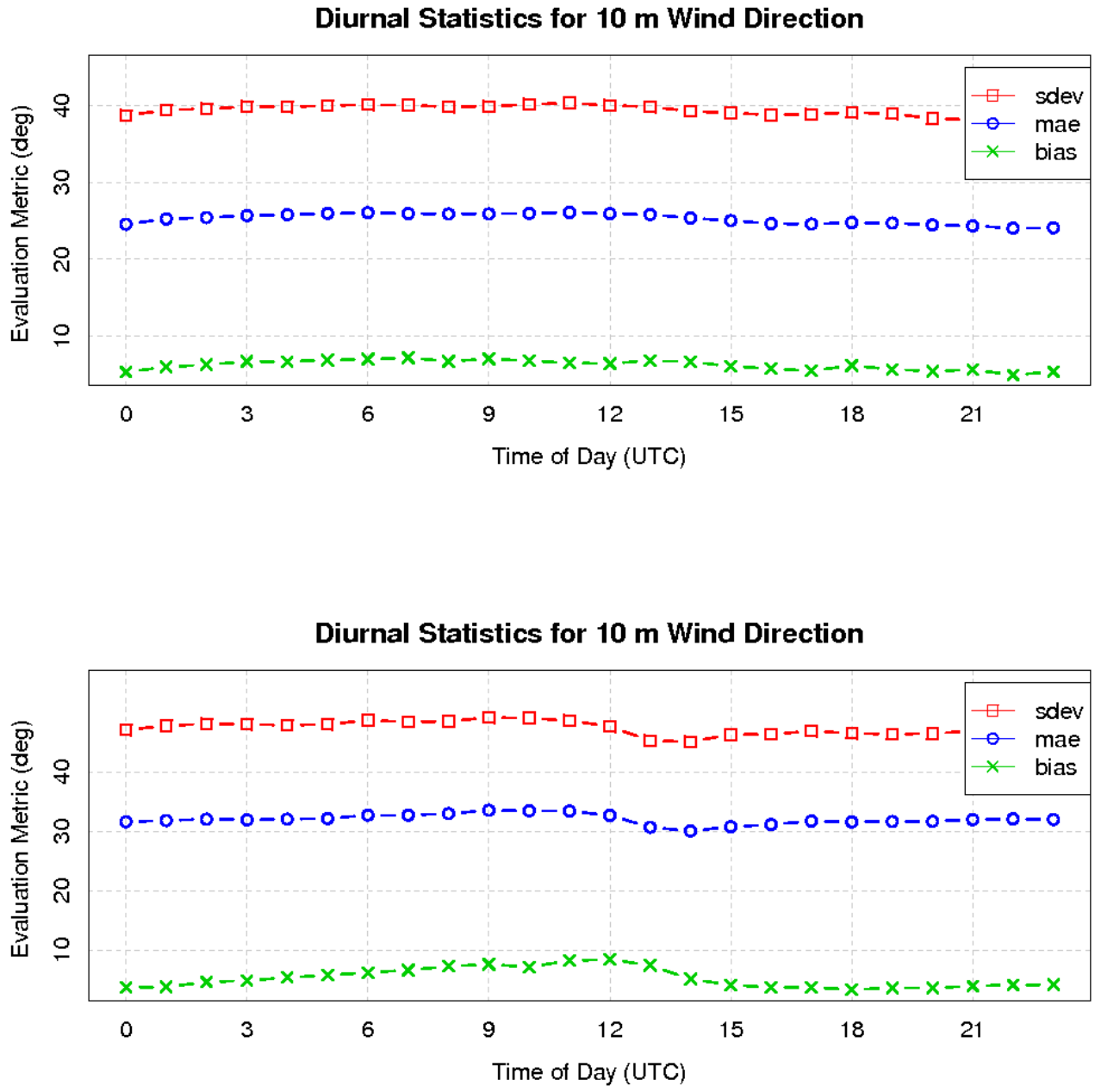

Figure 4-26. Diurnal 10-m wind direction error and bias (m/s) averaged over the 12-km CONUS domain for January (top) and July (bottom) 2014.

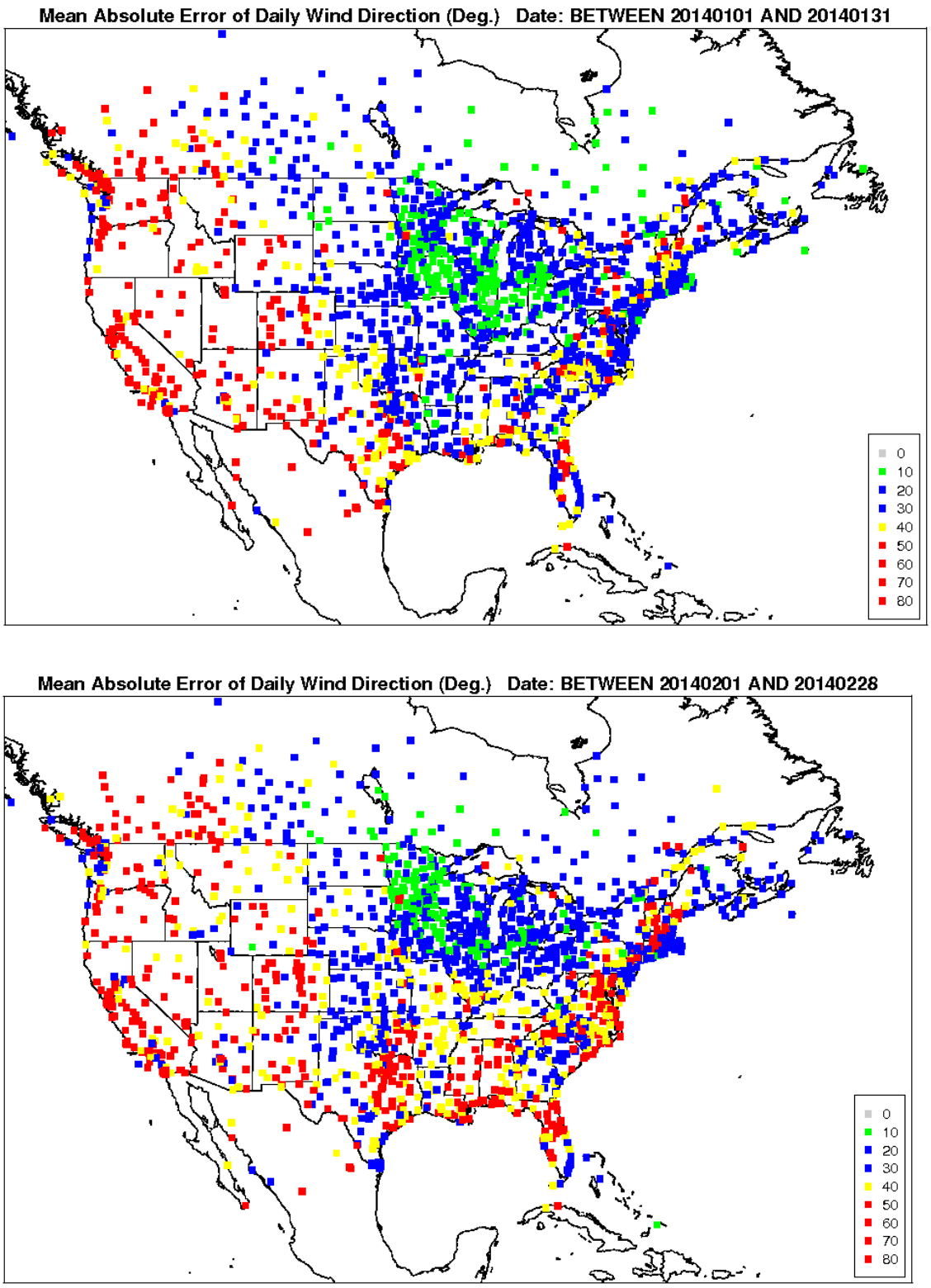

Figure 4-27. Spatial distribution of 10-m wind direction mean absolute error within the 12-km CONUS domain for January (top) and February (bottom).

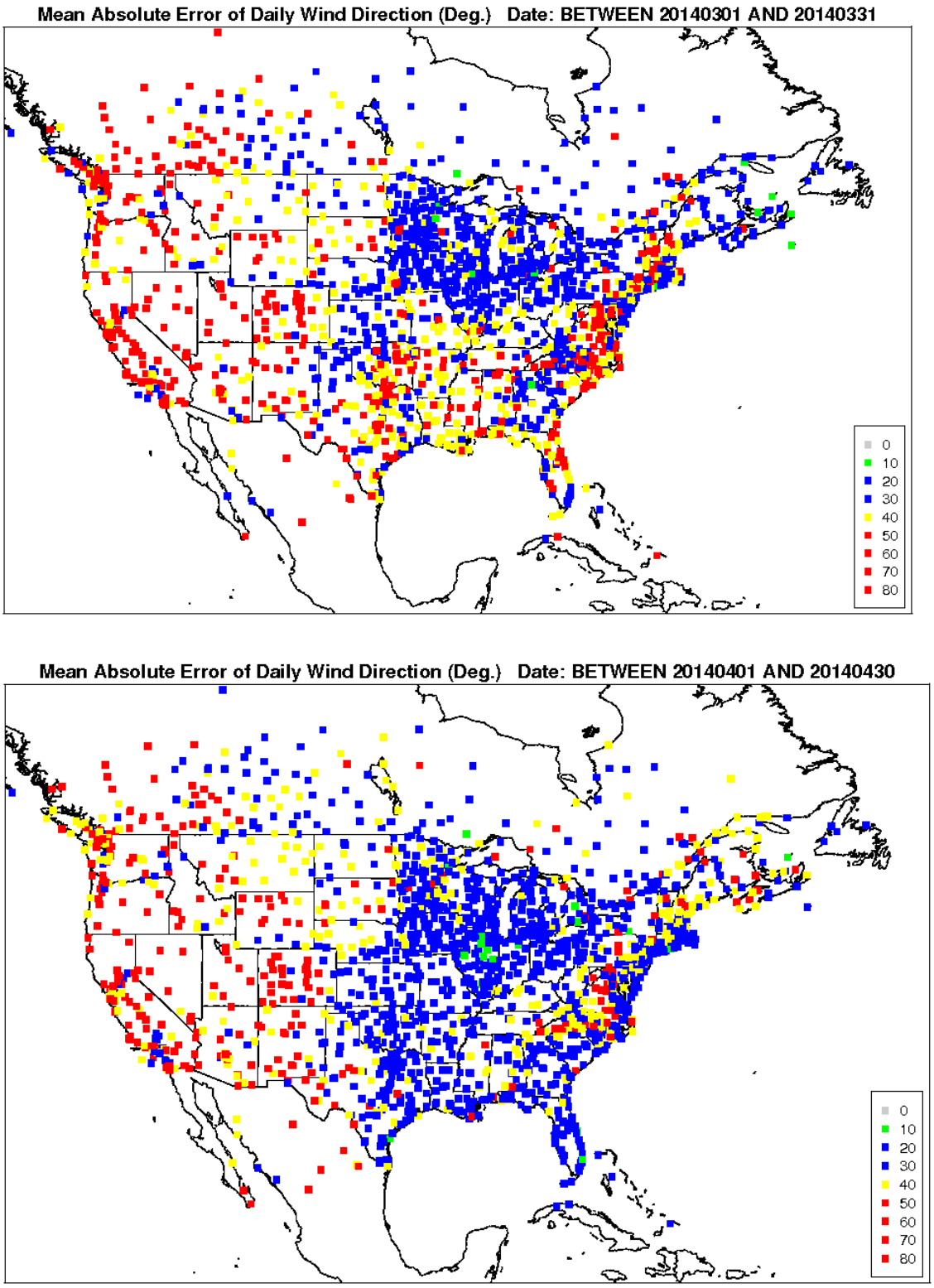

Figure 4-28. Spatial distribution of 10-m wind direction mean absolute error within the 12-km CONUS domain for March (top) and April (bottom).

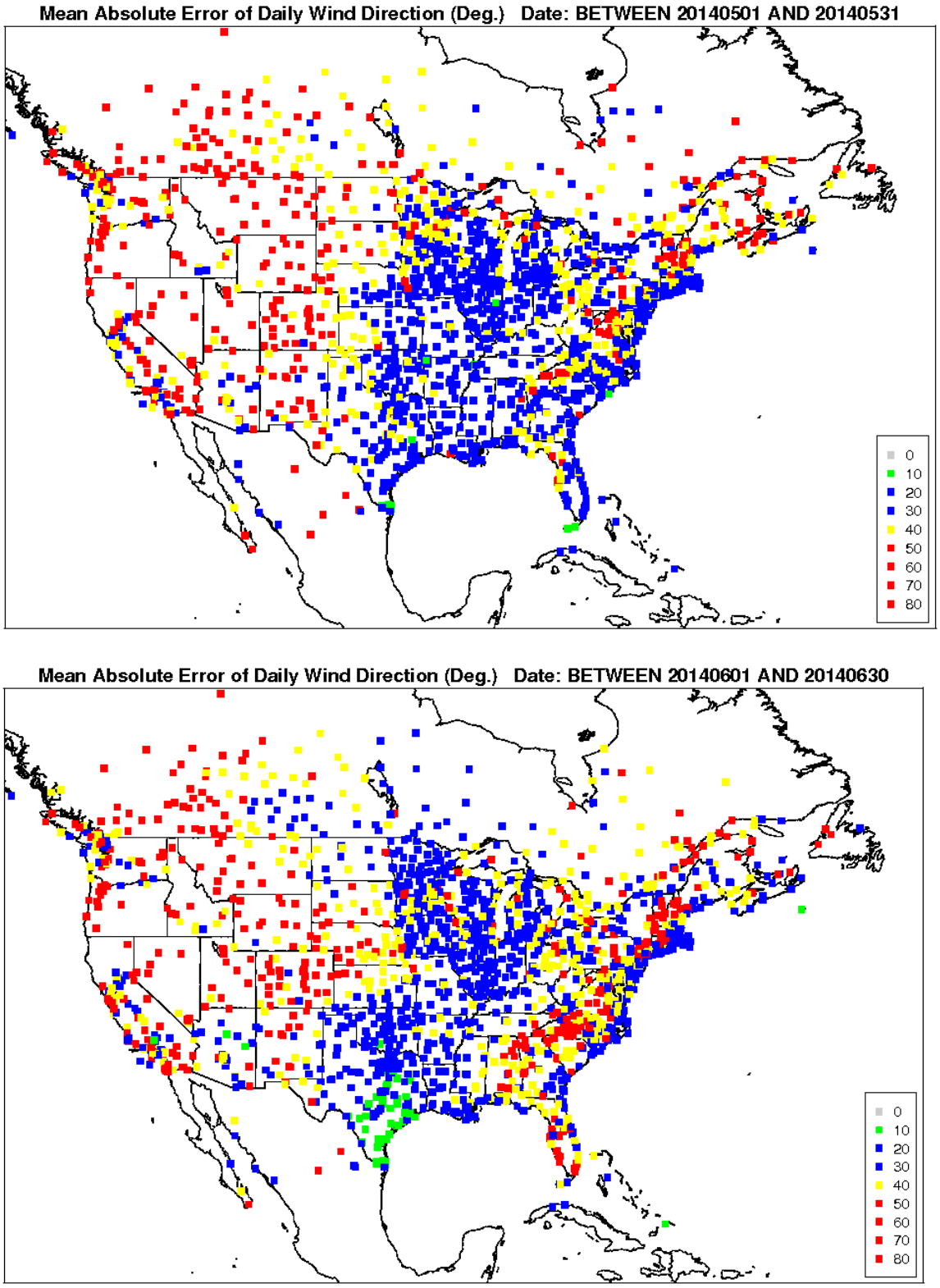

Figure 4-29. Spatial distribution of 10-m wind direction mean absolute error within the 12-km CONUS domain for May (top) and June (bottom).

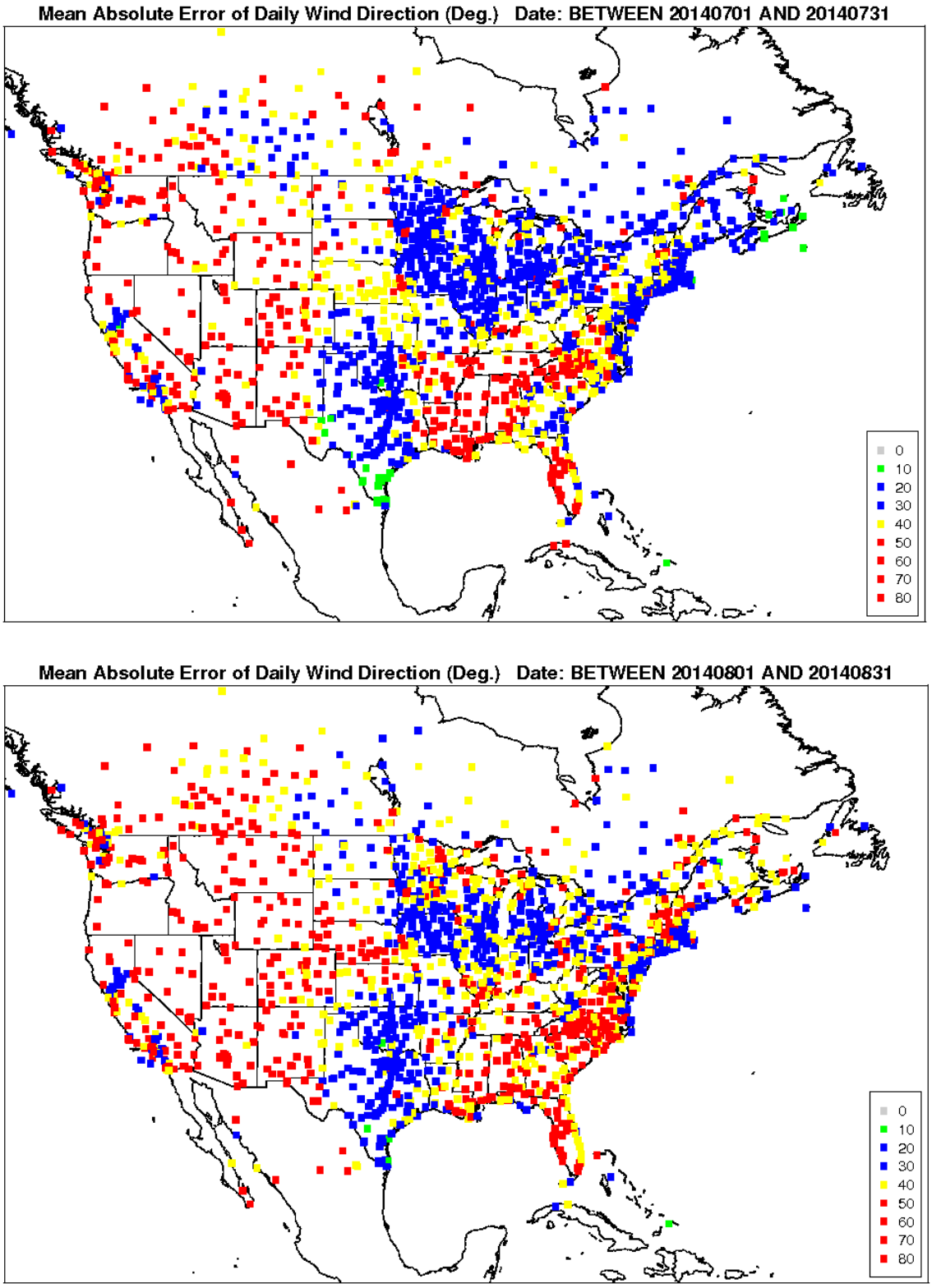

Figure 4-30. Spatial distribution of 10-m wind direction mean absolute error within the 12-km CONUS domain for July (top) and August (bottom).

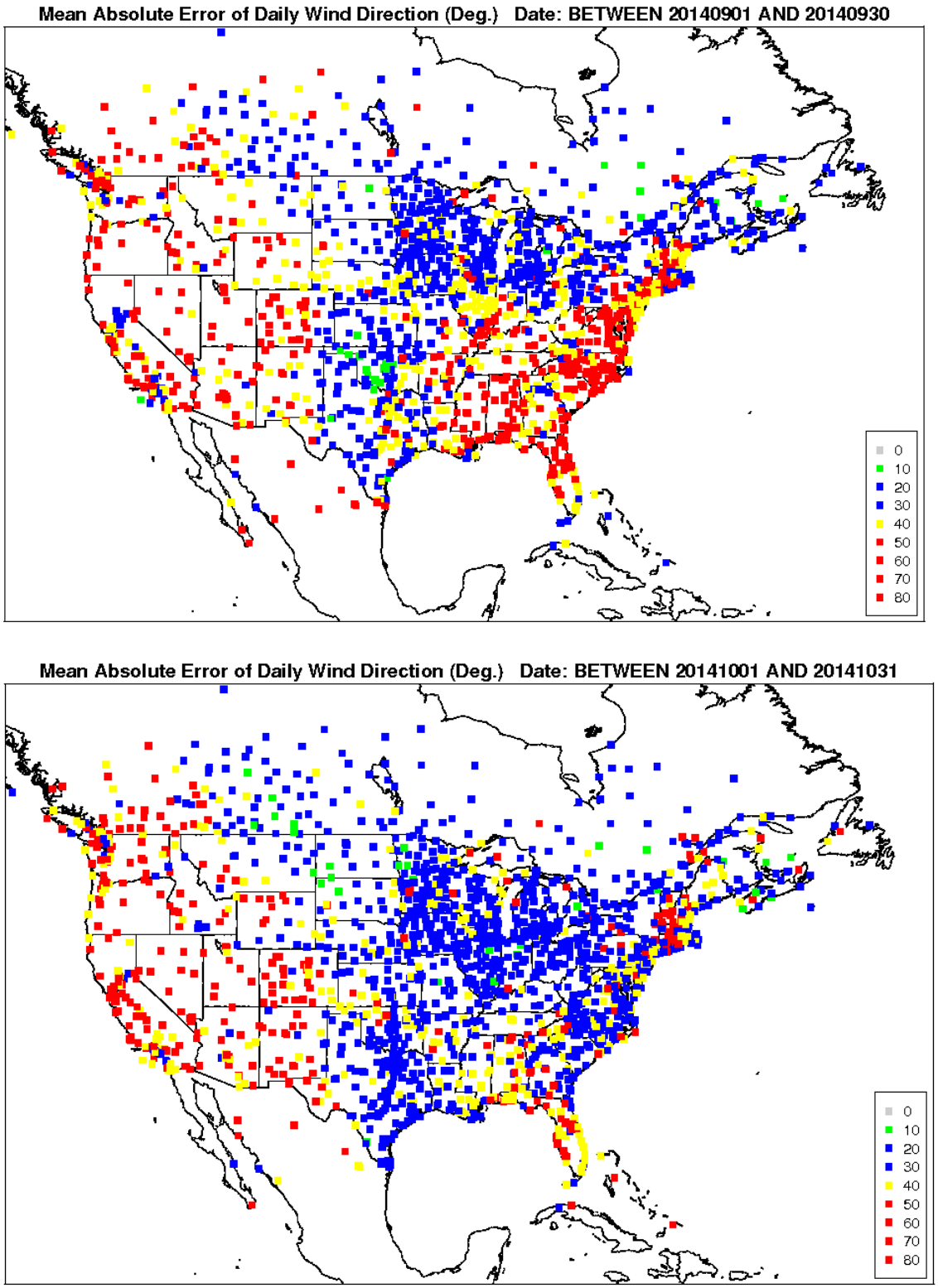

Figure 4-31. Spatial distribution of 10-m wind direction mean absolute error within the 12-km CONUS domain for September (top) and October (bottom).

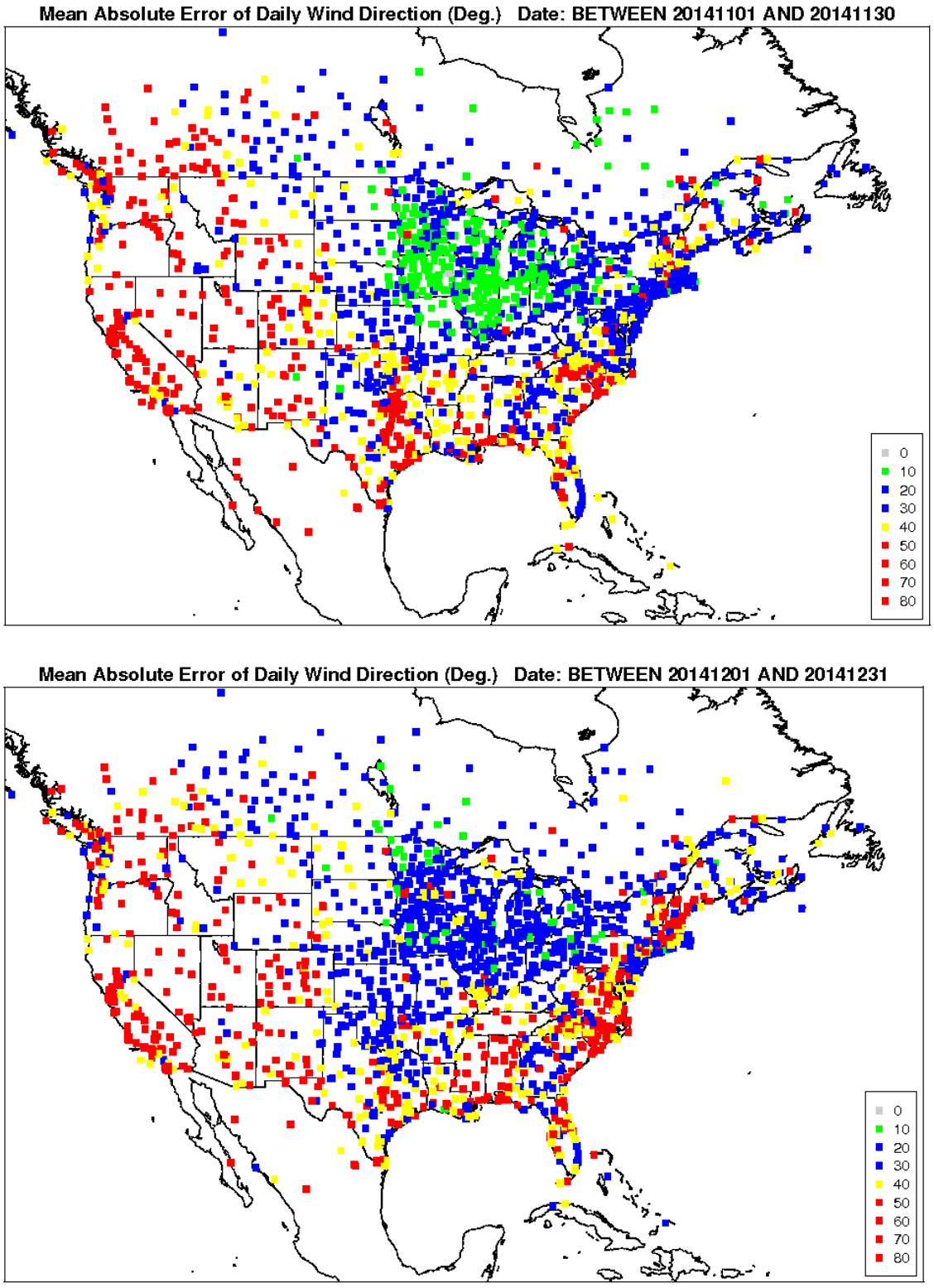

Figure 4-32. Spatial distribution of 10-m wind direction mean absolute error within the 12-km CONUS domain for November (top) and December (bottom).

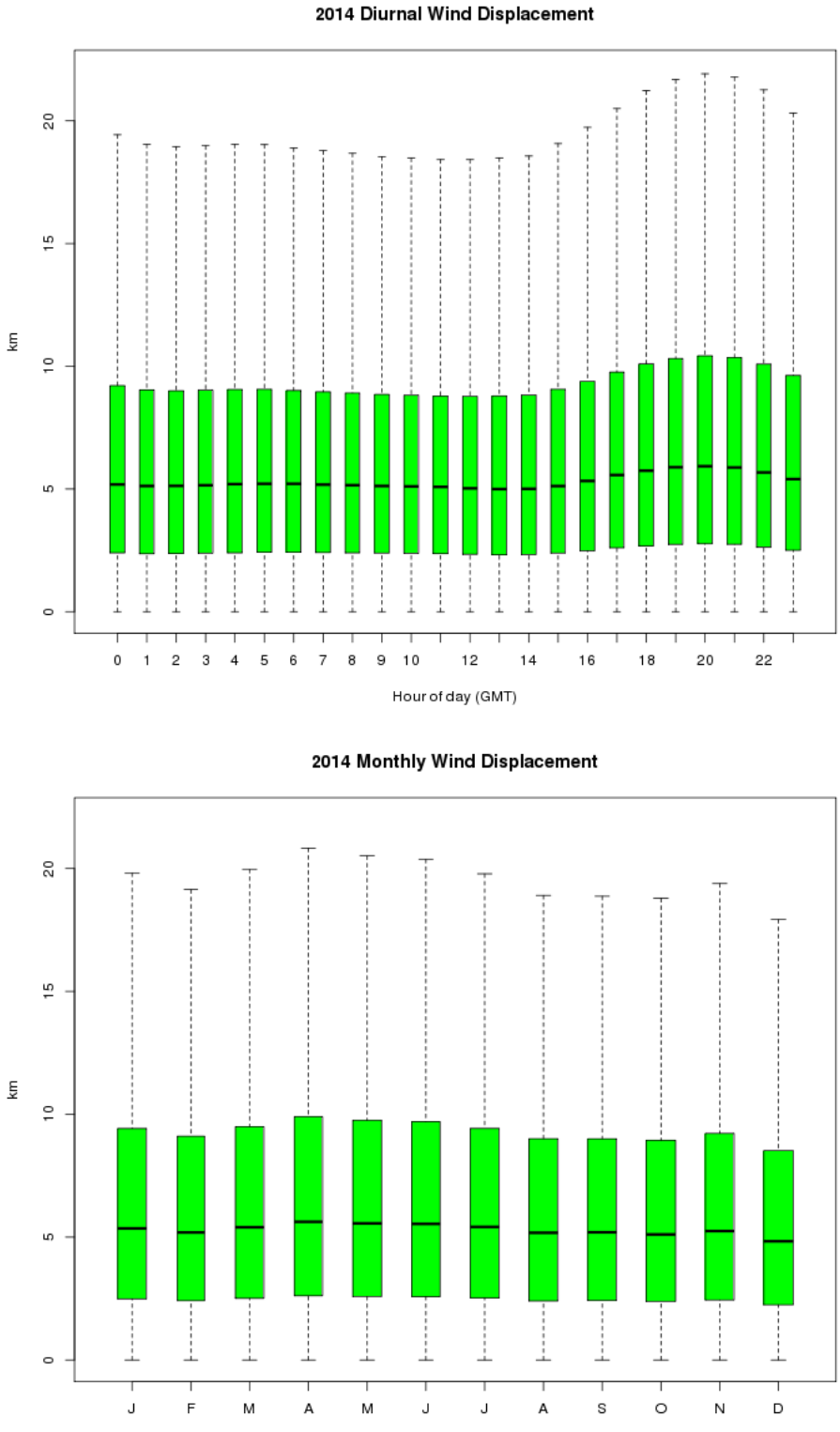

Figure 4-33. Distribution of wind displacement averaged for all statistics within the 12-km CONUS domain for each hour (top) and month (bottom).

Model Evaluation Results for Monthly Precipitation

The PRISM-accumulated monthly precipitation was compared to the WRF 12-km domain precipitation amounts for each month of 2014, January through December. The PRISM precipitation was aggregated to the WRF 12-km domain to take a difference in the monthly precipitation totals for each month (WRF minus PRISM). Below is a discussion of the precipitation for each month. Note that PRISM data does not include regions outside of the U.S.

January Precipitation 2014

Figure 4-34 compares the accumulated monthly precipitation from PRISM (top), WRF (middle), and WRF minus PRISM (bottom) for January 2014 within the CONUS. The WRF spatial pattern of monthly precipitation in January 2014 matches the PRISM patterns very well, in areas such as placement of higher rainfall totals for the Pacific Northwest and the eastern half of the CONUS. Climatologically, drier conditions existed from California into the Southwest and Southern Plains. For instance, New Mexico recorded its driest January in the 120-year record.[20] These record dry conditions are well simulated in WRF.

In examining WRF minus PRISM, the higher terrain locations within the Cascade and Rocky Mountains show the largest differences. WRF overestimates the precipitation totals in the higher terrain over the western half of the CONUS. However, the coastal locations in the Pacific Northwest are drier in WRF. The other region with large differences between observed and WRF-simulated rainfall totals is the Southeast U.S. In general, WRF underestimates the rainfall totals for much of the Southeast U.S., excluding southern Florida. It is important to note that station density is an important component of the observed precipitation PRISM product; therefore, some caution about the overestimation over the higher terrain, where station density is smaller, must be applied.

February Precipitation 2014

Figure 4-35 compares the accumulated monthly precipitation from PRISM (top), WRF (middle), and WRF minus PRISM (bottom) for February 2014 within the CONUS. The WRF spatial pattern of monthly precipitation in February 2014 matches the PRISM patterns very well. For instance, WRF simulates higher precipitation totals within the Northwest for locations within Wyoming, Idaho, and Montana. In particular, the precipitation totals in February for Montana and Wyoming rank as one of the top 10 wettest Februaries in the 120-year record.[21] Additionally, WRF is able to simulate the higher observed rainfall totals from Louisiana, extending northward into Tennessee and Kentucky. February was also very dry; one of the top 10 driest Februaries on record for Arizona, New Mexico, and Oklahoma. WRF captures the drier conditions that were persistent for much of the Southwest U.S.

In examining WRF minus PRISM, large differences occur in similar locations to the month of January. Overestimation of rainfall occurs for the higher terrain locations within the Cascade and Rocky Mountains, especially for Idaho and Wyoming. Additionally, the coastal locations in the Pacific Northwest are drier in WRF. The other region with large differences between observed and WRF

[20] https://www.ncdc.noaa.gov/sotc/national/201401
[21] https://www.ncdc.noaa.gov/sotc/national/201402

simulated rainfall totals occur within the Southeast U.S. In general, WRF underestimates the rainfall totals for much of the Southeast U.S., from Louisiana into the Carolinas. There is also a noticeable but small overestimation, generally less than one inch, for much of the Northeast U.S.

March Precipitation 2014

Figure 4-36 compares the accumulated monthly precipitation from PRISM (top), WRF (middle), and WRF minus PRISM (bottom) for March 2014 within the CONUS. WRF simulates the placement of higher rainfall totals for locations within CONUS, such as over Idaho, western Montana, and along the Gulf Coast of the Southeast U.S. Montana had its third wettest March in the 120-year record[22] and the placement of the higher precipitation totals in western Montana is well simulated by WRF.

In examining WRF minus PRISM, WRF overestimates the precipitation amounts from the Cascade Mountains into the northern Plains. Similar to the prior months, the precipitation within the Southeast U.S. is generally underestimated. In particular, WRF underestimates rainfall from northern Louisiana into Mississippi and Alabama. However, in March, unlike January and February, WRF overestimates the precipitation totals from Georgia into the Carolinas.

April Precipitation 2014

In April 2014, WRF simulates the correct placement of precipitation for locations such as the Northwest, upper Midwest (e.g. Wisconsin), and parts of the Southeast (e.g. Alabama), as shown in Figure 4-37. However, there are some locations where WRF fails to simulate heavier precipitation amounts such as the panhandle region of Florida and western Kentucky. The top 10 wettest Aprils recorded in the 120-year record occurred for Wisconsin, Minnesota, Alabama, Georgia, and Florida.[23] Some of the heaviest rainfall within Florida and Georgia are underestimated in WRF, despite the climatologically large rainfall anomalies.

In examining WRF minus PRISM, WRF over and underestimates rainfall for locations within the Southeast U.S., helping to highlight the problem simulating the exact rainfall placement. As in prior months, WRF overestimates precipitation in the higher elevations over the western half of the CONUS and the Northeast.

May Precipitation 2014

The placement of maximum precipitation in May 2014 was well simulated by WRF over the Northwest (e.g. Washington and Oregon) into the northern Plains/Midwest (Colorado, Nebraska, Minnesota and Wisconsin), as shown in Figure 4-38. WRF failed to simulate precipitation along the Gulf Coast from Texas to Florida. Additionally, the rainfall maximum along coastal locations and throughout the Northeast was above average, based on climatological records. Despite heavy rainfall over Texas, the

[22] https://www.ncdc.noaa.gov/sotc/national/201403
[23] https://www.ncdc.noaa.gov/sotc/national/201404

nearby neighboring state of Kansas had the 6th driest May in the 120-year record[24]. WRF does a good job at simulating the drier conditions within Kansas.

In examining WRF minus PRISM, WRF underestimates precipitation in the Northwest, Southeast and Northeast. WRF overestimates precipitation in the Southwest, and from South Carolina into western North Carolina/Kentucky.

June Precipitation 2014

In June 2014, WRF simulates the large precipitation that is oriented south to north within the Great Plains (from Kansas to Minnesota), shown in Figure 4-39. Numerous states within the Great Plains had their 10 wettest Junes within the 120-year record.[25] In particular, Minnesota broke the record for the wettest June. There are numerous other locations throughout the CONUS where the location of the maximum precipitation is simulated by WRF, including Florida and eastern North Carolina. Additionally, WRF does a good job at simulating the precipitation amounts for some of the driest locations, such as Arizona, which experienced its 3rd driest June on record.

In examining WRF minus PRISM, WRF underestimates precipitation for the Gulf Coast and the coastal locations within the Northeast. However, the difference for a majority of the CONUS illustrate WRF can over and underestimate rainfall over short distances, which indicates that the model does not have a consistent precipitation bias.

July Precipitation 2014

Figure 4-40 compares the accumulated monthly precipitation from PRISM (top), WRF (middle), and WRF minus PRISM (bottom) for July 2014 within the CONUS. The precipitation associated with the Southwest monsoon is captured in WRF; however, WRF overestimates the amount of rainfall throughout a good portion of the Southwest. The difference between WRF and PRISM precipitation shows rainfall totals in WRF is overestimated by 3 inches or more in July. This indicates a problem simulating the North American monsoon within WRF. Additionally, WRF overestimates rainfall within the Southeast into the Northeast. Many of the areas where WRF overestimates precipitation occur with climatologically above average precipitation (e.g. Southwest and Northeast).[26] The locations where WRF underestimates the monthly rainfall totals are located most within the Great Plains. Overall, the WRF precipitation in July hints at a potential problem with simulating the Great Plains Low-Level Jet during the summer.

August Precipitation 2014

Like July, WRF estimates higher and more widespread precipitation within the Southwest in August 2014 than PRISM, as shown in Figure 4-41. Again, the results illustrate an issue with WRF simulating the North American Monsoon. WRF simulates the location of heavy precipitation in the northern Great Plains from Montana into the Dakotas. Montana experienced its wettest August on record with other states with the

[24] https://www.ncdc.noaa.gov/sotc/national/201405
[25] https://www.ncdc.noaa.gov/sotc/national/201406
[26] https://www.ncdc.noaa.gov/sotc/national/201407

Great Plains also having its top 10 wettest August.[27] In Montana and portions of the Dakotas, WRF overestimates the precipitation. Other areas with observed precipitation maximum that are simulated in approximate locations include Florida, Louisiana, Carolinas, Tennessee, and Kentucky. With the exception of Louisiana, WRF overestimates the precipitation totals for August for these locations. Additionally, precipitation totals within the lower Great Plains are underestimated by WRF.

September Precipitation 2014

In September 2014, there continues to be an overestimation of precipitation from WRF for the Southwest that extends into the Rockies, as shown in Figure 4-42. In particular, precipitation in Arizona, New Mexico, and the Colorado Rockies are overestimated by as much as 4 inches. The results indicate a systematic problem from July through September with simulating precipitation associated with the North American Monsoon. However, it is important to also note that in additional to the monsoonal flow, remnants from a tropical cyclone helped to contribute to above average precipitation within the Southwest.[28] In the Southeast, WRF simulates the heavier observed precipitation from Florida northward into the eastern Carolinas. WRF also simulates that heavier precipitation occurred from Kansas northeastward into Wisconsin; however, precipitation totals are generally underestimated by WRF. WRF fails to capture the heavy precipitation along the Texas Gulf Coast.

October Precipitation 2014

In October 2014, heavy precipitation returned to the Pacific Northwest and WRF does a good job at capturing the location and the precipitation amounts, shown in Figure 4-43. Heavy precipitation also fell along the Mississippi River Valley with Kentucky, Missouri, and Tennessee, each having one of their ten wettest Octobers on record.[29] WRF simulates the heavy precipitation along the Mississippi River, but the rainfall totals are underestimated by WRF. In particular, WRF underestimates the rainfall for Georgia, Alabama, and Mississippi by as much as four inches in some locations. WRF also underestimates precipitation along the Atlantic coast from North Carolina to Maine.

November Precipitation 2014

In November 2014, WRF simulates the heavy precipitation along the Pacific Northwest, seen in Figure 4-44. However, WRF underestimates the precipitation totals in November. WRF also captures the heavier rainfall along northern California and the Sierra Nevada; however, the precipitation totals are again underestimated by WRF. An exception over the western half of the CONUS is in the Rocky Mountains, where WRF typically overestimates the precipitation totals in November (e.g. Idaho). WRF is able to simulate heavier precipitation from Texas and locations east. The observed north-south precipitation streaks are likely the result of precipitation associated with cold fronts/low pressure systems and these features are somewhat misplaced by WRF. For instance, WRF simulates large precipitation totals in eastern North Carolina, while the observed precipitation maximum is south over eastern South Carolina and Georgia. In general, WRF underestimates the precipitation totals within the Southeast.

[27] https://www.ncdc.noaa.gov/sotc/national/201408
[28] https://www.ncdc.noaa.gov/sotc/national/201409
[29] https://www.ncdc.noaa.gov/sotc/national/201410

December Precipitation 2014

In December 2014, the largest precipitation totals occur in the Northwest, Northeast, and Southeast, as shown in Figure 4-45. WRF estimates larger rainfall totals in the higher terrain locations over the western half of the CONUS with an exception of northern Sierra Nevada. In general, December rainfall totals along the west coast are underestimated by WRF when compared to PRISM. Another notable issue is the precipitation totals within the Southeast. Though WRF simulates heavier precipitation amounts, the precipitation totals are underestimated by 4 inches for most locations within the Southeast. WRF does a good job at simulating the precipitation within the Northeast, especially the rainfall maximum in Maine.

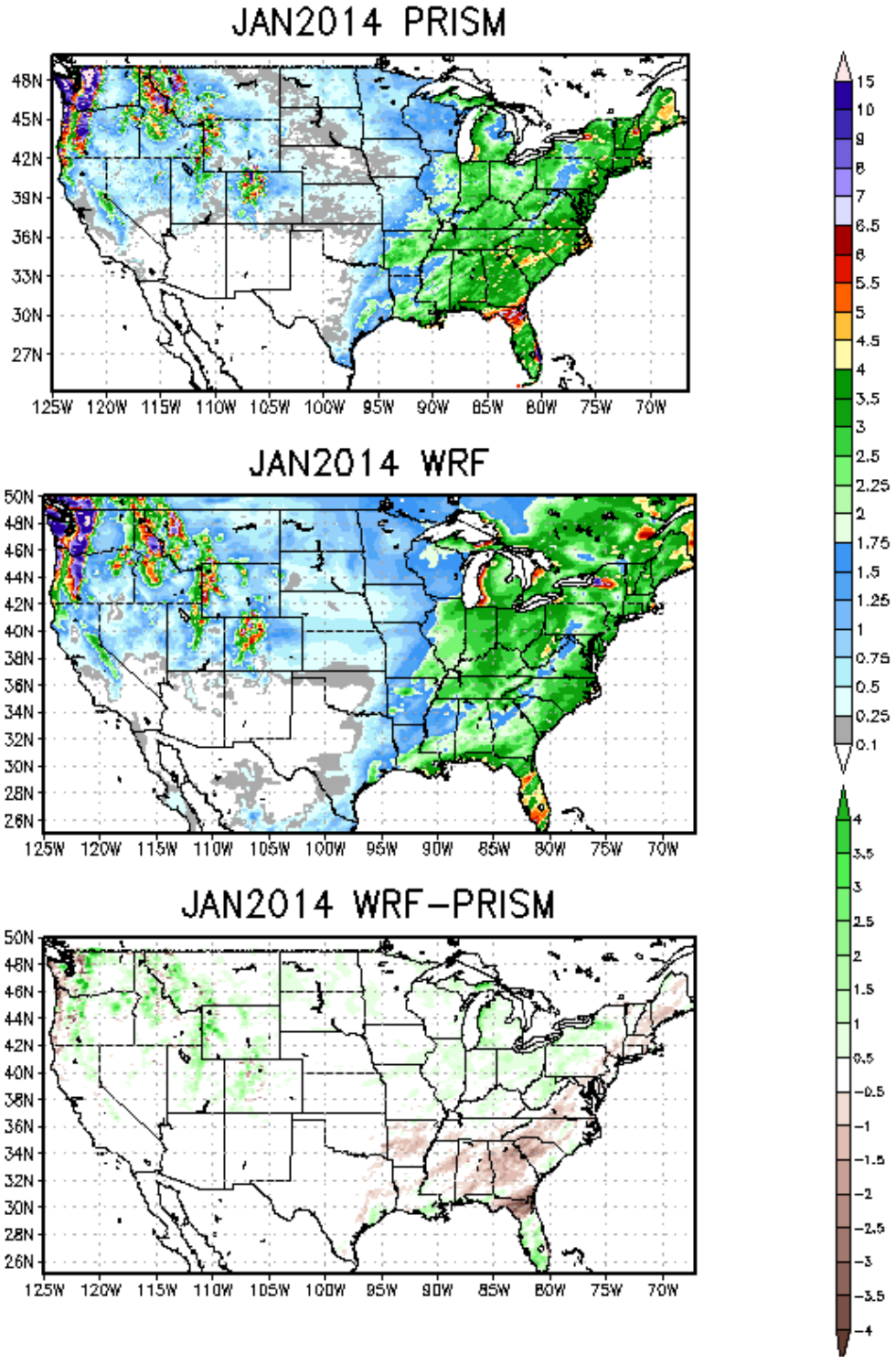

Figure 4-34. Comparison of monthly total precipitation (inches) from PRISM (top) and WRF (middle) and WRF minus PRISM (bottom) for the 12-km CONUS domain in January 2014.

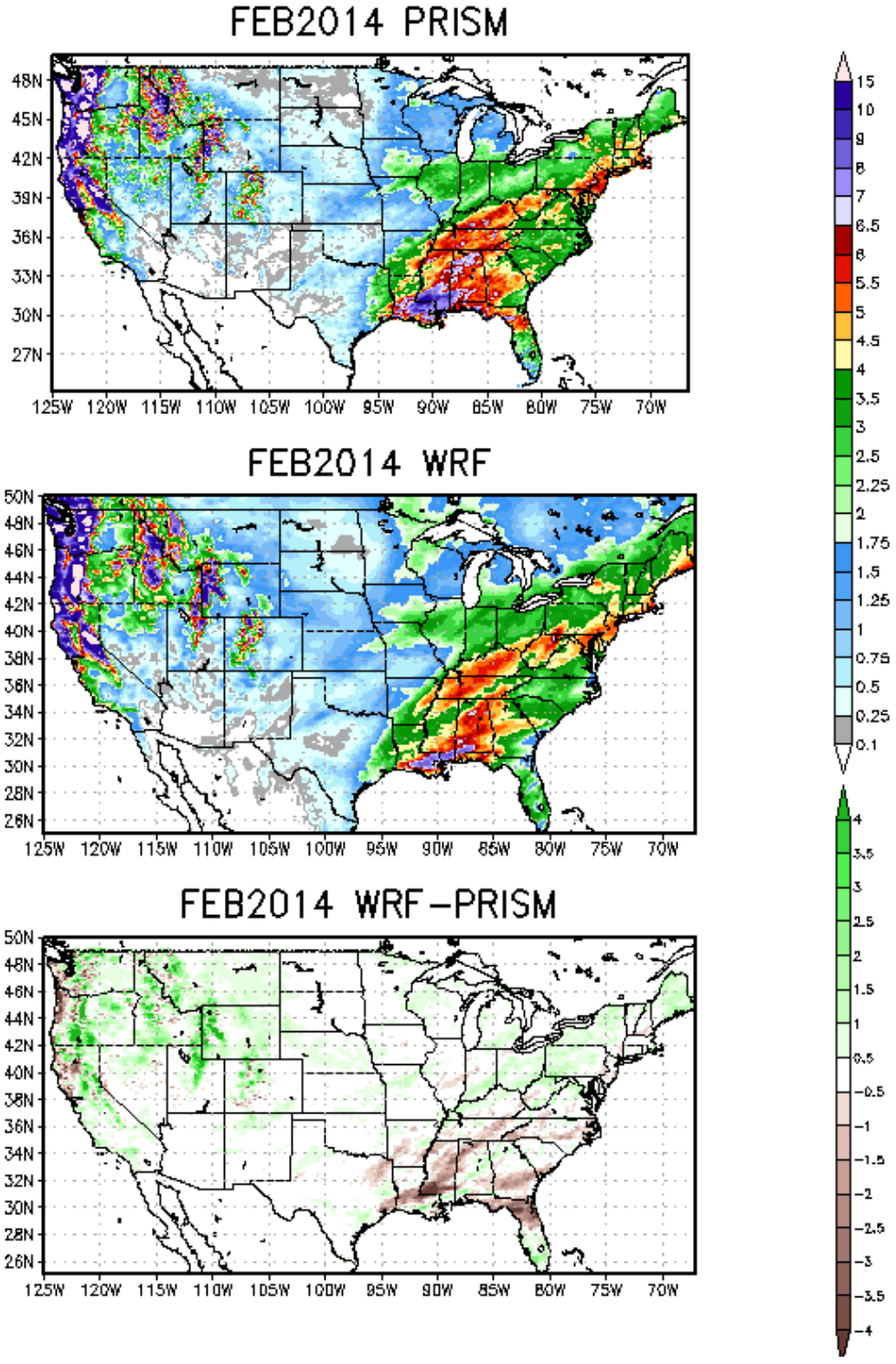

Figure 4-35. Comparison of monthly total precipitation (inches) from PRISM (top) and WRF (middle) and WRF minus PRISM (bottom) for the 12-km CONUS domain in February 2014.

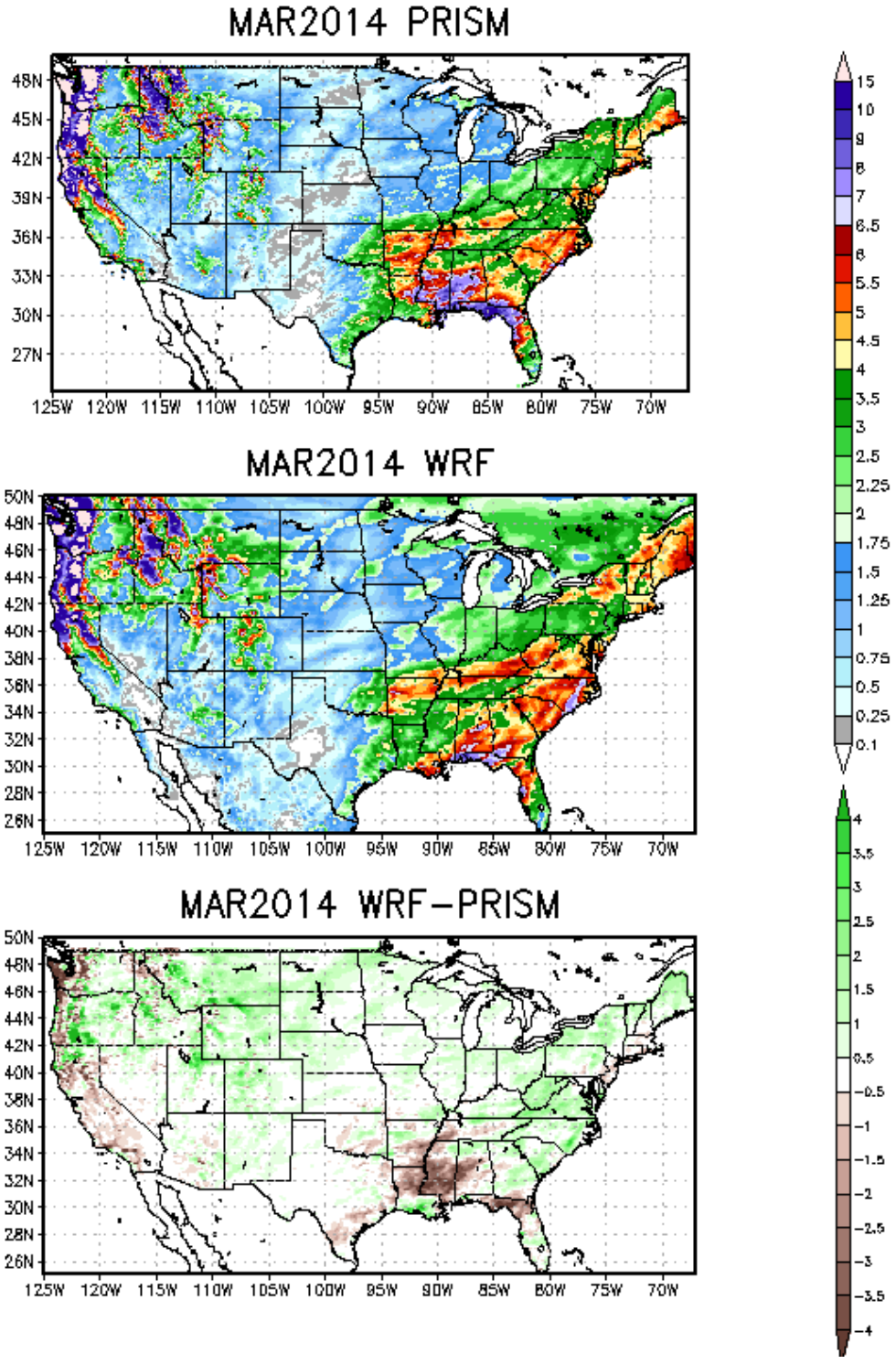

Figure 4-36. Comparison of monthly total precipitation (inches) from PRISM (top) and WRF (middle) and WRF minus PRISM (bottom) for the 12-km CONUS domain in March 2014.

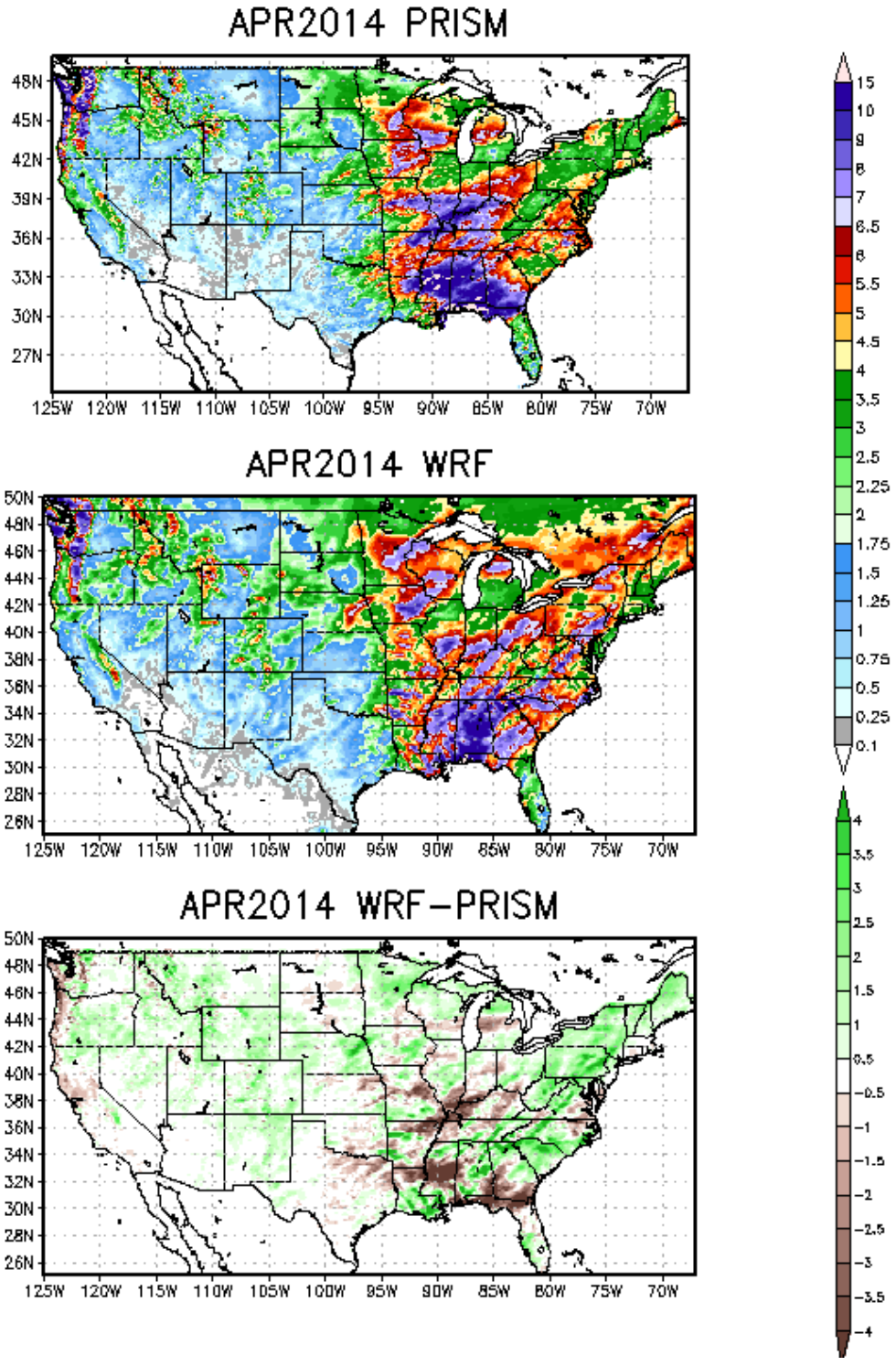

Figure 4-37. Comparison of monthly total precipitation (inches) from PRISM (top) and WRF (middle) and WRF minus PRISM (bottom) for the 12-km CONUS domain in April 2014.

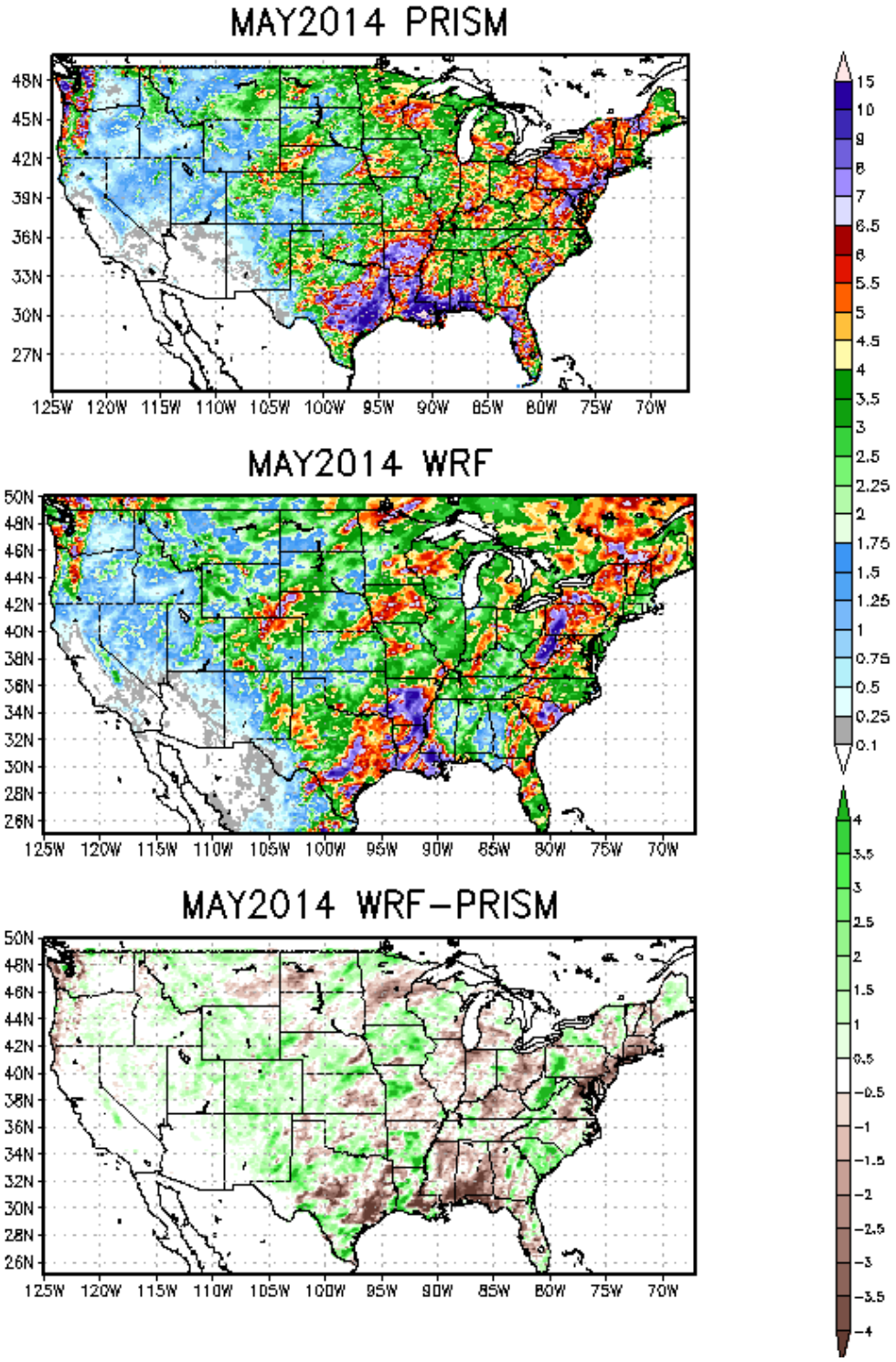
MAY2014 PRISM
MAY2014 WRF
MAY2014 WRF−PRISM
125W 120W 115W 110W 105W 100W 95W 90W 85W 80W 75W 70W
15
10
9
8
7
6.5
6
5.5
5
4.5
4
3.5
3
2.5
2.25
2
1.75
1.5
1.25
1
0.75
0.5
0.25
0.1
4
3.5
3
2.5
2
1.5
1
0.5
−0.5
−1
−1.5
−2
−2.5
−3
−3.5
−4

Figure 4-38. Comparison of monthly total precipitation (inches) from PRISM (top) and WRF (middle) and WRF minus PRISM (bottom) for the 12-km CONUS domain in May 2014.

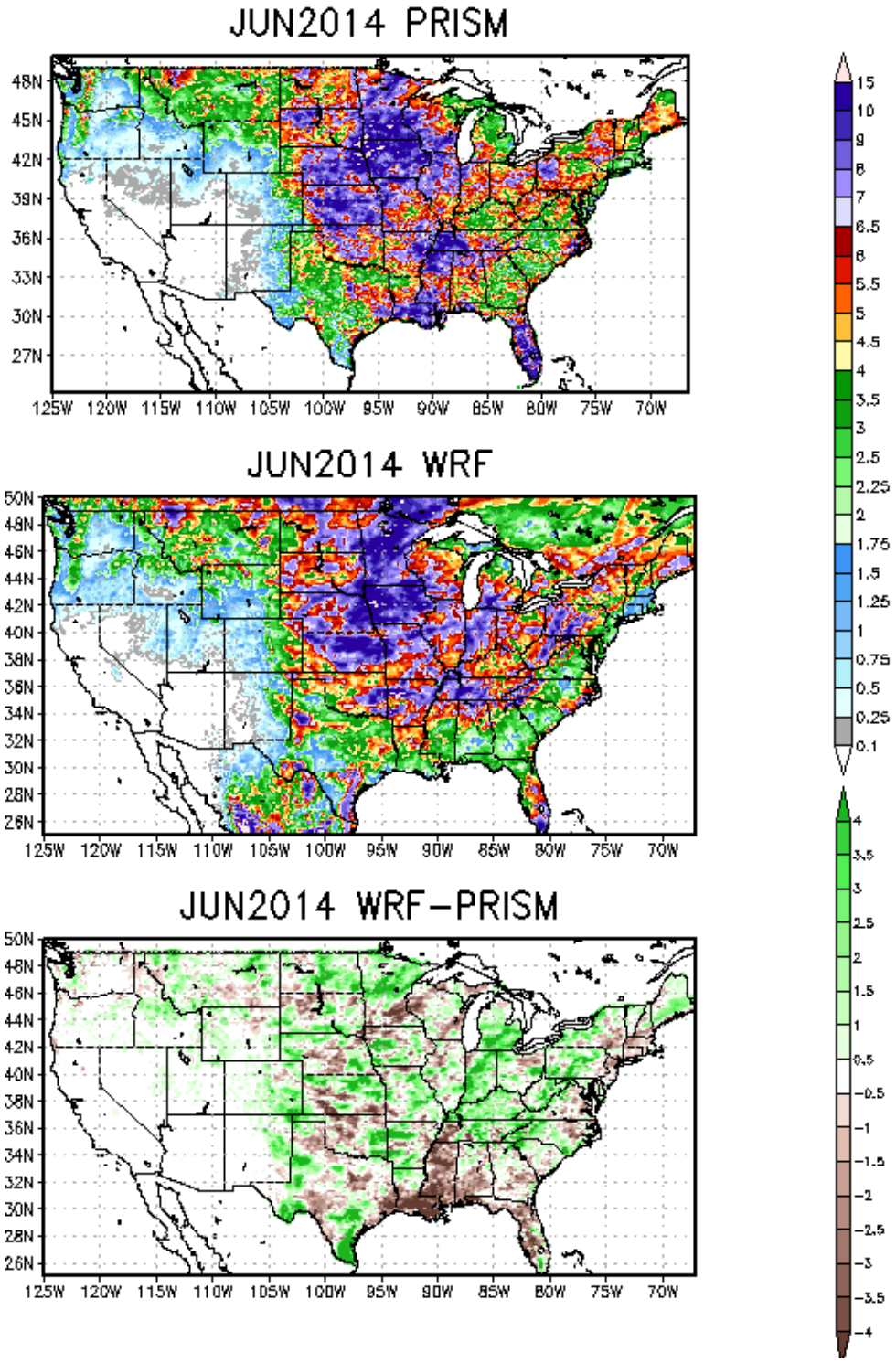

Figure 4-39. Comparison of monthly total precipitation (inches) from PRISM (top) and WRF (middle) and WRF minus PRISM (bottom) for the 12-km CONUS domain in June 2014.

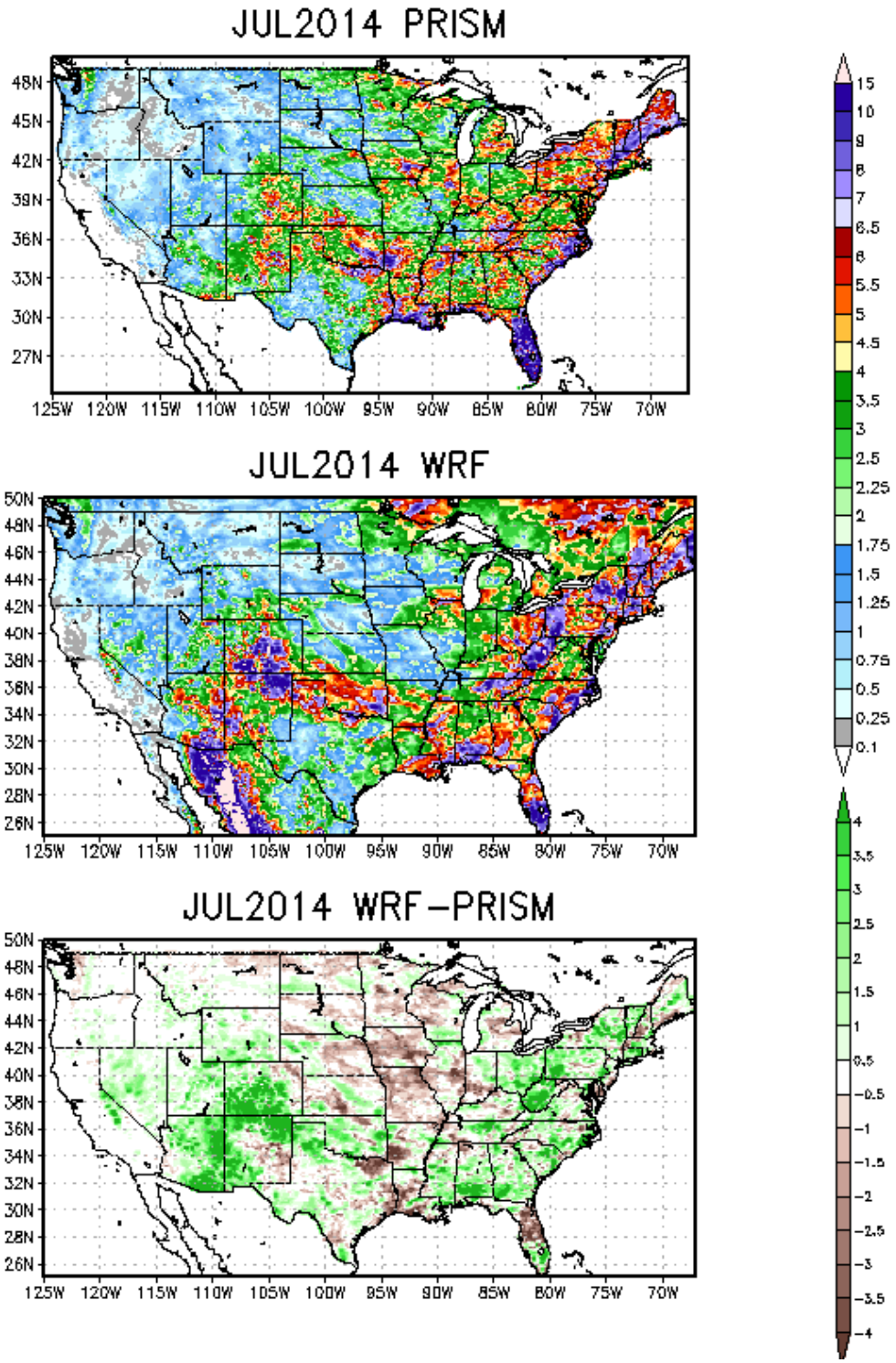

Figure 4-40. Comparison of monthly total precipitation (inches) from PRISM (top) and WRF (middle) and WRF minus PRISM (bottom) for the 12-km CONUS domain in July 2014.

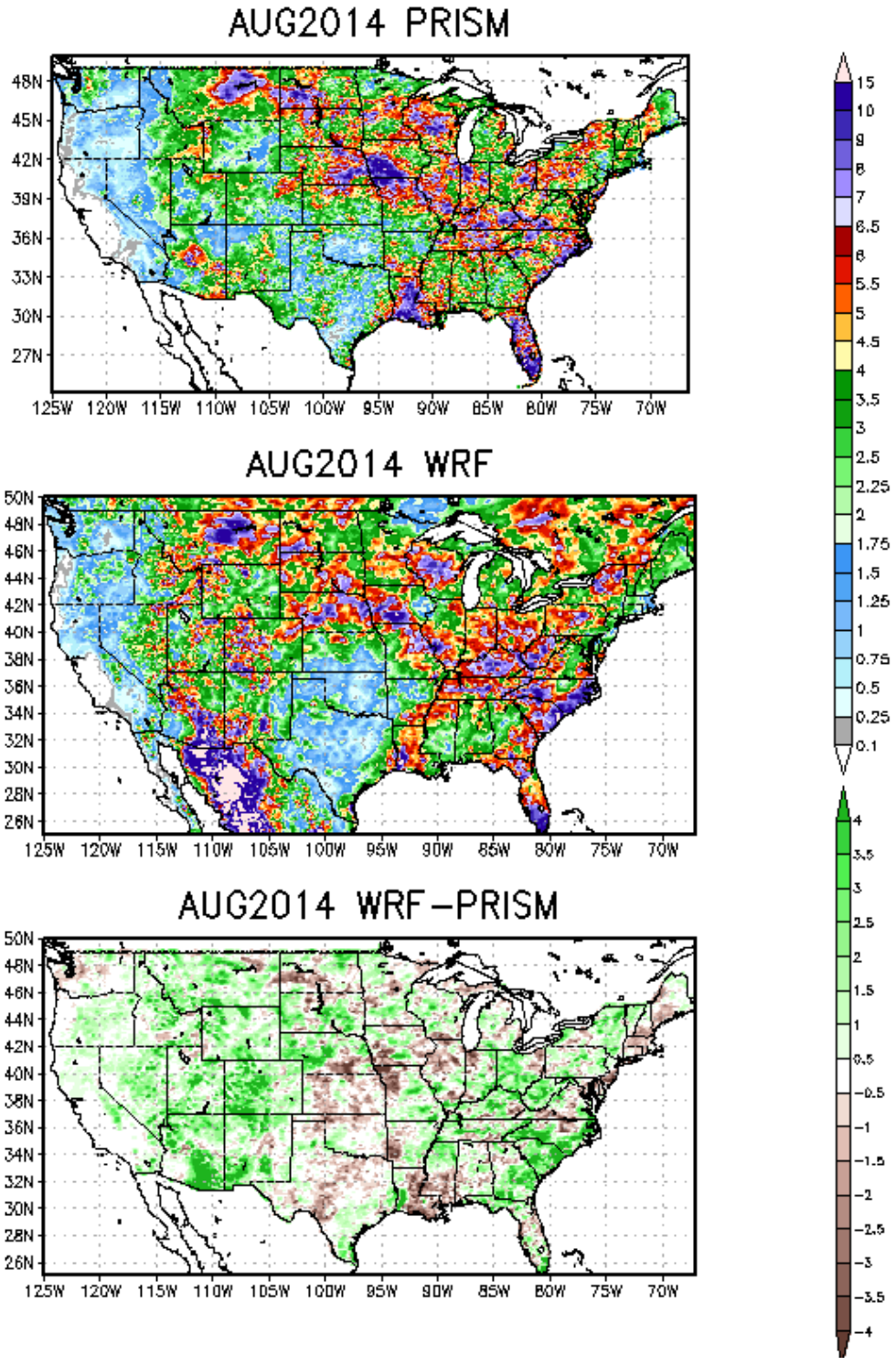

Figure 4-41. Comparison of monthly total precipitation (inches) from PRISM (top) and WRF (middle) and WRF minus PRISM (bottom) for the 12-km CONUS domain in August 2014.

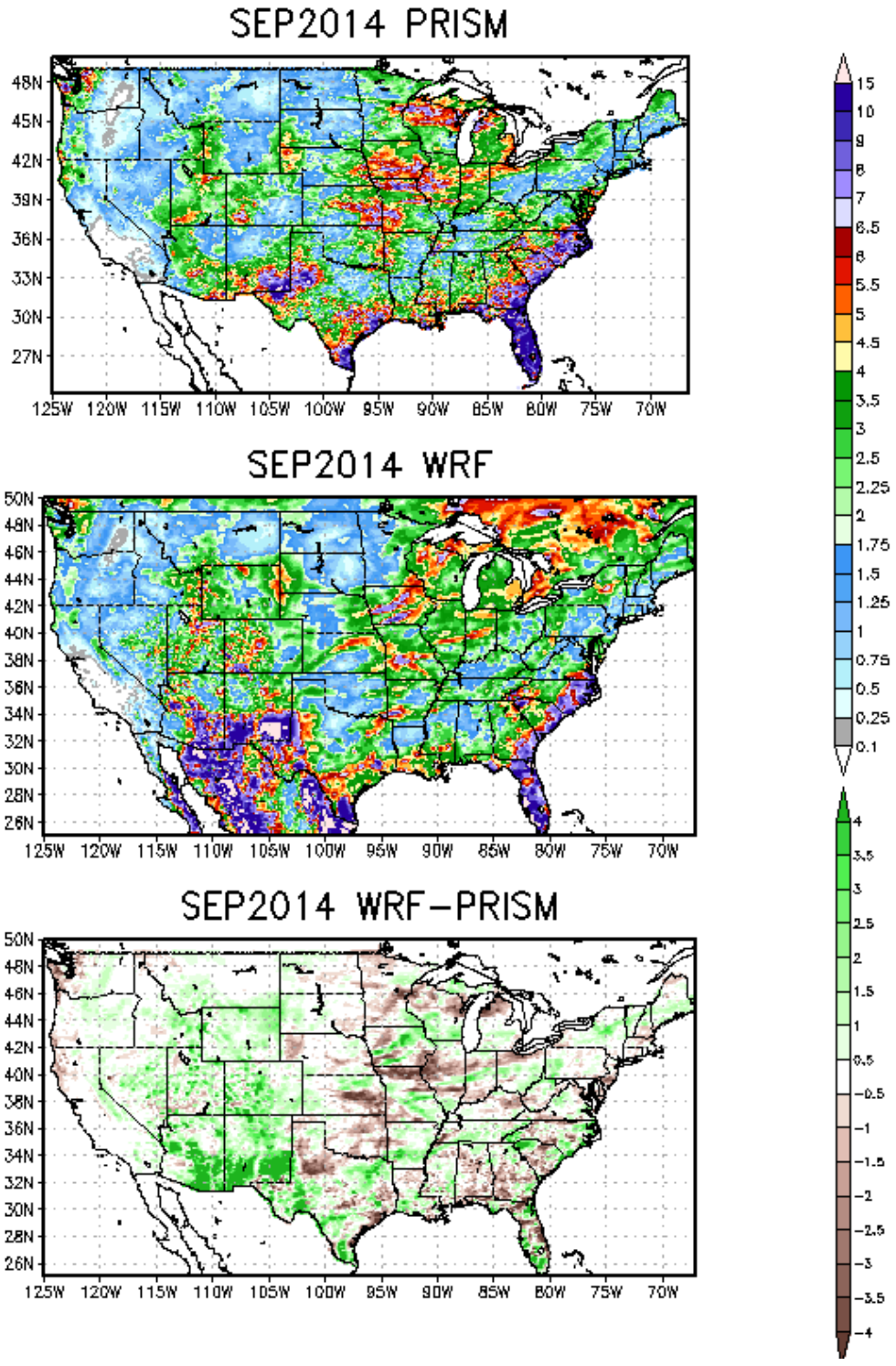

Figure 4-42. Comparison of monthly total precipitation (inches) from PRISM (top) and WRF (middle) and WRF minus PRISM (bottom) for the 12-km CONUS domain in September 2014.

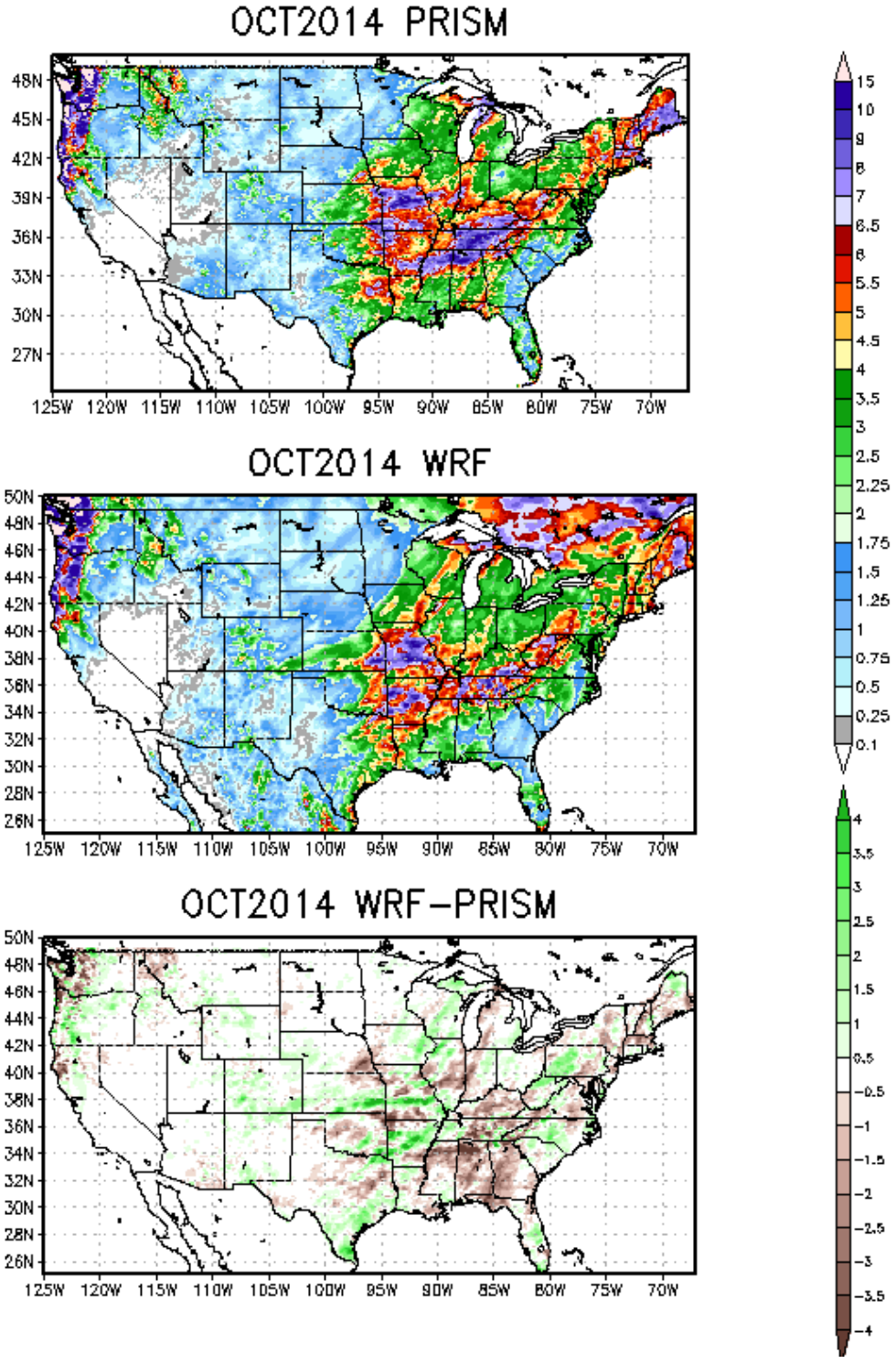

Figure 4-43. Comparison of monthly total precipitation (inches) from PRISM (top) and WRF (middle) and WRF minus PRISM (bottom) for the 12-km CONUS domain in October 2014.

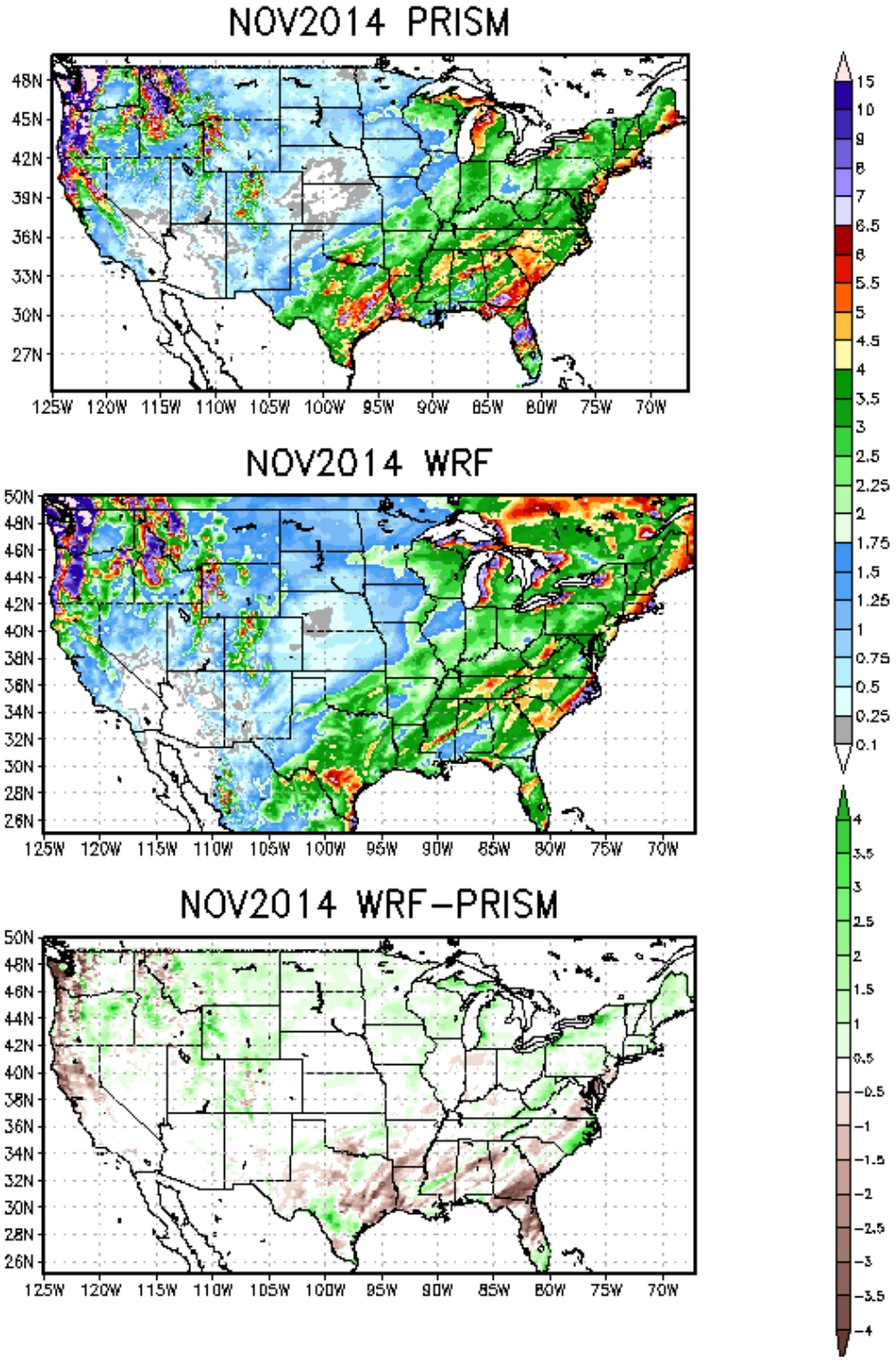

Figure 4-44. Comparison of monthly total precipitation (inches) from PRISM (top) and WRF (middle) and WRF minus PRISM (bottom) for the 12-km CONUS domain in November 2014.

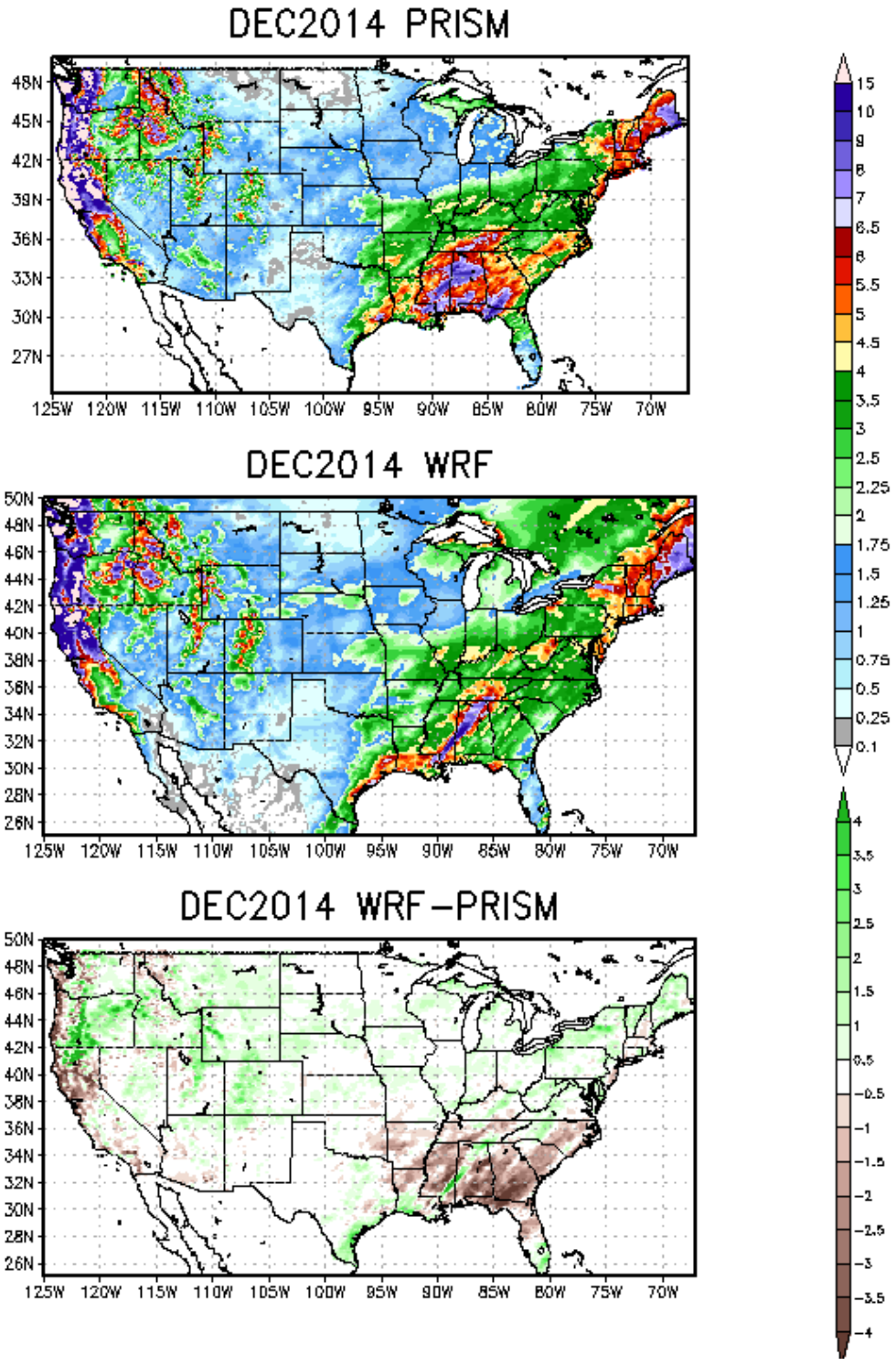

Figure 4-45. Comparison of monthly total precipitation (inches) from PRISM (top) and WRF (middle) and WRF minus PRISM (bottom) for the 12-km CONUS domain in December 2014.

Model Evaluation Results for Solar Radiation

Estimates of modeled biogenic emissions for estimating isoprene emissions are sensitive to the photosynthetically activated radiation, which is a fraction of the shortwave downward radiation.[30] Regional ozone chemistry and the formation of secondary organic aerosols are impacted by changes in the isoprene emissions. Below, we illustrate the model performance of shortwave downward radiation, which has important implications for regional air quality and provides an indirect assessment of how well the model captures cloud formation during daylight hours.

Figure 4-46 is a comparison of the shortwave downward radiation estimates compared to the surface based measurements at SURFRAD and ISIS network monitors averaged for all sites within the CONUS. The top panel is a comparison of the hourly estimates. The model underestimates the shortwave downward radiation during the early to late morning hours and overestimates the amount during the late afternoon into early evening. The over prediction during the afternoon is larger (upwards +100 W/m2) than the under prediction during the morning hours (-50 W/m2). These results hint at problems simulating the relative cloud cover amount during the morning and afternoon. In the bottom panel is a comparison of the monthly radiation estimates. During the late fall through winter into the early spring, the shortwave radiation bias is small. The bias grows by late spring into the summer with a peak in the over prediction of shortwave radiation during the months June and July. The over prediction is generally less than 100 W/m2. The median bias is close to zero for all months.

[30] Carlton, A.G., Baker. K.R., 2011. Photochemical Modeling of the Ozark Isoprene Volcano: MEGAN, BEIS, and Their Impacts on Air Quality Predictions. *Environmental Science and Technology* 45, 4438-4445.

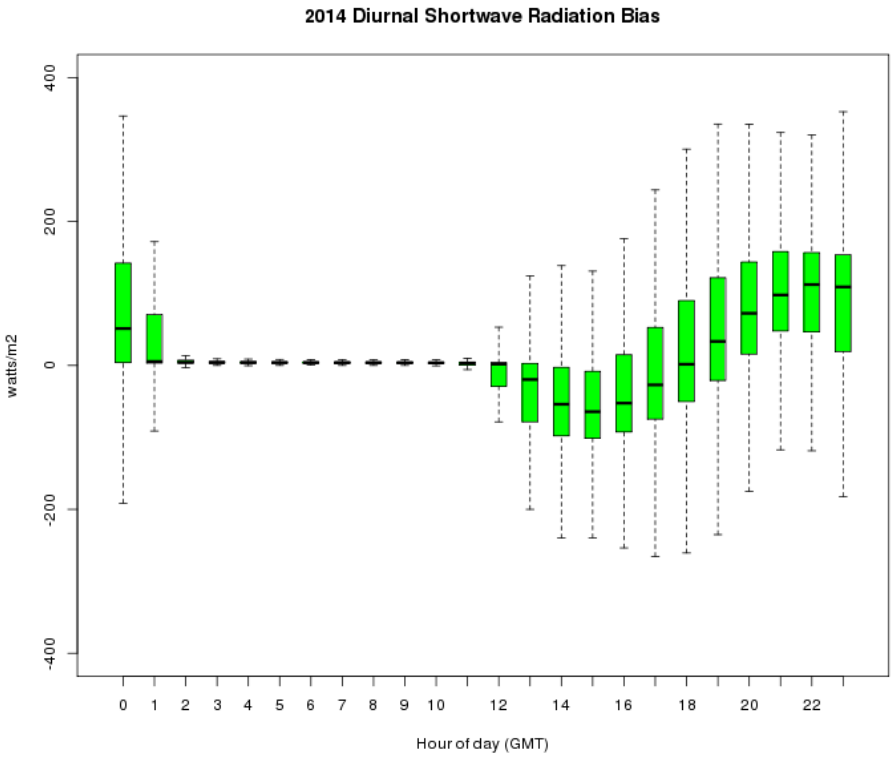
2014 Diurnal Shortwave Radiation Bias
watts/m2
400
200
0
-200
-400
0
1
2
3
4
5
6
7
8
9
10
12
14
16
18
20
22
Hour of day (GMT)

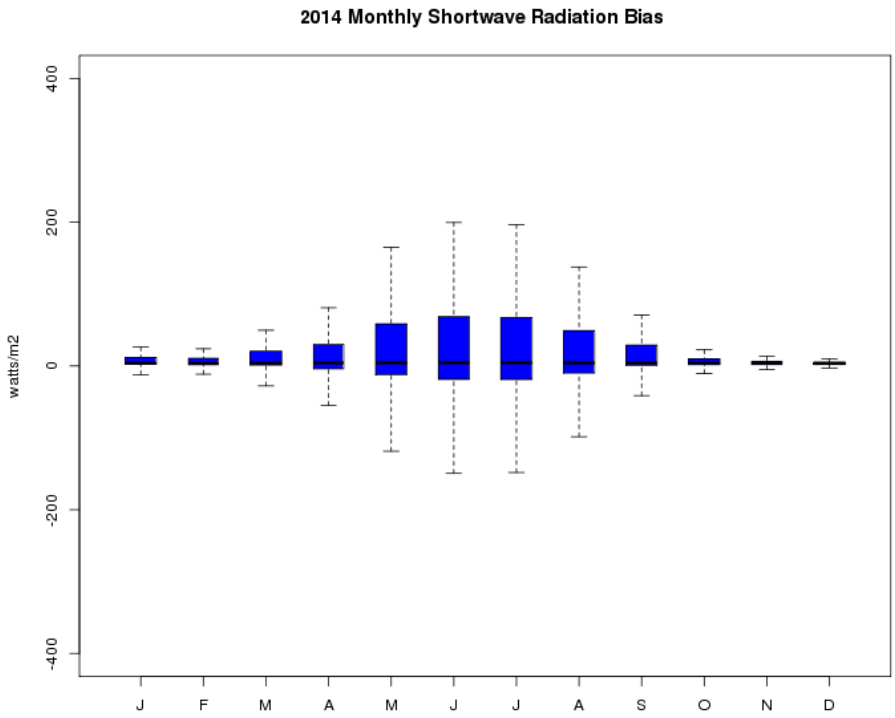

Figure 4-46. Model bias of shortwave radiation averaged over all SURFRAD and ISIS network monitors within the 12-km CONUS domain for each hour (top) and month (bottom).

5.0 ADDITIONAL RESULTS

An electronic docket is also included with this report that contains additional plots illustrating the 2014 WRF model performance.

Link to additional model evaluation plots for 2014 can be found at:

https://drive.google.com/folderview?id=0BxAQ24gAklsMMzI2bzJHbV94c3M&usp=sharin